# Non-linear buckling and large deflection analyses of isotropic and composite stiffened panels using an arbitrarily orientated stiffened element approach

by

Roberto Eduardo Ojeda Rabanal

B.Eng. (Hons) Universidad Austral de Chile, 2003

Submitted in fulfilment of the requirement for the degree of

Doctor of Philosophy

at the

National Centre for Maritime Engineering and Hydrodynamics

Australian Maritime College

University of Tasmania

June 2011

# Declarations

## Declaration of Originality

I certify that this thesis contains no material which has been accepted for a degree or diploma by the University or any other institution, except by the way of background information duly acknowledged in this thesis, and to the best of my knowledge and belief contains no material previously published or written by another person except where due acknowledgment is made in the text of the thesis, nor does the thesis contains any material that infringes copyright.

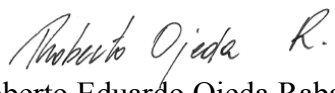

Roberto Eduardo Ojeda Rabanal

Date: 30/06/2011

## Statement of Authority of Access

This thesis may be made available for loan. Copying of any part of this thesis is prohibited for two years from the date this statement was signed; after that time limited copying is permitted in accordance with the Copyright Act 1968.

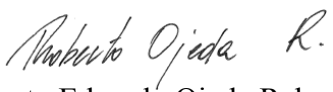

Roberto Eduardo Ojeda Rabanal

Date: 30/06/2011

# Abstract

*A new approach for the non-linear buckling and large deflection analyses of isotropic and composite stiffened panels, as used in high speed craft, is presented.*

*Eight node isoparametric elements, formulated according to Marguerre shallow shell theory, are combined with three node beam elements, using the concept of equal displacements at the panel-stiffener interface, to represent the stiffened panels. Non-linear equilibrium equations are derived using the principle of virtual work applied to a continuum with a total Lagrangian description of motion.*

*The arbitrarily stiffened, shallow shell element is capable of modelling eccentric or concentric stiffeners attached to flat or imperfect panels under in-plane or transverse loads. Special modelling considerations for the loading and boundary conditions, required in the linear and non-linear buckling analyses of stiffened panels using arbitrarily stiffened finite elements, are suggested and discussed for the first time.*

*The Newton-Raphson incremental-iterative solution technique is used to obtain the non-linear response path. Results obtained in this investigation are compared with those available in the open literature to demonstrate the validity and efficiency of the proposed approach. Good agreement is found in all the investigated cases.*

*para mi querido Viejo...*

*"no hay que llegar primero, sino que hay que saber llegar..."*

*José Alfredo Jiménez*

# Acknowledgments

*First, I would like to thank my supervisors, A/Prof Gangadhara Prusty, A/Prof Norman Lawrence and A/Prof Giles Thomas, for guiding my research and for their patience. I am especially grateful of A/Prof Gangadhara Prusty for giving me the opportunity of conducting this research project and for continuing my supervision after his departure from the Australian Maritime College to the University on New South Wales.*

*I would like to thank the Australian Maritime College – National Centre for Maritime Engineering and Hydrodynamics for awarding me the IPRS and John Bicknell scholarships which made this investigation possible.*

*I offer my most sincere thanks to Mr Luciano Mason, not only for the invaluable help he provided in the development of the computer code, but also for his support and encouragement throughout the most difficult times of my candidature.*

*I would also like to thank A/Prof Paul Brandner, not only for his careful editing of the final manuscript, but most importantly for his friendship and camaraderie.*

*Finally, this thesis would have never been finalized without the support of my Family, especially the understanding and caring from my wife Carmen. For her, I will be always in debt...*

# Table of Contents

# List of figures

# List of tables

# Nomenclature

## General Rules and Notation

- The most used symbols are declared here.
- Symbols are generally defined where they appear in the text for the first time.
- Bold face is used to denote matrices and vectors, e.g. **u**

## Subscripts

| | |
|---|---|
| $st$ | Stiffener/Slave element |
| $int$ | Internal |
| $ini$ | Initial |
| $ext$ | External |
| $0$ | Linear |
| $1$ | Initial |
| $NL$ | Non-linear |

## Superscript

| | |
|---|---|
| $a$ | axial |
| $b$ | Bending |
| $p$ | In-plane |
| $s$ | Shear |

## Mathematical Operators

$\partial$ Partial derivative

$d$ Variational operator

## Roman letters

$A_{st}$ Stiffener cross sectional Area

$\mathbf{B}_0$ Linear strain-displacement matrix of the master element

$\mathbf{B}_I$ Initial strain-displacement matrix of the master element

$\mathbf{B}_{NL}$ Non-linear strain-displacement matrix of the master element

$C_{st}$ Stiffener edge couple for eccentrically stiffened panels under compressive loads

$E$ Young's modulus for an isotropic material

$F_{st}$ Extra in-plane load due to the stiffener

$D$ Bending stiffness of the unstiffened panel

$\hat{\mathbf{D}}$ Generalized rigidity matrix of the master element

$G$ Shear modulus for an isotropic material

$h$ Stiffener height

$I_{st}$ Stiffener second moment of area

$\mathbf{I}$ Identity matrix

$J_{st}$ Stiffener polar moment of inertia

$\mathbf{K}_0$ Linear stiffness matrix of the master element

$\mathbf{K}_\sigma$ Geometric stiffness matrix of the master element

$\mathbf{K_S}$ Secant stiffness matrix of the master element

$\mathbf{K_T}$ Tangent stiffness matrix of the master element

$N_i$ Shape function of the $i^{th}$ node of the master element

| | |
|---|---|
| $\mathbf{N}_i$ | Shape function matrix of the $i^{th}$ node of the master element |
| $\mathbf{N}$ | Shape function matrix of the master element |
| $\mathbf{T}$ | Slave element transformation matrix |
| $t$ | Panel thickness |
| $t_s$ | Stiffener thickness |
| $\mathbf{u}$ | Displacement vector |
| $\hat{\mathbf{u}}$ | Mid-surface displacement vector |
| $d\hat{\mathbf{u}}$ | Virtual mid-surface displacement vector |
| $dW_{int}$ | Internal virtual work |
| $dW_{ext}$ | External virtual work |

## Greek letters

| | |
|---|---|
| $\boldsymbol{\varepsilon}$ | Green's strain vector |
| $\hat{\boldsymbol{\varepsilon}}$ | Generalised Green's strain vector |
| $d\hat{\boldsymbol{\varepsilon}}$ | Variation of the generalized Green's strain vector |
| $\boldsymbol{\delta}$ | Nodal displacements of the master element |
| $\boldsymbol{\delta}_i$ | Displacements of the $i^{th}$ node of the master element |
| $d\boldsymbol{\delta}$ | Virtual displacements of the master element |
| $\boldsymbol{\Lambda}$ | Slave element orientation matrix |
| $\boldsymbol{\zeta}$ | Second Piola-Kirchhoff stress vector |
| $\boldsymbol{\zeta}$ | Generalised second Piola-Kirchhoff stress vector |
| $\upsilon$ | Poisson's ratio for an isotropic material |

## Abbreviations

| | |
|---|---|
| CAE | Computer Assisted Engineering |
| CAD | Computer Aided Design |
| CR | Co-rotational description of motion |
| DOF | Degree Of Freedom |
| EBT | Euler Beam Theory |
| TBT | Timoshenko Beam Theory |
| FRP | Fibre Reinforced Plastics |
| FSDT | First order Shear Deformation Theory |
| HOST | Higher Order Shear deformation Theory |
| HSC | High Speed Craft |
| IMO | International Maritime Organization |
| SCF | Shear Correction Factor |
| TL | Total Lagrangian description of motion |
| UL | Updated Lagrangian description of motion |

# Chapter 1. General Introduction

## 1.1 Background

In recent years the requirements for fast marine transportation and fast deployment capabilities, for commercial and naval vessels respectively, have led designers of High-Speed Craft (HSC) [1] to push their creations to the very edge of their operational limits.

Since the structural failure of a HSC could have fatal consequences for the crew and passengers; generate major economical losses for ship-owners/operators; and seriously damage the reputation of the designer/shipbuilder, it is fundamental to ensure that the structure will be safe, i.e. that it would not fail under the prescribed design loads. This is not a simple task since HSC need to resist extreme loadings caused by higher operational speeds, such as slamming, which are yet to be fully understood (Thomas, 2003).

In addition to being safe, the vessel must be as efficient as possible. According to Molland (2008), the efficiency of a HSC can be gauged using the transport efficiency factor, which is the ratio of the product of payload and speed to the total installed power. From this definition it can be easily appreciated that an increment of the payload would increase the overall efficiency of the vessel.

A common way to achieve an increment in payload is to reduce the weight of the structure. However, a reduction in structural weight is normally linked to a reduction in scantlings that could lead to an unwanted reduction in structural safety, and/or to the use of exotic materials which could be expensive. Designers are hence forced to

[1] A high-speed craft is, as defined by International Maritime Organization (IMO), a craft capable of a maximum speed, in meters per second, equal or exceeding $3.7\nabla^{0.1667}$, where $\nabla$ is the volume of displacement corresponding to the design waterline in cubic metres.

find an optimum structure that efficiently balances strength, cost, and weight requirements without sacrificing safety.

Since traditional structural design methods, i.e. empirical rules, cannot distinguish between structural adequacy and over-adequacy, the search for this optimum configuration in HSC is normally conducted using a rational-based approach (Hughes, 1988) where the design is directly and entirely based on structural theory and computer based methods of structural analysis, and which obtains an optimum structure on the basis of a designer-selected measure of merit.

Until recently the numerical models used by marine structural designers for the rational-based structural analysis of marine structures have been mainly linear, i.e. based on the assumption that deflections of the structure remain small, i.e. less than half the thickness of the panel skin in magnitude.

However, due to the lower stiffness of the materials used in HSC, the geometrically non-linear behaviour of laterally loaded panels is significant even at low load levels (Moy *et al.*, 1996, Bau-Madsen *et al.*, 1993) and consequently, a linear analysis may lead to under/overestimates of the displacement levels resulting in the design of under/overdesigned, structures.

Moreover, it is now common for designers of HSC to conduct an ultimate failure analysis of the ship's hull girder in order to determine a safe operational limit for the vessel structure (Chen *et al.*, 2003, Chen and Guedes Soares, 2007). This type of analysis requires an understanding of both the pre and post-buckling behaviour of the structure. The post-buckling behaviour of a stiffened panel is a highly non-linear problem that a linear finite element model will be unable to analyse.

Finally, the search for an optimum structure is a very resource intensive process, as it involves repetitive calculations coupled to changes to the structural configuration parameters, i.e. stiffener orientation, eccentricity, spacing, and cross sectional dimensions. Consequently, if the analysis tool is computationally inefficient, every calculation will slow down the optimization process. The optimization process could be further delayed if the analysis tool lacks in modelling flexibility, as every iterative change in the structural arrangement could become an extremely laborious and tedious task for the designer.

Summarizing, the design of an optimal HSC structure is a complex balancing act. The complexity of the non-linear structural problem in hand, combined with the iterative nature of the calculations required in the design process of a HSC, creates the necessity for an efficient numerical modelling technique that reduces both the computational processing time, as well as the time required to generate and/or modify the structural configuration in the numerical model.

## 1.2 Problem definition

The structure of a HSC can be idealized as a thin-walled box girder (or girders in the case of a multihull). The walls of this box girder usually consist of a combination of flat and curved unstiffened and stiffened panels.

Structural engineers define an unstiffened panel as a monocoque structure. The word monocoque results from the combination of *coque*, which is the French word for the shell of a shellfish (as well as the word for ship hull), and *mono*, a Greek word which in this context specifies that the skin is the sole contributor to the overall stiffness and strength of the panel. Therefore a monocoque can be understood as a structure where only the skin contributes to the overall stiffness of the panel.

If the load is increased, the skin may be thickened in order to provide additional strength and stiffness. However, by increasing the skin thickness such a design will not be efficient in respect to the weight of material used.

A stiffened panel on the other hand is defined by structural engineers as a semi-monocoque (Figure 1-1).

Here the addition of the Greek work *semi* specifies that the skin is not the single contributor to the overall strength and stiffness of the panel, since this configuration uses an internal framework to increase the overall bending stiffness of the panel.

Normally, the stiffening members are arranged in an orthogonal grid-like pattern. However, in particular cases such as stern and bow panels of a ship hull, stiffeners are also placed at arbitrary orientations within the panel boundaries (Brubak *et al.*, 2007).

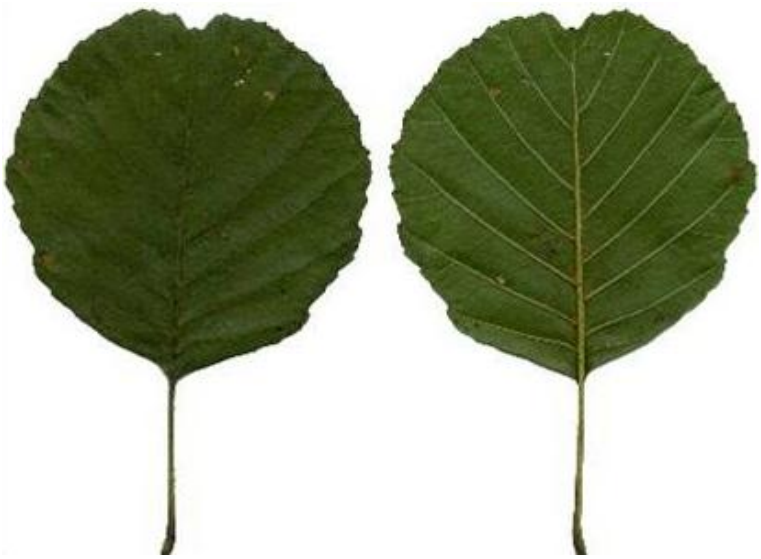

**Figure 1-1 Nature's example of a semi-monocoque structure.**

The members of the framework, known as stiffeners, add negligible weight to the overall structure compared to their large influence on strength and stability of the panel (Bedair, 1998).

Stiffened panels can exhibit a variety of failure modes, some overall and some local in nature. The quantitative and qualitative assessment of these failure modes is crucial to the understanding of the overall structural response of a HSC.

As the optimum preliminary sizing of structural components at the conceptual design phase of new structures requires a large number of structural optimizations, and considering the fact that computational time and resources in the preliminary are limited, the use of detailed finite element models as part of this rational-based optimization of stiffened structures is not affordable (Lamberti *et al.*, 2003).

Designers are forced to reach a compromise between the complexity in the structural analysis model, e.g. local models instead of a global model and/or linearised analysis instead of non-linear analysis, and that of the optimization method (local versus global optimization). When designing new concepts where good initial designs are not available, design optimization needs to be performed, and this is not currently possible with complex models.

The structural problem is further complicated in the analysis of HSC where materials with high strength-to-weight ratio such as aluminium alloys and, more recently, composite materials are normally used to save weight.

Composites made of Fibre-Reinforced Plastics (FRP) are often superior to steel and aluminium as building material for HSC due to their high stiffness-to-weight ratio and corrosion resistance. Nevertheless, poor fabrication quality, and high cost added to perceived lack of high-quality, initially limited the application of FRP composite to a few non-critical ship structures and small boats.

However, it has been reported (Mouritz *et al.*, 2001) that, since the mid-1980s, the overall length of FRP ships has increased steadily and that currently composite ships of up to 80-90 m long are being constructed or have already been built. This development has been driven by the need to enhance the operational performance (e.g increased range, stealth characteristics, stability, payload) but at the same time reduce the ownership cost of surface and submarine vessels, through better manufacturing processes and lower material costs.

Mouritz *et al.* (2001) suggest that, if the trend continues, hulls for mid-size warships, such as frigates that are typically 120-160 m long, may be constructed from FRP composites from about 2020. This hypothetical trend is already a reality in the aerospace industry where the new Boeing 787 will soon become the first airliner with a composite only fuselage.

**Figure 1-2 FRP composite fuselage of the Boeing 787 (Boffoli 2007).**

According to Mouritz *et al.* (2001), this progressive change could be accelerated if simple to use models for optimising the design of large, complex load-bearing naval structures become available.

Such models are of special importance in the preliminary design of composite structures given that the scaling laws for composites are complex due to their anisotropic properties, making the modification of existing load-bearing structure designs more difficult than with metals.

Furthermore, although experimental testing of composite structures is still necessary to validate the results of analytical and numerical models, extensive testing of composite structural components is extremely expensive and therefore unviable. A cost effective structural analysis tool, capable of evaluating the performance of composite structures, would be a significant aid in reducing the number of required experimental tests (Tay *et al.*, 2008).

## 1.3 Scope of work

Clearly, it is vital that the HSC is not operated outside the structural design envelope. In order to calculate an optimum design envelope, an iterative structural design process has to be conducted. This design process should be as accurate and fast as economically practicable.

Consequently, in this investigation, a non-linear analysis tool was developed to introduce and evaluate quick design modifications, which allows designers to conduct a streamlined and iterative design process efficiently.

The requirements of this tool, and at the same time the goals in this investigation, are:

1. The tool must be able to quickly evaluate the performance of unstiffened and stiffened panels, with a preliminary design level of accuracy and with minimum modelling cost.

2. The tool must be capable of performing non-linear calculations for panels made from metallic and composite materials accurately and efficiently.

3. The tool must be able to modify the parameters that define the panel configuration, i.e. stiffener spacing, orientation, cross section and eccentricity, quickly to allow a thorough exploration of the design space.

4. The position of the stiffener(s) within the panel must not impose any kind of topological restrictions that may affect the efficiency of the modelling tool.

5. The tool must be capable of representing not only the behaviour of stiffened and unstiffened panels under the action of transverse loads, but also under the action of in-plane compressive loads.

6. In order to model the non-linear compressive behaviour, the tool must include initial deformations of the unstiffened and stiffened panels

## 1.4 Thesis outline

The investigation conducted to develop and validate the analysis tool described in the previous Section is reported in the present thesis. The thesis is comprised of 7 chapters in total:

- Chapters 1 and 2 mainly consist of an introduction to the problem in hand and provide a detailed literature review of the available modelling techniques and existing work in the field of non-linear structural analysis of stiffened panels, with special attention to the developments of arbitrarily orientated stiffened finite element formulations.

- Chapter 3 contains an extensive and detailed description of the mathematical formulation implemented in this investigation, for the non-linear analysis of stiffened panels using arbitrarily stiffened elements. The chapter includes a description of the theories used in the formulation of both the shallow shell master element as well as the Timoshenko beam slave element.

- Chapter 4 discusses the procedures used to formulate and solve the non-linear equations of the stiffened element. This chapter includes the discussion of a new method used to account for the effects of in-plane loads in arbitrarily

stiffened panels, as well as a description of the technique used to calculate and incorporate initial deformations into the stiffened panel models.

- In Chapter 5 the performance of the stiffened element in representing the non-linear behaviour of stiffened panels under transverse loads is validated against experimental and numerical data available in the open literature and data obtained using the general purpose finite element package ANSYS.

- Similarly, in Chapter 6 the performance of the stiffened element in representing the non-linear behaviour of stiffened panels under in-plane loads is validated against experimental and numerical data available in the open literature and data obtained using the general purpose finite element package ANSYS. Furthermore, the effects of the in-plane load modelling technique suggested in chapter 4 are discussed and validated.

- Finally, Chapter 7 provides a summary of the investigation and the overall conclusions arising from the current research. Recommendations for further research based on the present study are also presented in this chapter.

# Chapter 2. Literature Review

## 2.1 Introduction

The goal of this chapter is to establish an overview of available techniques for modelling the non-linear behaviour of stiffened structures with a design stage level of accuracy. The purpose of this is to provide an extensive basis for choosing the best approach to formulate an element which meets the aims of the present study described in Section 1.3.

Although progress in the analysis of stiffened structures has been reported in the past by several authors (Satsangi and Mukhopadhyay, 1989, Mukhopadhyay and Mukherjee, 1989, Sinha and Mukhopadhyay, 1995, Mukhopadhyay and Sinha, 1992, Norwood, 1995), these reviews were focused mainly on the linear response of such structures. Consequently, as part of the present investigation, a literature review focusing on the non-linear response of stiffened structures was conducted and published to highlight the advances and the state-of-the-art in the field (Ojeda *et al.*, 2008). The most relevant outcomes of that review are presented in this Chapter to guide the selection of the most suitable modelling tool.

The cited references were selected to illustrate the variety of models being used in the broad area of stiffened structural analysis and are not necessarily the only significant contribution on the subject. The discussion is kept to a descriptive level, and for all the mathematical details, the reader is advised to refer to the cited literature. Undoubtedly, a survey of this type will not do justice to all the contributions for which the author apologizes.

## 2.2 Stiffened panel modelling approaches

A variety of methods are available for the non-linear analysis of stiffened panels, ranging from simple closed form solutions to complicated three dimensional discretised solutions.

The analysis cost typically increases with the level of detail modelled and the fidelity of the analysis procedure used (Lamberti *et al.*, 2003). The most common analysis models or methods are as follows:

1. Analytical and semi-analytical methods;
2. Finite strip method;
3. Finite element method.

### 2.2.1 Analytical and semi-analytical method

The simplest approach to analyse stiffened structures is to use an analytical model in which the structure is converted to an equivalent plate/shell with constant thickness by smearing out the stiffeners. The model is suitable for obtaining load paths, stiffness constraints and overall or general buckling load estimates. However, these models cannot be used for stress calculations or to capture local and stiffener buckling failures. Moreover further difficulties appear when using this approach if the stiffeners are not identical in both directions since the resulting thickness becomes non-uniform.

The "smeared stiffener" approach was used by Shen (1998) for the post-buckling analysis of imperfect stiffened laminated cylindrical shells under combined external pressure and thermal loading. The author used a boundary layer theory of shell buckling which includes the effects of non-linear pre-buckling deformations, non-linear large deflections in the post-buckling range and initial deformations of the shell.

Nonetheless the "smeared approach" fails to capture the local effects of the stiffeners, thereby making it unsuitable to study the response of stiffened panels, where the stiffeners are spaced unevenly or are of different cross section; hence the applicability of the "smeared" approach is very much restricted.

Recently, and in order to overcome these difficulties, Steen *et al.* (Steen and Byklum, 2005, Steen *et al.*, 2004b, Steen *et al.*, 2001, Steen *et al.*, 2004a) have proposed three semi-analytical models to study the post-buckling ultimate strength of stiffened panels:

an unstiffened model, an orthogonally stiffened model and an arbitrary stiffened model. These models can be classified as semi-analytical in the sense that they are based on the recognised plate theory of Marguerre (1938) in combination with numerical techniques for solution of governing differential equations. Both the unstiffened and the orthogonally stiffened models are capable of assessing post-buckling strength whereas the arbitrary orientated stiffened model is limited only to linear analyses. Furthermore, none of these models are capable of analysing composite laminated panels.

### 2.2.2 **Finite strip method**

The finite strip method was devised for structural analysis in the late 1960's (Cheung and Tham, 1998). This method treats the stiffened panels as an assemblage of plates or shells. For each component in the assemblage, the field equations are solved and boundary conditions at the interfaces are matched between adjoining members. The field equations for each component can be solved exactly or approximately using assumed displacements.

The finite strip method is suitable for the analysis of stiffened panels manufactured from layered composite materials. Loughlan (1994) and Loughlan and Delaunoy (1993) used the finite strip method to study the effects of fibre orientation on the buckling of composite stiffened plates. A multi-term finite strip approach was required to predict the complex buckling behaviour of composite stiffened panels under shear loads. The method was later extended by Loughlan (1996) for the buckling analysis of composite box sections. In both cases only structures reinforced with stiffeners running parallel with the direction of the strips where considered.

The conventional finite strip method allows different segments to have different properties, but does not allow variations of thickness or properties in each segment. This restricts the models to have length-wise or breadth-wise uniform properties. Local details (e.g. cutouts, localized loads) are difficult to model.

The spline finite strip method was developed to overcome some of the limitations of the conventional finite strip method by adopting a cubic B-spline function to improve the interpolation in the direction of the strip.

This approach has been proven suitable for the vibration (Wang and Dawe, 1997), buckling (Wang and Dawe, 1997, Dawe, 2002), and transient (Dawe, 2002) analyses of

prismatically stiffened composite plates as well as for the vibration and buckling analysis of stiffened sandwich plates (Yuan and Dawe, 2004).

An example of the application of this spline finite strip method to the study of stiffened plates is the work of Sheikh and Mukhopadhyay (Sheikh and Mukhopadhyay, 2002, Sheikh and Mukhopadhyay, 2000). The authors extended the analysis capabilities of their previously developed linear formulation (Sheikh and Mukhopadhyay, 1993, Sheikh and Mukhopadhyay, 1992) to perform large deflection and non-linear transient vibration analysis of stiffened plates. The main advantage of the formulation lies in the treatment of the stiffeners which does not need to be placed along the edges of the strips. However, the main limitation of this approach is that the stiffener ends have to pass through two opposite edges of the strips.

### 2.2.3 **Finite element method**

The finite element method (Zienkiewicz and Taylor, 1994) involves replacing the panel domain with a discrete number of interpolation regions (elements) of known stiffness. The versatility of this method relies on its ability to cater for arbitrary geometry, material anisotropy, ease of formulation as well as its ability to include a wide range of boundary conditions and loads (Prusty, 2001b).

Since its first introduction to the analysis of ship structures by Paulling (1964), the finite element method has become established as the standard tool for the analysis of ship structures (Thomas, 2003).

Although the finite element method is considered to be one of the most accurate and versatile techniques available, a careful selection of the modelling approach is paramount to perform efficient analyses, as an inappropriate model can use large amounts of computer storage as well as modelling and processing time (Sheikh and Mukhopadhyay, 2002).

The most detailed finite element models available are those that use three dimensional elements, also known as solid elements, to represent the complete structural domain of the panel. These models are generated by dividing (meshing) the stiffened panel domain into a series of small tetrahedral and/or hexahedra interpolation regions or elements.

Although being the most detailed discretisation technique available, three dimensional finite element models of stiffened panels are used in few particular applications.

One of these applications is the analysis of thermal induced deformations created by welding. Camilleri *et al.*, (2005) used highly detailed finite element models, created in the general purpose finite element code ANSYS with the eight node hexahedra element SOLID 45, to optimize the welding scheme with respect to minimum out-of-plane deformation in orthogonally stiffened panels. In this analysis three dimensional elements were used to describe in detail the state of stress surrounding the zone affected by welding in order to predict the thermal distortions accurately.

Another area of application of three dimensional finite element models is the field of fracture mechanics, where highly detailed three dimensional finite element models are normally used to track the progression of failure. An example of such application are the failure predictions for rib-stiffened panels presented by Key *et al.* (2004). These authors used ABAQUS eight node hexahedra elements, augmented with the multi-continuum technology progressive failure model, to predict and analyse the separation of the stiffener from the skin at the interface. Again, this problem required a highly detailed description of the state of stress at the skin-stiffener interface for an accurate prediction of the progression of failure.

The main reason for the limited application of three dimensional models in the analysis of stiffened panels, is that these elements are considered wasteful and problematic (Cook, 1995). They are considered wasteful as they compute the transverse normal stress which is negligible in such a thin structure and, more importantly, they are considered problematic as three dimensional element models are normally much harder to prepare, tedious to check for errors, and most importantly, the higly demanding of computer resources.

Indeed, in order to control the shape and quality of the mesh, the domain topology, normally defined using Computer Aided Design (CAD) software, must be divided as shown in Figure 2-1. Such divisions increase the complexity of the model and force the user to perform tedious Boolean operations to subdivide the domain. Such operations might be cumbersome if multiple and/or non-uniformly shaped stiffeners were present in the model.

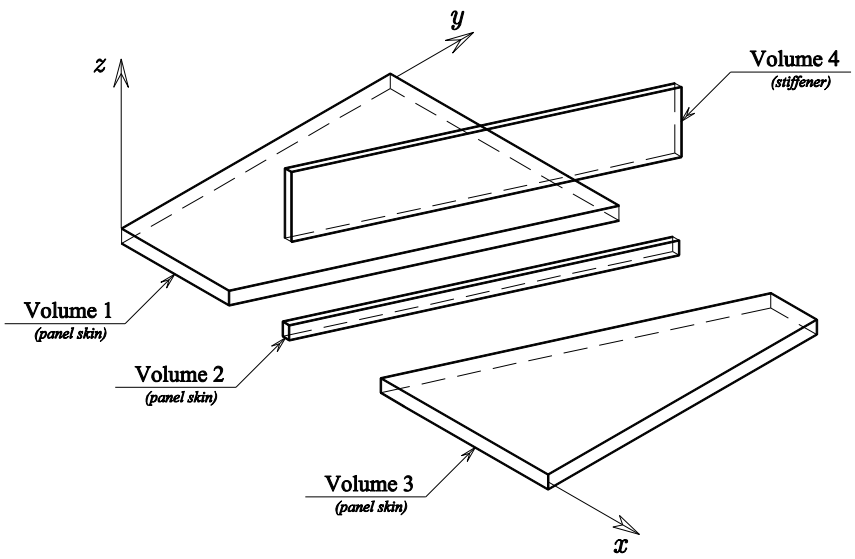


**Figure 2-1 Topology requirements for a three dimensional finite element mesh.**

In addition, Cook (1995) suggests that because of the dimensions of a stiffened panel, the three dimensional elements become distorted in modelling the thin panel skin and stiffener volumes. This, according to Cook, invites locking, which is an overly stiff representation of some of the deformation modes of the structure. The locking problem could be avoided by using a greater number of more compact elements. However, this would increase the total number of degrees of freedom of the structure, which in turn would make the solution numerically inefficient.

A better option for generating a model of a stiffened panel using finite elements is to represent the panel domain using two dimensional elements. Two dimensional elements are obtained by collapsing a three dimensional element in the thickness direction and by omitting the transverse normal stress in their formulation. Two dimensional elements can be quadrilateral or triangular in shape, with a quadrilateral element mesh yielding usually more accurate results than a mesh of similar density based on triangular elements.

Consequently, such elements required only the definition of a two dimensional domain (surface), which is normally divided, in order to control the shape and quality of the mesh, as illustrated in Figure 2-2.

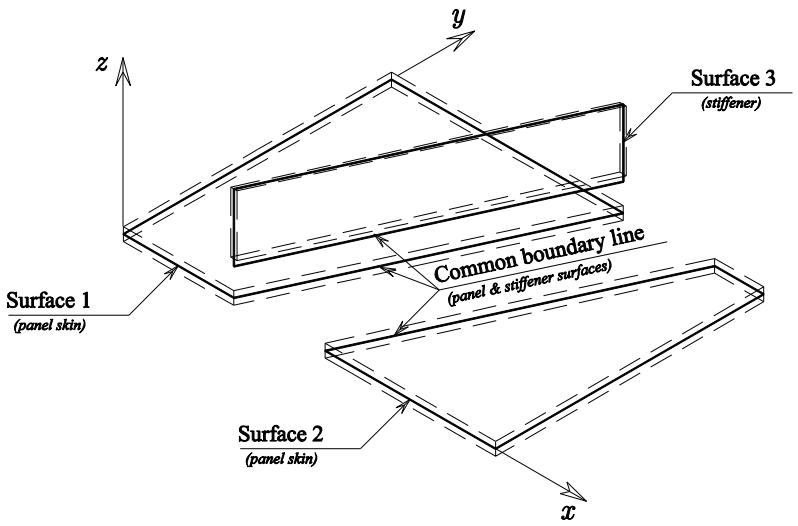


**Figure 2-2 Topology requirements for a two dimensional finite element mesh.**

It is important to note that, in this division, a line that is common to all three areas must exist in order to ensure that the panel and stiffener behaves as a semi-monocoque structure.

An example of the application of two dimensional finite elements to the analysis of stiffened structures is the investigation reported by Chen and Guedes Soares (2007, 2008) on the longitudinal strength of composite ship hulls. In this investigation, the hull girder was idealized as an assembly of stiffened composite panels modelled using degenerated laminated composite shell elements for both the panel skin and the stiffener. Using a progressive failure algorithm, the ultimate strength of each stiffened panel was predicted by nonlinear finite element analysis. Based on the individual panel failure results, the longitudinal strength of the ship's hull girder was estimated using an iterative method similar to that suggested by Gordo *et al.* (1996).

More recently, and also using two dimensional finite elements, the post-buckling behaviour and strength of multi-stiffened aluminium panels under combined axial compression and lateral pressure was investigated by Khedmati *et al.* (2010).

In that investigation, a finite element model, previously generated by Rigo *et al.* (Rigo *et al.*, 2003) using the general purpose finite element package ANSYS, was used to

study the influence of both initial deflections and the heat affected zone on the post-buckling behaviour and collapse characteristics of aluminium stiffened panels under combined axial compression and lateral pressure.

Nevertheless, although stiffened panel model generated using two dimensional elements are more computationally efficient than those generated using three dimensional elements, a large number of equations are still required to discretise the stiffener domain. Furthermore, in such models the user is still required to perform Boolean operations to obtain a domain topology that is suitable for a two dimensional element mesh.

The inefficiency of idealising stiffened structures with only three or two dimensional finite elements has led researchers to search for more computationally efficient models. A more efficient way of representing a stiffened panel, using the finite element method, is to combine two different types of elements in the same model. This is normally achieved by combining two dimensional (plate/shells) and one-dimensional (beam) elements as shown in Figure 2-3. Here, two dimensional elements are used to discretise the skin of the panel (Surface 1 and Surface 2) whilst the one-dimensional elements are used to discretise the stiffener (along the common line).

An admissible, combined model demands compatible displacements fields for both the beam and the shell elements. Therefore, the interpolation functions approximating the displacement fields in beams must be the same as the ones approximating the corresponding displacement field in the shell elements. This approach, known as the discrete stiffener approach, was used by Liao & Reddy (1990) to present a degenerated continuum-based, laminated, isoparametric, stiffened shell element in conjunction with a degenerated, isoparametric beam element to investigate the static, geometric, non-linear response of composite stiffened shells.

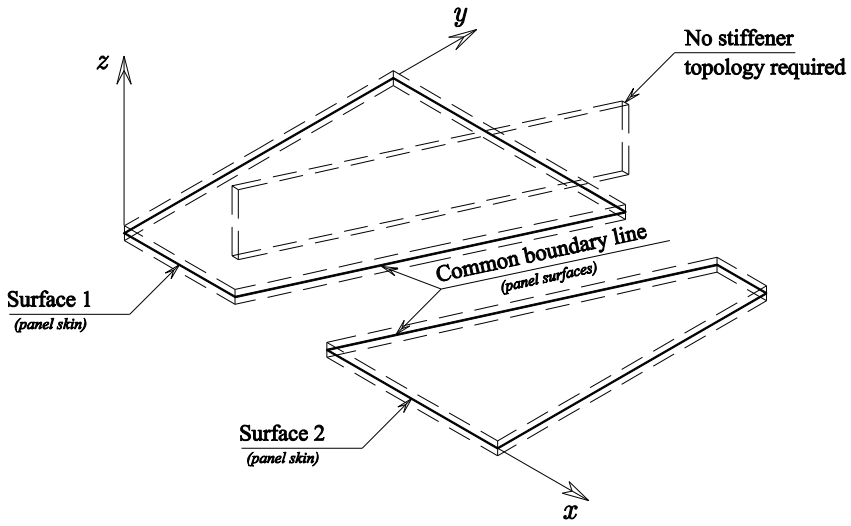


**Figure 2-3 Topology requirements for a discretely stiffened finite element mesh.**

The degenerated shell and beam elements were obtained by imposing appropriate kinematic constraints on the three dimensional isoparametric solid element as presented by Bathe & Bolourchi (1980). Similarly, Qun *et al.* (1999) used the discrete stiffener approach to develop a finite element program for the static analysis of concentrically stiffened isotropic plates and shells with large deflection and rotations. A generalized conforming triangular flat shell element with drilling degrees of freedom and the three dimensional beam element with Hermite interpolation was used to represent the stiffened structure.

The discrete stiffener approach has not been limited to the global analysis of stiffened shells. The local behaviour of discretely stiffened laminated composite cylindrical shells has been investigated by Kassegne & Reddy (1998). The layer-wise theory (Reddy, 1987) was used to model the composite laminate. The layer-wise model is essentially a 3D model in a 2D format, where the 3D displacement field is expanded as a function of a surface wise 2D displacement field and a one-dimensional interpolation through the thickness. Hence it is capable of representing the local layer behaviour. The authors acknowledged that the discrete layer-wise model might be too expensive computationally for shells with a large number of stiffeners.

Koko & Olson (1991a) used a super-element approach for the large deflection elasto-plastic analysis of orthogonally stiffened plates. The super-elements are designed to contain all the basic modes of deformation so that only one plate element per bay and one beam element per span are needed to analyse a stiffened structure, therefore reducing the storage requirement and solution times. The authors further extended the proposed method for the non-linear modal and transient analyses of stiffened plates (Koko and Olson, 1991b, 1992). Later, and inspired by the satisfactory performance of the super-elements for the non-linear analysis stiffened plates, Jiang & Olson (1994) further developed this approach to study the non-linear behaviour of stiffened shells. The proposed method was limited to the study of isotropic rectangular plates and shells, stiffened in mutually perpendicular directions. Hence, and similar to the discrete stiffener approach, this particular super-element approach is restricted by the condition that the stiffeners must pass through the edges of the super-element.

Another interesting approach was reported by Günay (1999). The author presented a geometrically non-linear finite element analysis of laminated stiffened cylindrical shallow shells using composite shallow shell elements with stringer-type stiffeners. In his analysis, a two sided meshing system was generated to represent cylindrical shell with stiffeners in a three dimensional co-ordinate system. No attempts were made to model stiffeners of various shapes and/or having arbitrary orientation in the plate/shell panel.

A significant disadvantage of the discretely stiffened models discussed so far is that the orientation of the stiffeners is restricted by the mesh, because the beam and shell elements are connected to each other at their nodal points. Therefore, a beam element can be placed only along the boundaries of the areas of the panel.

Consequently, the distribution of stiffeners modelled by beam elements has a very restrictive influence on the meshing of the skin, which may be very inefficient, especially when repeated analyses are to be performed to estimate the optimum spacing and orientation of stiffeners in a panel.

An optimal combined model should involve the placement of the beam element within the plate or shell element at an arbitrary orientation (Barut *et al.*, 2000), as shown in Figure 2-4.

This requires the definition of the displacement fields at any point within a slave element (beam element) in terms of the field variables of a master element (plate or shell element). Since the beam kinematic field is described by the shell kinematic field, only the master plates or shells are needed to discretise the entire stiffened shell structure. Thus eliminating the modelling difficulties attributed to the conventional beam-plate and beam-shell models.

This approach is referred to as the arbitrary-orientated stiffener approach and has been widely applied for more than two decades to the linear analysis of stiffened plates (Ray and Satsangi, 1996, Ray and Satsangi, 1999, Kumar and Mukhopadhyay, 2002, Kumar *et al.*, 2002, Kumar and Srivastava, 2003, Satsangi and Ray, 1998, Chattopadhyay *et al.*, 1993, Barik and Mukhopadhyay, 2002, Palani *et al.*, 1993, Palani *et al.*, 1992, Kumar and Mukhopadhyay, 2000b, Thompson *et al.*, 1988, Mukherjee and Chattopadhyay, 1994, Chattopadhyay *et al.*, 1992, Mukhopadhyay, 1981) and stiffened shells (Samanta and Mukhopadhyay, 1998, Prusty, 2001b, Nayak and Bandyopadhyay, 2002, Prusty, 2001a, Prusty and Satsangi, 2001b, Prusty and Satsangi, 2001a, Prusty, 2003, Prusty *et al.*, 2001a, Prusty *et al.*, 2001b).

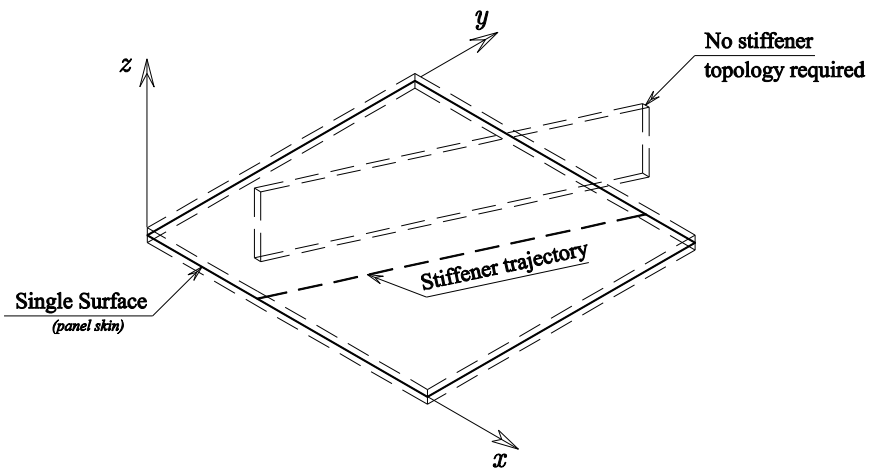


**Figure 2-4 Topology requirements for a arbitrarily stiffened finite element mesh.**

An excellent example of the application of the arbitrarily-orientated stiffener to the analysis of ship structures is the computer program Advance Ship Structural Analysis (ASSA) developed by Kumar and Mukhopadhyay (Kumar and Mukhopadhyay, 2002, Kumar *et al.*, 2002, Kumar and Mukhopadhyay, 2000a) for the global linear structural analysis of ship hulls. This program uses a 3 node Allman-discrete Kirchhoff-Mindlin stiffened plate element to represent isotropic and composite stiffened panels without the restriction of having to align the mesh with the trajectories of the stiffeners. It has been reported (Kumar and Mukhopadhyay, 2002) that a reduction of nearly 50% in the total number of degrees of freedom, for the same level of accuracy, of a generic ship model was achieved by using this stiffened element instead of a conventional discretely stiffened model.

However, the vast majority of the reported formulations are limited to linear analysis. In fact the reported work on the application of the arbitrarily-orientated stiffener approach to the large deflection analysis of stiffened plates and shells is scarce.

The first application was reported by Rao *et al.* (1993). The authors presented the finite element static analysis of the large deflection response of isotropic stiffened plates using an isoparametric quadratic stiffened plate bending element. The stiffened element was a development of the linear formulation presented by Mukhopadhyay *et al.* (1984). The authors excluded the contribution of the stiffener non-linearities in the formulation.

This effect was later included by Chattopadhyay *et al.* (1995). In this later work, the large deflections of laminated composite stiffened plates were analysed using an eight noded isoparametric element. The element formulation was based on Reissner-Mindlin's hypothesis with a total Lagrangian description of motion. In both works, the arbitrary orientated stiffener approach was applied so that the stiffener may lay within the element, with the limitation that the stiffener ends had to pass through two opposite edges of the element. The presented formulation was not capable of modelling stiffeners of arbitrary cross-section.

The arbitrary-orientated stiffener approach was also applied to the geometrically non-linear analysis of stiffened shells by Goswami and Mukhopadhyay (1995). Geometrically non-linear finite element static, modal and transient analyses of laminated composite stiffened shells were carried out using a nine noded Lagrangian curved shear flexible isoparametric stiffened element with five degrees of freedom per

node. Again the formulation accounts for arbitrarily orientated stiffeners with the limitation that stiffeners have to pass through two opposite edges of the element. Hence it is not possible to model stiffeners that are required to pass through two adjacent edges of the shell element. Additionally, the formulation is restricted to the analysis of shallow shells.

In view of this restriction, Samanta and Mukhopadhyay (1999) presented a formulation for the large deflections of deep isotropic stiffened shells. The analysis was conducted using a combination of Allman's plane stress triangle and the discrete Kirchhoff triangle plate bending element which was previously used (Samanta and Mukhopadhyay, 1998, Samanta and Mukhopadhyay, 2004) by the authors to analyse the small deflections of stiffened plates and shells. The proposed formulation was limited to thin, isotropic plates and shells reinforced with stiffeners of rectangular cross-section only.

Ray and Satsangi (1998) presented an arbitrary orientated finite element formulation for the geometrically non-linear analysis of laminated hat-stiffened plates. The stiffened panel was discretised using eight node plate and three node beam isoparametric elements derived previously for the linear analysis of hat-stiffened composite plates (Ray and Satsangi, 1996). Although the authors suggested that the stiffener can be incorporated at any arbitrary orientation within the plate element, no validation work was presented to support their claim.

As part of the present investigation, and in the absence of knowledge of the earlier work by Ray and Satsangi, Ojeda *et al.* (2007) conducted a similar investigation which demonstrated, through numerical validation, that the arbitrarily orientated stiffened approach was indeed capable of representing truly arbitrarily orientated stiffened panels.

More recently, Barut *et al.* (2000) presented a stiffened shell element formulation for the geometric non-linear analysis of composite laminated stiffened shells. It is a four node, triangular, $C^0$ anisoparametric element with five degrees of freedom at the corner nodes and two degrees of freedom at the centre node. The formulation accounts for transverse shear deformation and material anisotropy in both the shell and stiffener. The laminated stiffeners may be arbitrary in orientation and cross section. Whilst the element is capable of taking large deflections and rotations into account, the presented

formulation has not been proven to be capable of solving deep shell examples. Although the study discusses the incorporation of arbitrarily shaped and arbitrarily orientated stiffeners, only one example for a laminated cross-ply stiffened shell with rectangular stiffeners was covered.

It can be seen that the reported work has focused on studying the non-linear response of stiffened plates and shells under transverse loads. However, deck, side and bottom panels of a ship hull are not only subjected to the action of transverse loads, but also subjected to the action of large in-plane forces which may induce stability failure.

The classical approach to elastic stability analysis, also known as bifurcation buckling analysis, involves the linearization of the pre-buckling state, which leads to an Eigen-value problem to obtain the buckling load parameter (Eigen-value) and the buckling mode shape (Eigen-vector).

In order to study the bifurcation buckling behaviour of stiffened panels authors have used the arbitrary orientated stiffener approach to determine the linear buckling loads. The first work reported on this area was presented by Mukhopadhyay and Mukherjee (1990). The authors used an eight-node isoparametric stiffened plate element, previously developed to solve stiffened plate bending problems (Mukhopadhyay *et al.*, 1990, Mukhopadhyay and Satsangi, 1984), to calculate the buckling load parameter of isotropic flat stiffened panels.

Later, and in order to avoid shear locking, a phenomenon usually encountered in earlier isoparametric elements, Kumar and Mukhopadhyay (1999) presented a stiffened element for buckling analysis of laminated stiffened plates based on the combination of Allman's plane stress triangular element and a discrete Kirchhoff-Mindlin plate bending element. The element was used to calculate the linear buckling loads of composite stiffened plates under uni-axial and shear edge-loads.

Another approach to avoid shear locking was presented by Barik and Mukhopadhyay (2002), they presented a stiffened-plate bending element derived by combining the four-node rectangular plane-stress element having 8 degrees of freedom with the simplest rectangular plate-bending element having 12 degrees of freedom (commonly known as the ACM Element, after Adini, Clough and Melosh).

However, all these investigations assumed a uniform state of stress in the plate for the construction of the initial stress matrix, yielding a fast but very limited solution. Therefore this approach becomes unviable if either the panel edge loading is non-uniform or if the boundary conditions are not symmetric, as in these cases a non-uniform state of stress would need to be considered in the construction of the initial stress matrix.

A more general procedure requires the calculation of the state of stress, using a linear static solution, before the Eigenvalue buckling analysis in order to obtain the true stress distribution.

Srivastava *et al.* (2003) used this procedure to investigate the buckling response of isotropic stiffened plates subjected to partial edge loading, i.e. when the initial stresses are no longer uniform. In this investigation the authors conducted firstly a plane-stress static analysis in which the initial stress distribution due to the non-uniform loading was calculated followed by a bifurcation buckling analysis in which the buckling parameter due to the non-uniform stress distribution was obtained.

Although this study investigates the effect of concentrated and partially distributed loads on the edges of the panel, no attention was given to how the load acting on the stiffener cross section affects the in-plane behaviour of the stiffened element.

Moreover, although previous investigations using the arbitrarily orientated stiffener approach have reported on the effect of stiffener eccentricity on linear buckling, no author has reported on the modelling implication of stiffener edge loading in such configurations.

It must be noted that an eccentric stiffener couples the in-plane and bending behaviour of the panel. Therefore, if not modelled properly, a purely in-plane load on the edge of the panel creates a fictitious out-of-plane deformation. This deformation will generate bending stress and consequently will generate an incorrect state of stress in the plate yielding an incorrect value for the buckling load parameter. It is likely that this modelling issue has been overlooked since, as previously discussed, most authors have assumed a stress field and have not carried out a linear static calculation before the Eigen-value analysis.

The major drawback of all the Eigen-value buckling analyses discussed so far is that they completely neglect the effect of initial deformations in the panel. If a stiffened panel under the action of in-plane compressive forces has a finite initial deformation there is no longer distinct bifurcation buckling behaviour. Rather, the panel deforms in a continuous manner as the external loads are increased. This highly non-linear behaviour is especially important because the reserve capacity that exists after the initial panel deformation takes place (Byklum and Amdahl, 2002).

## 2.3 Conclusions

From the review, it can be seen that the arbitrarily stiffened element approach is the most efficient technique to generate finite element models of stiffened panels capable of producing results with a preliminary design level accuracy.

Although the large deflection of stiffened panels has been previously studied using arbitrarily orientated stiffened elements, all formulations fail to account for the initial deformations present in real structures. These deformations have a critical effect on the structural response of stiffened panels under the action of in-plane compressive loads.

Since the understanding of this behaviour is critical to produce an optimal design, there is a need for an effective and efficient analysis tool for the study of the complex structural non-linear response of arbitrary stiffened panels.

In this work a more general stiffened element formulation, capable of studying not only the large deflection under transverse loads but also the post-buckling of stiffened panels with initial deformations is developed based on Marguerre's (1938) shallow shell theory.

# Chapter 3. Finite Element Formulation

## 3.1 Introduction

As described in previous sections, an arbitrarily stiffened element consists of the combination of a master and a slave element as shown in Figure 3-1. Here, the skin of the panel is represented by the master elements, numbered using Roman numerals, whilst the stiffener is represented by the slave elements, numbered using Latin numerals.

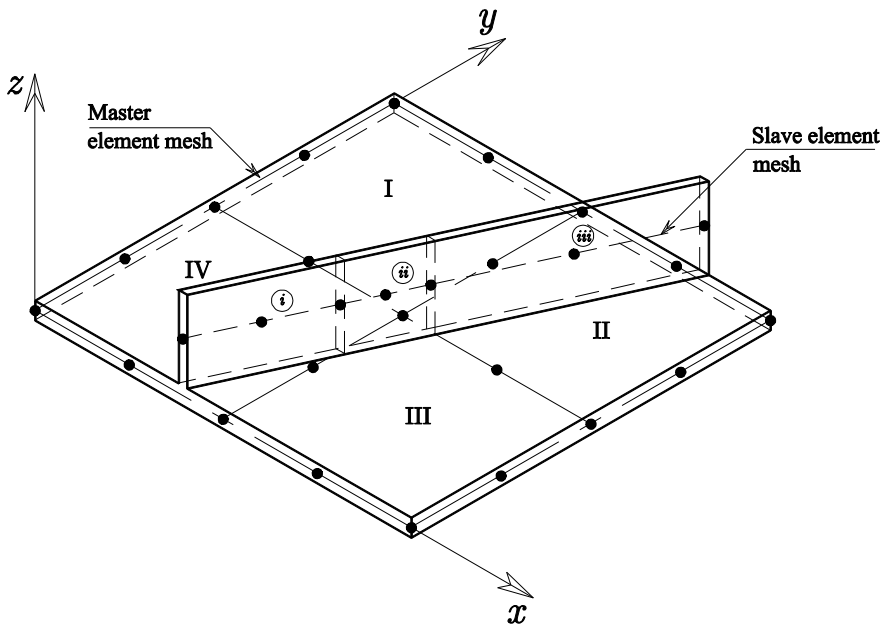


**Figure 3-1 Details of the finite element mesh of a stiffened panel using arbitrarily stiffened elements.**

The figure shows that in this model both stiffened and unstiffened elements are present. In the stiffened panel master elements II III and IV receive the stiffness contribution of the slave elements *iii*, *ii* and *i* respectively, whilst element I will remain unstiffened.

In the following sections the finite element expression for both the master and the slave elements is presented. The middle plane of the panel was selected as the reference plane of the master element. Both elements are combined using the assumption of equal displacements (Hughes and Davies, 1975, Hughes *et al.*, 1976) and rotations (Mukhopadhyay and Satsangi, 1984) at the slave-master element interface. This assumption requires that the cross section of the slave element and master element before deformation remain co-planar after deformation, i.e. the cross section of the beam element lies on the same plane as that of the shell element after deformation (Barut *et al.*, 2000).

In order to derive the kinematic description of the deformation of a continuous body it is required first to define a frame of reference. The two possible frames of reference in continuum mechanics are the Eulerian (spatial) and the Lagrangian (material) frames of reference.

In an Eulerian frame of reference the attention is focused on the motion of the material through a stationary control volume and it is therefore preferred for the analysis of fluid mechanics problems.

Unlike an Eulerian frame of reference, in a Lagrangian frame of reference we follow all particles of the body in their motion, from their original to final configuration and it is therefore preferred for the solution of solid mechanics problems and is consequently selected as the frame of reference in this work.

For a Lagrangian frame of reference, three possible kinematic descriptions of motion are currently in use in finite element programs that solve non-linear structural problems. They can be distinguished from each other by the choice of reference configuration.

The first and most popular is the Total Lagrangian (TL) description of motion. Here the reference configuration is seldom or never changed. Normally it is kept equal to the initial configuration throughout the analysis. Stresses and strains are measured with respect to this initial configuration.

The second description is the Updated Lagrangian (UL) description of motion, where the last target configuration, once reached, becomes the next reference configuration. Therefore stresses and strains are redefined once the reference configuration is updated.

This description is primarily used in treatments of very large strains and flow like behaviour

Finally, in the co-rotational (CR) description the reference configuration is divided. Stresses and strains are measured from the co-rotated configuration while the base configuration is maintained as reference for measuring rigid body motion.

Although the co-rotational description of motion is gaining popularity for some structural elements, the Total Lagrangian description of motion remains the most widely used in the formulation of continuum-based finite element and is therefore used in this work.

## 3.2 Formulation of the master element

In this Section the mathematical formulation of the master element is presented. The formulation uses an eight node isoparametric non-linear shallow shell element defined within a total Lagrangian frame of reference, based on a nine node Lagrangian element presented by Pica and Wood (1980).

The eight node element was selected since it is already available in the element library of almost every commercial finite element package which may facilitate the adoption of this formulation in existing programs. The shallow shell element is capable of modelling not only panels made of isotropic materials but laminated materials as well.

### 3.2.1 Displacement field in a shallow shell

In any three dimensional solid the displacement field varies in the three Cartesian directions. However a three dimensional approach to the description of the displacement field of a shallow shell is very complicated and inefficient (Cook, 1995).

Consequently, the three dimensional field description in thin-walled members, such as plates and shallow shells, is normally abandoned in favour of a simpler two-dimensional theories. In these theories it is assumed that the variation of the in-plane displacement along the thickness direction can be represented using kinematic hypotheses such as Kirchhoff's or Reissner-Mindlin's hypothesis (Reissner, 1945, Mindlin, 1951).

Kirchhoff's hypothesis postulates that the displacements can be described by assuming that a line that is straight and normal to the mid-surface before loading will remain straight and normal to the deformed mid-surface after a load has been applied. As a result of this assumption shear deformation is neglected, i.e. deformation is due entirely to bending and in-plane stretching. This limits the application of this hypothesis to the study of thin plates/shallow shells only.

Moreover, the use of Kirchhoff's hypothesis is a limiting factor in the study of composite laminated panels using equivalent single layer theories. In effect, as noted by Reddy and Robbins (1994), laminated panels have relatively low shear stiffness compared to the in-plane stiffness, and therefore experience large transverse shear strains, which an element based on Kirchhoff's hypothesis are incapable of represent.

In contrast to Kirchhoff's hypothesis, Reissner-Mindlin's hypothesis states that the plate normals remain straight but not necessarily normal to the deformed mid-surface after loading. Hence, this hypothesis allows shear deformation to take place and so expanding its application to the study of moderately thick plates and shells. Since the inclusion of transverse shear deformation has the advantage of providing a better representation of the behaviour of thick and/or composite shallow shells the Reissner-Mindlin's hypothesis was adopted in this work.

According to the Reissner-Mindlin's hypothesis, the three dimensional Cartesian displacement vector $\mathbf{u} = \left[u, v, w\right]^T$ of any material point within the panel $\mathbf{x} = x, y, z$ can be expressed using the generalised displacement vector $\hat{\mathbf{u}}$ presented in Equation 3.1

$$\hat{\mathbf{u}} = \begin{Bmatrix} \hat{u} \\ \hat{v} \\ \hat{w} \\ \theta_x \\ \theta_y \end{Bmatrix} \tag{3.1}$$

where $\hat{u}$, $\hat{v}$, $\hat{w}$ are the mid-surface translations and $\theta_x$, $\theta_y$ the mid-surface rotations defined in Figure 3-2.

For a shallow shell, i.e. an imperfect panel, the three dimensional components of the Cartesian displacement vector **u** at any point is expressed using Reissner-Mindlin hypothesis as

$$\begin{aligned} u &= \hat{u}(x,y) - z\theta_x(x,y) \\ v &= \hat{v}(x,y) - z\theta_y(x,y) \\ w &= \hat{w} = \hat{w}_0(x,y) + \hat{w}_1(x,y) \end{aligned} \qquad 3.2$$

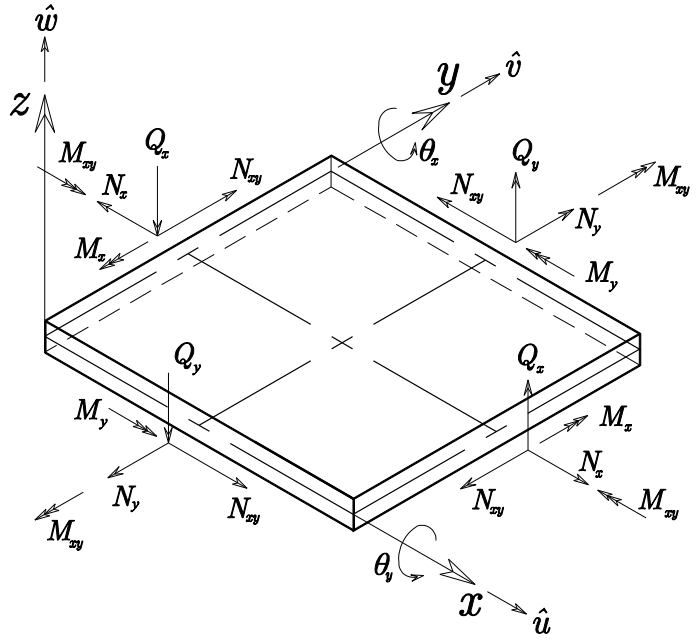


**Figure 3-2 Definition of the mid-surface quantities of the shallow shell.**

Here, $\hat{w}_0\ x,y$ is the stress-free, mid-surface deformation in the $z$ direction and $\hat{w}_1\ x,y$ is the net deformation in the $z$ direction. The total deformation in the $z$ direction, $\hat{w}$, is defined as shown in Figure 3-3.

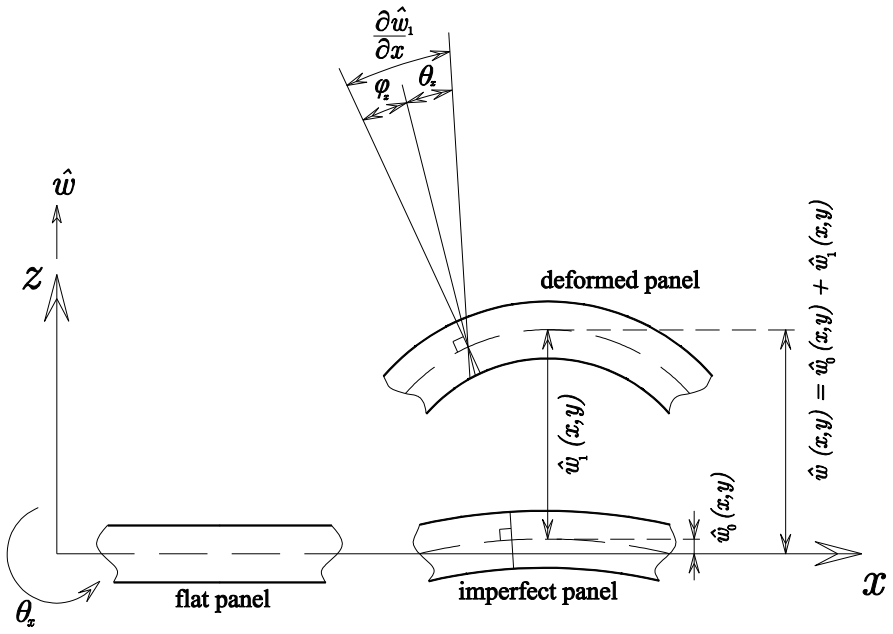


**Figure 3-3 Transverse deformations of the shallow shell.**

If the plate mid-surface of the panel is free from initial deformations, i.e. $\hat{w}_0 = 0$, Equation 3.2 becomes

$$\begin{aligned} u &= \hat{u}\ (x,y)\ - z\theta_x\ (x,y) \\ v &= \hat{v}\ (x,y)\ - z\theta_y\ (x,y) \\ w &= \hat{w}_1\ (x,y) \end{aligned} \qquad 3.3$$

Equation 3.3 describes the displacements of a perfectly flat panel.

### 3.2.2 Strain measure in a shallow shell

The six components of strain, in a solid undergoing large deformation, can be described using Green's strain vector as

$$\boldsymbol{\varepsilon} = \begin{Bmatrix} \varepsilon_x \\ \varepsilon_y \\ \varepsilon_z \\ \gamma_{xy} \\ \gamma_{xz} \\ \gamma_{yz} \end{Bmatrix} = \begin{bmatrix} \dfrac{\partial u}{\partial x} + \dfrac{1}{2}\left(\dfrac{\partial u}{\partial x}\right)^2 + \dfrac{1}{2}\left(\dfrac{\partial v}{\partial x}\right)^2 + \dfrac{1}{2}\left(\dfrac{\partial w}{\partial x}\right)^2 \\ \dfrac{\partial v}{\partial y} + \dfrac{1}{2}\left(\dfrac{\partial u}{\partial y}\right)^2 + \dfrac{1}{2}\left(\dfrac{\partial v}{\partial y}\right)^2 + \dfrac{1}{2}\left(\dfrac{\partial w}{\partial y}\right)^2 \\ \dfrac{\partial w}{\partial z} + \dfrac{1}{2}\left(\dfrac{\partial u}{\partial z}\right)^2 + \dfrac{1}{2}\left(\dfrac{\partial v}{\partial z}\right)^2 + \dfrac{1}{2}\left(\dfrac{\partial w}{\partial z}\right)^2 \\ \dfrac{\partial u}{\partial y} + \dfrac{\partial v}{\partial x} + \dfrac{\partial u}{\partial x}\dfrac{\partial u}{\partial y} + \dfrac{\partial v}{\partial x}\dfrac{\partial v}{\partial y} + \dfrac{\partial w}{\partial x}\dfrac{\partial w}{\partial y} \\ \dfrac{\partial u}{\partial z} + \dfrac{\partial w}{\partial x} + \dfrac{\partial u}{\partial x}\dfrac{\partial u}{\partial z} + \dfrac{\partial v}{\partial x}\dfrac{\partial v}{\partial z} + \dfrac{\partial w}{\partial x}\dfrac{\partial w}{\partial z} \\ \dfrac{\partial v}{\partial z} + \dfrac{\partial w}{\partial y} + \dfrac{\partial u}{\partial y}\dfrac{\partial u}{\partial z} + \dfrac{\partial v}{\partial y}\dfrac{\partial v}{\partial z} + \dfrac{\partial w}{\partial y}\dfrac{\partial w}{\partial z} \end{bmatrix} \tag{3.4}$$

However, since the thickness of the panel is small compared to the other two dimensions, it can be assumed that the normal strain component in the trough-the-thickness direction, $\varepsilon_z$, to be negligible and hence the strain vector of Equation 3.4 can reduced to

$$\boldsymbol{\varepsilon} = \begin{Bmatrix} \varepsilon_x \\ \varepsilon_y \\ \gamma_{xy} \\ \gamma_{xz} \\ \gamma_{yz} \end{Bmatrix} = \begin{Bmatrix} \dfrac{\partial u}{\partial x} + \dfrac{1}{2}\left(\dfrac{\partial u}{\partial x}\right)^2 + \dfrac{1}{2}\left(\dfrac{\partial v}{\partial x}\right)^2 + \dfrac{1}{2}\left(\dfrac{\partial w}{\partial x}\right)^2 \\ \dfrac{\partial v}{\partial y} + \dfrac{1}{2}\left(\dfrac{\partial u}{\partial y}\right)^2 + \dfrac{1}{2}\left(\dfrac{\partial v}{\partial y}\right)^2 + \dfrac{1}{2}\left(\dfrac{\partial w}{\partial y}\right)^2 \\ \dfrac{\partial u}{\partial y} + \dfrac{\partial v}{\partial x} + \dfrac{\partial u}{\partial x}\dfrac{\partial u}{\partial y} + \dfrac{\partial v}{\partial x}\dfrac{\partial v}{\partial y} + \dfrac{\partial w}{\partial x}\dfrac{\partial w}{\partial y} \\ \dfrac{\partial u}{\partial z} + \dfrac{\partial w}{\partial x} + \dfrac{\partial u}{\partial x}\dfrac{\partial u}{\partial z} + \dfrac{\partial v}{\partial x}\dfrac{\partial v}{\partial z} + \dfrac{\partial w}{\partial x}\dfrac{\partial w}{\partial z} \\ \dfrac{\partial v}{\partial z} + \dfrac{\partial w}{\partial y} + \dfrac{\partial u}{\partial y}\dfrac{\partial u}{\partial z} + \dfrac{\partial v}{\partial y}\dfrac{\partial v}{\partial z} + \dfrac{\partial w}{\partial y}\dfrac{\partial w}{\partial z} \end{Bmatrix} \tag{3.5}$$

It can be appreciated that this strain definition, which has been adopted by other authors (Chattopadhyay *et al.*, 1995, Rao *et al.*, 1993, Ray and Satsangi, 1998) to formulate their respective geometrically non-linear master stiffened element, does not include initial stress-free, out-of-plane deformations in the panel.

As the inclusion of initial out-of-plane deformation is a crucial part of the non-linear buckling analysis of panels under in-plane loads, the previously mentioned stiffened plate elements are confined to the analysis of flat panels under transverse loads only.

In order to overcome this limitation, this investigation includes initial out-of-plane deformation using the strain definition suggested by Pica and Wood (1980). These researchers suggest that the strain vector presented in Equation 3.5 is modified by subtracting the initial stress-free deformations from the total strain as

$$\boldsymbol{\varepsilon} = \begin{Bmatrix} \varepsilon_x \\ \varepsilon_y \\ \gamma_{xy} \\ \gamma_{xz} \\ \gamma_{yz} \end{Bmatrix} = \begin{Bmatrix} \dfrac{\partial u}{\partial x} + \dfrac{1}{2}\left(\dfrac{\partial u}{\partial x}\right)^2 + \dfrac{1}{2}\left(\dfrac{\partial v}{\partial x}\right)^2 + \dfrac{1}{2}\left(\dfrac{\partial w}{\partial x}\right)^2 \\ \dfrac{\partial v}{\partial y} + \dfrac{1}{2}\left(\dfrac{\partial u}{\partial y}\right)^2 + \dfrac{1}{2}\left(\dfrac{\partial v}{\partial y}\right)^2 + \dfrac{1}{2}\left(\dfrac{\partial w}{\partial y}\right)^2 \\ \dfrac{\partial u}{\partial y} + \dfrac{\partial v}{\partial x} + \dfrac{\partial u}{\partial x}\dfrac{\partial u}{\partial y} + \dfrac{\partial v}{\partial x}\dfrac{\partial v}{\partial y} + \dfrac{\partial w}{\partial x}\dfrac{\partial w}{\partial y} \\ \dfrac{\partial u}{\partial z} + \dfrac{\partial w}{\partial x} + \dfrac{\partial u}{\partial x}\dfrac{\partial u}{\partial z} + \dfrac{\partial v}{\partial x}\dfrac{\partial v}{\partial z} + \dfrac{\partial w}{\partial x}\dfrac{\partial w}{\partial z} \\ \dfrac{\partial v}{\partial z} + \dfrac{\partial w}{\partial y} + \dfrac{\partial u}{\partial y}\dfrac{\partial u}{\partial z} + \dfrac{\partial v}{\partial y}\dfrac{\partial v}{\partial z} + \dfrac{\partial w}{\partial y}\dfrac{\partial w}{\partial z} \end{Bmatrix} - \begin{Bmatrix} \dfrac{1}{2}\left(\dfrac{\partial w_0}{\partial x}\right)^2 \\ \dfrac{1}{2}\left(\dfrac{\partial w_0}{\partial x}\right)^2 \\ \dfrac{\partial w_0}{\partial x}\dfrac{\partial w_0}{\partial y} \\ \dfrac{\partial w_0}{\partial x} + \dfrac{\partial w_0}{\partial x}\dfrac{\partial w_0}{\partial z} \\ \dfrac{\partial w_0}{\partial y} + \dfrac{\partial w_0}{\partial y}\dfrac{\partial w_0}{\partial z} \end{Bmatrix} \tag{3.6}$$

Equation 3.6 is simplified even further using the von Kármán assumption. According to this assumption all quadratic terms, except for those corresponding to rotation of the mid-surface, are dropped from Green's strain vector.

This simplification rests on the assumption that, the vertical component of displacement of the plate, $w$, is independent of the vertical coordinate $z$ and, that the gradients of $u$ and $v$ are small and therefore their high order contribution to Equation 3.6 can be neglected. As a result of this simplification the strain vector can be further reduced to

$$\boldsymbol{\varepsilon} = \begin{Bmatrix} \varepsilon_x \\ \varepsilon_y \\ \gamma_{xy} \\ \gamma_{xz} \\ \gamma_{yz} \end{Bmatrix} = \begin{Bmatrix} \dfrac{\partial u}{\partial x} \\ \dfrac{\partial v}{\partial y} \\ \dfrac{\partial u}{\partial y} + \dfrac{\partial v}{\partial x} \\ \dfrac{\partial u}{\partial z} + \dfrac{\partial w}{\partial x} \\ \dfrac{\partial v}{\partial z} + \dfrac{\partial w}{\partial y} \end{Bmatrix} + \begin{Bmatrix} \dfrac{1}{2}\left(\dfrac{\partial w}{\partial x}\right)^2 \\ \dfrac{1}{2}\left(\dfrac{\partial w}{\partial y}\right)^2 \\ \dfrac{\partial w}{\partial x}\dfrac{\partial w}{\partial y} \\ 0 \\ 0 \end{Bmatrix} - \begin{Bmatrix} \dfrac{1}{2}\left(\dfrac{\partial w_0}{\partial x}\right)^2 \\ \dfrac{1}{2}\left(\dfrac{\partial w_0}{\partial x}\right)^2 \\ \dfrac{\partial w_0}{\partial x}\dfrac{\partial w_0}{\partial y} \\ 0 \\ 0 \end{Bmatrix} \tag{3.7}$$

### 3.2.3 **Stress measure in a shallow shell**

For each geometrically non-linear measure of strain, there is a conjugate stress measure. In this case, since the original configuration has been chosen as the reference configuration (TL description of motion), the stress vector associated with the Green strain measure described in Equation 3.4 is the second Piola-Kirchhoff stress vector.

The second Piola-Kirchhoff stress measure expresses the transformed current force per unit of undeformed area (original configuration). In Section 3.2.2 it was stated that the normal strain component in the through-the-thickness direction, $\varepsilon_z$, to be negligible. Consequently, in this derivation of the stresses of a shallow shell it can also be assumed that the magnitude of the normal stress component in this direction, $\sigma_z$, to be negligible.

By integrating the second Piola-Kirchhoff stresses over the thickness of the shallow shell the resultant values of the forces and moments by unit length at the mid-surface of the shallow shell are obtained as

$$\boldsymbol{\zeta} = \begin{Bmatrix} N_x \\ N_y \\ N_{xy} \\ M_x \\ M_y \\ M_{xy} \\ Q_x \\ Q_y \end{Bmatrix} = \begin{Bmatrix} \int_{-\frac{t}{2}}^{\frac{t}{2}} \sigma_x dz \\ \int_{-\frac{t}{2}}^{\frac{t}{2}} \sigma_y dz \\ \int_{-\frac{t}{2}}^{\frac{t}{2}} \tau_{xy} dz \\ \int_{-\frac{t}{2}}^{\frac{t}{2}} \sigma_x z dz \\ \int_{-\frac{t}{2}}^{\frac{t}{2}} \sigma_y z dz \\ \int_{-\frac{t}{2}}^{\frac{t}{2}} \tau_{xy} z dz \\ \int_{-\frac{t}{2}}^{\frac{t}{2}} \tau_{xz} dz \\ \int_{-\frac{t}{2}}^{\frac{t}{2}} \tau_{yz} dz \end{Bmatrix} \qquad 3.8$$

The direction of these mid-surface resultant forces and moments is defined in Figure 3-2.

### 3.2.4 **Strain-curvature relations of the shallow shell**

Using Reissner Mindlin's hypothesis to describe the displacement field, i.e. substituting Equation 3.2 into Equation 3.7, the simplified Green's strain vector, corresponding to the generalized mid-surface stresses presented in Equation 3.8, is now expressed in terms of the mid-surface displacements and curvatures as

$$\hat{\boldsymbol{\varepsilon}} = \begin{Bmatrix} \varepsilon_x \\ \varepsilon_y \\ k_x \\ k_y \\ k_{xy} \\ \gamma_{xy} \\ \gamma_{xz} \\ \gamma_{yz} \end{Bmatrix} = \begin{Bmatrix} \dfrac{\partial \hat{u}}{\partial x} \\ \dfrac{\partial \hat{v}}{\partial y} \\ \dfrac{\partial \hat{u}}{\partial y} + \dfrac{\partial \hat{v}}{\partial x} \\ -z\dfrac{\partial \theta_x}{\partial x} \\ -z\dfrac{\partial \theta_y}{\partial y} \\ -z\left(\dfrac{\partial \theta_x}{\partial y}\dfrac{\partial \theta_y}{\partial x}\right) \\ \dfrac{\partial \hat{w}_1}{\partial x} - \theta_x \\ \dfrac{\partial \hat{w}_1}{\partial x} - \theta_x \end{Bmatrix} + \begin{Bmatrix} \dfrac{1}{2}\left(\dfrac{\partial \hat{w}_1}{\partial x} + \dfrac{\partial \hat{w}_0}{\partial x}\right)^2 \\ \dfrac{1}{2}\left(\dfrac{\partial \hat{w}_1}{\partial y} + \dfrac{\partial \hat{w}_0}{\partial y}\right)^2 \\ \left(\dfrac{\partial \hat{w}_1}{\partial x} + \dfrac{\partial \hat{w}_0}{\partial x}\right)\left(\dfrac{\partial \hat{w}_1}{\partial y} + \dfrac{\partial \hat{w}_0}{\partial y}\right) \\ 0 \\ 0 \\ 0 \\ 0 \\ 0 \end{Bmatrix} - \begin{Bmatrix} \dfrac{1}{2}\left(\dfrac{\partial \hat{w}_0}{\partial x}\right)^2 \\ \dfrac{1}{2}\left(\dfrac{\partial \hat{w}_0}{\partial x}\right)^2 \\ \dfrac{\partial \hat{w}_0}{\partial x}\dfrac{\partial \hat{w}_0}{\partial y} \\ 0 \\ 0 \\ 0 \\ 0 \\ 0 \end{Bmatrix} \tag{3.9}$$

Equation 3.9 represents the generalized strains of Marguerre's (1938) shallow shell theory. By operating in the two last column vectors of Equation 3.9, it is possible to separate the linear contribution of the initial deformation from the non-linear component of the in-plane strain as

$$\hat{\boldsymbol{\varepsilon}} = \begin{Bmatrix} \varepsilon_x \\ \varepsilon_y \\ k_{xy} \\ k_x \\ k_y \\ \gamma_{xy} \\ \gamma_{xz} \\ \gamma_{yz} \end{Bmatrix} = \underbrace{\begin{Bmatrix} \dfrac{\partial \hat{u}}{\partial x} \\ \dfrac{\partial \hat{v}}{\partial y} \\ \dfrac{\partial \hat{u}}{\partial y} + \dfrac{\partial \hat{v}}{\partial x} \\ -z\dfrac{\partial \theta_x}{\partial x} \\ -z\dfrac{\partial \theta_y}{\partial y} \\ -z\left(\dfrac{\partial \theta_x}{\partial y}\dfrac{\partial \theta_y}{\partial x}\right) \\ \dfrac{\partial \hat{w}_1}{\partial x} - \theta_x \\ \dfrac{\partial \hat{w}_1}{\partial x} - \theta_x \end{Bmatrix}}_{Linear} + \underbrace{\begin{Bmatrix} \dfrac{\partial \hat{w}_0}{\partial x}\dfrac{\partial \hat{w}_1}{\partial x} \\ \dfrac{\partial \hat{w}_0}{\partial y}\dfrac{\partial \hat{w}_1}{\partial y} \\ \dfrac{\partial \hat{w}_0}{\partial x}\dfrac{\partial \hat{w}_1}{\partial y} + \dfrac{\partial \hat{w}_1}{\partial x}\dfrac{\partial \hat{w}_0}{\partial y} \\ 0 \\ 0 \\ 0 \\ 0 \\ 0 \end{Bmatrix}}_{Intial} + \underbrace{\begin{Bmatrix} \dfrac{1}{2}\left(\dfrac{\partial \hat{w}_1}{\partial x}\right)^2 \\ \dfrac{1}{2}\left(\dfrac{\partial \hat{w}_1}{\partial x}\right)^2 \\ \dfrac{\partial \hat{w}_1}{\partial x}\dfrac{\partial \hat{w}_1}{\partial y} \\ 0 \\ 0 \\ 0 \\ 0 \\ 0 \end{Bmatrix}}_{Non-Linear} \tag{3.10}$$

where the three column vectors are respectively the linear ($\hat{\boldsymbol{\varepsilon}}_0$), initial ($\hat{\boldsymbol{\varepsilon}}_I$) and non-linear ($\hat{\boldsymbol{\varepsilon}}_{NL}$) components of the strain of the shallow shell as

$$\hat{\boldsymbol{\varepsilon}} = \hat{\boldsymbol{\varepsilon}}_0 + \hat{\boldsymbol{\varepsilon}}_I + \hat{\boldsymbol{\varepsilon}}_{NL} \tag{3.11}$$

If the panel is free from initial deformations, the initial strains vanish and the second vector is dropped from Equation 3.10. In that case Equation 3.11 represents the strains of a perfectly flat panel.

### 3.2.5 Variation of strain in the shallow shell

In this Section, the variation of strain $d\hat{\boldsymbol{\varepsilon}}$ due to the virtual displacement $d\hat{\mathbf{u}}$ is discussed. The variation in the generalized mid-surface strains, $\hat{\boldsymbol{\varepsilon}}$, presented in Equation 3.11, due to the virtual displacement $d\hat{\mathbf{u}}$ is defined as

$$d\hat{\boldsymbol{\varepsilon}} = d\hat{\boldsymbol{\varepsilon}}_0 + d\hat{\boldsymbol{\varepsilon}}_I + d\hat{\boldsymbol{\varepsilon}}_{NL} \tag{3.12}$$

Since $\hat{\boldsymbol{\varepsilon}}_0$ is a linear function of the mid-surface displacements, $\hat{\mathbf{u}}$, its variation is expresses as

$$d\hat{\boldsymbol{\varepsilon}}_0 = \mathbf{L}\, d\hat{\mathbf{u}} \tag{3.13}$$

where

$$\mathbf{L} = \begin{bmatrix} \frac{\partial}{\partial x} & 0 & 0 & 0 & 0 \\ 0 & \frac{\partial}{\partial y} & 0 & 0 & 0 \\ \frac{\partial}{\partial y} & \frac{\partial}{\partial x} & 0 & 0 & 0 \\ 0 & 0 & 0 & -\frac{\partial}{\partial x} & 0 \\ 0 & 0 & 0 & 0 & -\frac{\partial}{\partial y} \\ 0 & 0 & 0 & -\frac{\partial}{\partial y} & -\frac{\partial}{\partial x} \\ 0 & 0 & \frac{\partial}{\partial x} & -1 & 0 \\ 0 & 0 & \frac{\partial}{\partial y} & 0 & -1 \end{bmatrix} \tag{3.14}$$

and

$$d\hat{\mathbf{u}} = d\begin{Bmatrix} \hat{u} \\ \hat{v} \\ \hat{w} \\ \theta_x \\ \theta_y \end{Bmatrix} \tag{3.15}$$

In order to obtain the variation of the non-linear, $\hat{\boldsymbol{\varepsilon}}_{NL}$, and initial strains, $\hat{\boldsymbol{\varepsilon}}_{I}$, defined in the second and third columns of Equation 3.10, the gradient of the lateral deformation, $\hat{w}_1$, and initial deformations, $\hat{w}_0$, of the panel are defined first, as suggested by Zienkiewicz and Taylor (1994), as

$$\boldsymbol{\theta} = \left[\frac{\partial \hat{w}_k}{\partial x}, \frac{\partial \hat{w}_k}{\partial y}\right]^T, \quad with\ k = 0,1 \tag{3.16}$$

Using this expression, and noting that both vectors contribute only to the in-plane strains of the shallow shell, their respective variation is obtained in terms of the virtual gradient as

$$d\hat{\boldsymbol{\varepsilon}}_I^{\,p} = \mathbf{A_0} d\boldsymbol{\theta}$$
$$d\hat{\boldsymbol{\varepsilon}}_{NL}^{\,p} = \mathbf{A_1} d\boldsymbol{\theta} \qquad 3.17$$

where

$$\mathbf{A}_k = \begin{bmatrix} \dfrac{\partial \hat{w}_k}{\partial x} & 0 \\ 0 & \dfrac{\partial \hat{w}_k}{\partial y} \\ \dfrac{\partial \hat{w}_k}{\partial y} & \dfrac{\partial \hat{w}_k}{\partial x} \end{bmatrix}, \quad with\ k = 0,1 \qquad 3.18$$

and

$$d\boldsymbol{\theta} = d\left[\frac{\partial \hat{w}_1}{\partial x}, \frac{\partial \hat{w}_1}{\partial y}\right]^T \qquad 3.19$$

### 3.2.6 Stress-strain relations of a shallow shell

In this Section, the stress-strain relations, or constitutive relations, that characterise the individual material and its deformations as a reaction to applied loads, i.e. the relationship between stresses and strains, for both isotropic and orthotropic laminated materials is presented.

The stress-strain relations for isotropic materials were obtained following the traditional derivation used in plate and shell theory, whereas the stress-strain relations for the laminated material were obtained according to an equivalent single layer model based on First-order Shear Deformation Theory (FSDT). This theory was adopted following the suggestion of Rowher *et al.* (2004) that, for laminated structures with usual slenderness ratios and smooth loading, the FSDT can be regarded as the most efficient choice to obtain results with preliminary design level of accuracy.

#### *3.2.6.1 Isotropic materials*

For a linear elastic isotropic, homogeneous materials, with no stress and strain in the $z$ direction ($\sigma_z = 0$), the second Piola-Kirchhoff stresses $\boldsymbol{\zeta}$ are related to Green's strain $\boldsymbol{\varepsilon}$ by Hooke's law as

$$\boldsymbol{\zeta} = \mathbf{D}\boldsymbol{\varepsilon} \tag{3.20}$$

Where $\mathbf{D}$ is the matrix of constitutive coefficients presented in Equation 3.21, and $E$ and $\nu$ are the modulus of elasticity and the Poisson's ratio of the material respectively.

$$\mathbf{D} = \frac{E}{1-\nu^2}\begin{bmatrix} 1 & \nu & 0 & 0 & 0 \\ \nu & 1 & 0 & 0 & 0 \\ 0 & 0 & \frac{1-\nu}{2} & 0 & 0 \\ 0 & 0 & 0 & \frac{1-\nu}{2} & 0 \\ 0 & 0 & 0 & 0 & \frac{1-\nu}{2} \end{bmatrix} \tag{3.21}$$

Integrating Equation 3.20 explicitly through the plate thickness $t$ enables the stress resultants $\boldsymbol{\zeta}$ of Equations 3.8 to be written in terms of the generalized strains $\hat{\boldsymbol{\varepsilon}}$ of equations as

$$\boldsymbol{\zeta} = \hat{\mathbf{D}}\hat{\boldsymbol{\varepsilon}} \tag{3.22}$$

Where $\hat{\mathbf{D}}$ is the matrix of generalized constitutive coefficients or rigidity matrix for isotropic materials defined in Equation 3.23.

$$\hat{\mathbf{D}} = \frac{Et}{1-\nu^2}\begin{bmatrix} 1 & \nu & 0 & 0 & 0 & 0 & 0 & 0 \\ \nu & 1 & 0 & 0 & 0 & 0 & 0 & 0 \\ 0 & 0 & \frac{1-\nu}{2} & 0 & 0 & 0 & 0 & 0 \\ 0 & 0 & 0 & \frac{t^2}{12} & \frac{\nu t^2}{12} & 0 & 0 & 0 \\ 0 & 0 & 0 & \frac{\nu t^2}{12} & \frac{t^2}{12} & 0 & 0 & 0 \\ 0 & 0 & 0 & 0 & 0 & \frac{t^2}{24}\frac{1-\nu}{} & 0 & 0 \\ 0 & 0 & 0 & 0 & 0 & 0 & k\frac{1-\nu}{2} & 0 \\ 0 & 0 & 0 & 0 & 0 & 0 & 0 & k\frac{1-\nu}{2} \end{bmatrix} \tag{3.23}$$

Here, $k$ is the shear correction factor to allow for non-uniform shear stress distribution throughout the thickness of the plate.

### 3.2.6.2 Laminated material

An equivalent single layer model assumes that the laminate consists of a number of perfectly bonded laminas, or laminate, which are individually treated as homogeneous and orthotropic. Furthermore, the material in each lamina is considered to be linear and elastic. For the $k^{th}$ lamina in the laminate, the plane stress-reduced constitutive relationship with respect to the lamina coordinate system ( $x_1, x_2, x_3$ ) defined in Figure 3-4 are given by Reddy (1997) as

$$\begin{Bmatrix} \sigma_1 \\ \sigma_2 \\ \sigma_6 \\ \sigma_4 \\ \sigma_5 \end{Bmatrix}^k = \begin{bmatrix} Q_{11} & Q_{12} & 0 & 0 & 0 \\ Q_{21} & Q_{22} & 0 & 0 & 0 \\ 0 & 0 & Q_{66} & 0 & 0 \\ 0 & 0 & 0 & Q_{44} & 0 \\ 0 & 0 & 0 & 0 & Q_{55} \end{bmatrix}^k \begin{Bmatrix} \varepsilon_1 \\ \varepsilon_2 \\ \varepsilon_6 \\ \varepsilon_4 \\ \varepsilon_5 \end{Bmatrix}^k \tag{3.24}$$

or

$$\boldsymbol{\zeta}_{12}{}^k = \mathbf{Q}_{12}{}^k \boldsymbol{\varepsilon}_{12}{}^k \tag{3.25}$$

with each non-zero compliance coefficient, $Q_{ij}$, defined as

$$\begin{aligned} &Q_{11} = \frac{E_{11}}{1-\nu_{12}\nu_{21}}; \quad Q_{12} = \frac{\nu_{12}E_{22}}{1-\nu_{12}\nu_{21}}; \quad Q_{22} = \frac{E_{22}}{1-\nu_{12}\nu_{21}}; \\ &Q_{66} = G_{12}; \quad Q_{44} = G_{23}; \quad Q_{55} = G_{13} \end{aligned} \tag{3.26}$$

where, $E_{11}, E_{22}, G_{12}, G_{13}, G_{23}, \nu_{12}, \nu_{21}$ are the orthotropic material properties of the $k^{th}$ lamina in the laminate.

The plane stress-reduced constitutive relationship matrix, presented in Equation 3.24, can modified to relate the stresses and strains defined in the global coordinate system ( $x, y, z$ ), by applying the transformation

$$\mathbf{Q}_{xy} = \bar{\mathbf{T}}\mathbf{Q}_{12}\bar{\mathbf{T}}^T \tag{3.27}$$

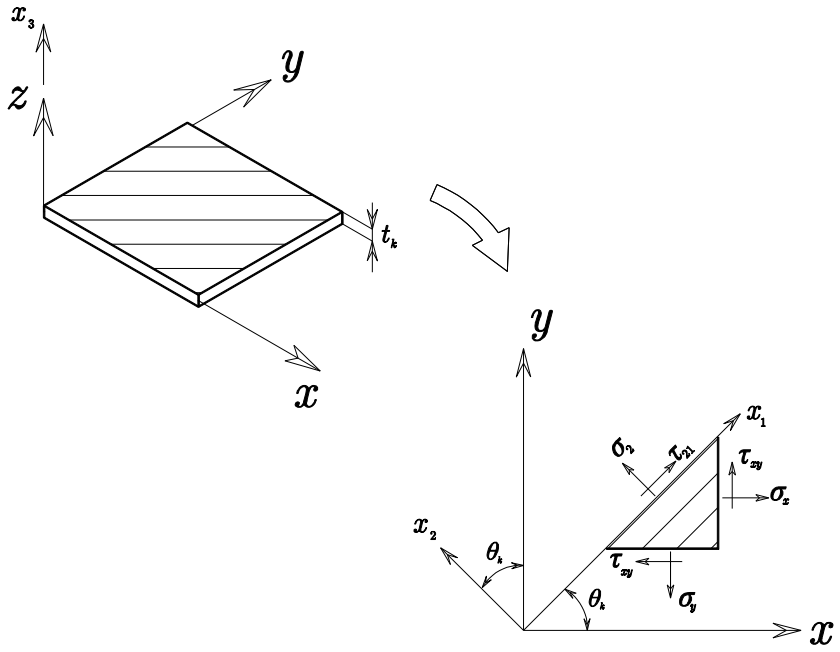


**Figure 3-4 Free body diagram and orientation of a lamina.**

where the transformation matrix of the $k^{th}$ lamina in the laminate is defined as

$$\bar{\mathbf{T}} = \begin{bmatrix} \cos^2\theta_k & \sin^2\theta_k & \sin^2\theta_k & 0 & 0 \\ \sin^2\theta_k & \cos^2\theta_k & -\sin^2\theta_k & 0 & 0 \\ -\sin\theta_k\cos\theta_k & \sin\theta_k\cos\theta_k & \cos^2\theta_k - \sin^2\theta_k & 0 & 0 \\ 0 & 0 & 0 & \cos\theta_k & \sin\theta_k \\ 0 & 0 & 0 & -\sin\theta_k & \cos\theta_k \end{bmatrix} \quad 3.28$$

In Equation 3.28 the angle $\theta_k$ that defines the orientation of the $k^{th}$ lamina in the laminate, and which direction is defined as described in Figure 3-4.

Finally stress resultants $\boldsymbol{\zeta}$ of a composite laminate can be expressed as a function of the mid-surface strains as

$$\boldsymbol{\zeta} = \hat{\mathbf{D}}\hat{\boldsymbol{\varepsilon}} \quad 3.29$$

where the rigidity matrix of the laminate, $\hat{\mathbf{D}}$, is defined as

$$\hat{\mathbf{D}} = \begin{bmatrix} \bar{A}_{11} & \bar{A}_{12} & \bar{A}_{13} & \bar{B}_{11} & \bar{B}_{12} & \bar{B}_{13} & 0 & 0 \\ \bar{A}_{21} & \bar{A}_{22} & \bar{A}_{23} & \bar{B}_{21} & \bar{B}_{22} & \bar{B}_{23} & 0 & 0 \\ \bar{A}_{31} & \bar{A}_{32} & \bar{A}_{33} & \bar{B}_{31} & \bar{B}_{32} & \bar{B}_{33} & 0 & 0 \\ \bar{B}_{11} & \bar{B}_{12} & \bar{B}_{13} & \bar{D}_{11} & \bar{D}_{12} & \bar{D}_{13} & 0 & 0 \\ \bar{B}_{21} & \bar{B}_{22} & \bar{B}_{23} & \bar{D}_{21} & \bar{D}_{22} & \bar{D}_{23} & 0 & 0 \\ \bar{B}_{31} & \bar{B}_{32} & \bar{B}_{33} & \bar{D}_{31} & \bar{D}_{32} & \bar{D}_{33} & 0 & 0 \\ 0 & 0 & 0 & 0 & 0 & 0 & \bar{S}_{11} & \bar{S}_{12} \\ 0 & 0 & 0 & 0 & 0 & 0 & \bar{S}_{21} & \bar{S}_{22} \end{bmatrix} \tag{3.30}$$

where the in-plane stiffness $\bar{\mathbf{A}}$, the coupled bending-stretching stiffness $\bar{\mathbf{B}}$ and the bending stiffness $\bar{\mathbf{D}}$, are calculated for the laminate with $n$ laminas defined in Figure 3-5, by integrating the compliance matrix $\mathbf{Q}_{xy}$ in the thickness direction as

$$\bar{\mathbf{A}}, \bar{\mathbf{B}}, \bar{\mathbf{D}} = \sum_{k=1}^{n} \int_{Z_k - 1}^{Z_k} \mathbf{Q}_{xy}{}^{k} \ \ 1, z, z^2 \ \ dz \tag{3.31}$$

Whilst the coefficients of shear stiffness matrix, $\bar{\mathbf{S}}$, are determined as

$$\bar{\mathbf{S}} = \sum_{k=1}^{n} k_{s_i} k_{s_j} \int_{Z_k - 1}^{Z_k} \mathbf{Q}_{xy}{}^{k} dz \tag{3.32}$$

where $k_s$ is the shear correction factor (SCF) used to account for the fact that the transverse shear stress is not constant in each lamina of the laminate, as assumed by the FSDT. The SCF can be calculated using transverse shear energy and equilibrium considerations as suggested by Whitney (1972).

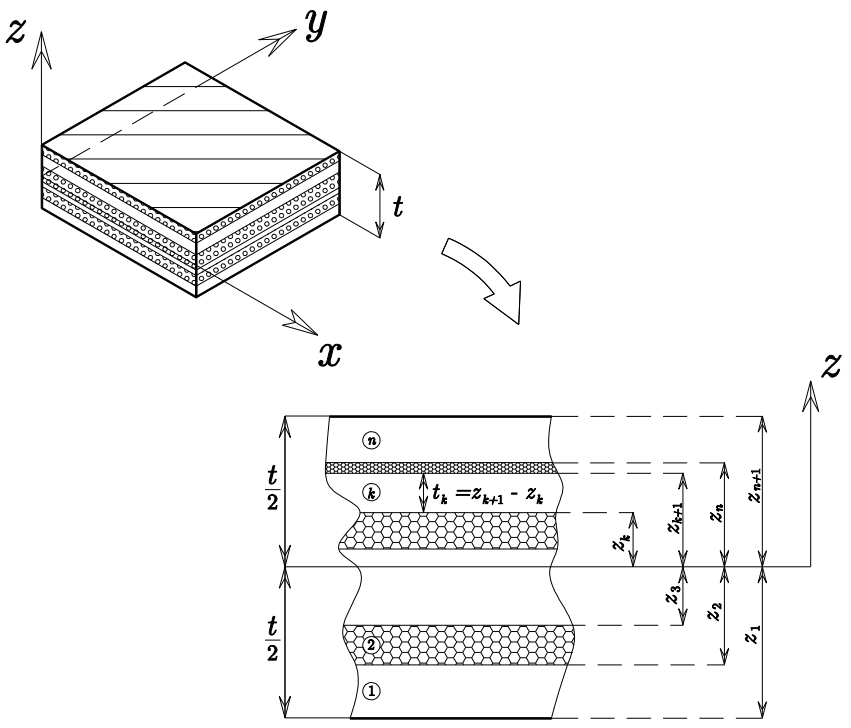


**Figure 3-5 Details of the laminate.**

### 3.2.7 **Formulation of the finite element equations of the master element**

The $C^0$ continuity, isoparametric element having eight nodes and five degrees of freedom per node presented by Cook *et al.* (1989) is used in the present investigation to formulate the equilibrium equations of the shallow shell. A diagram that represents the interpolation region of the element, as well as the element global and natural coordinate systems is presented in Figure 3-6.

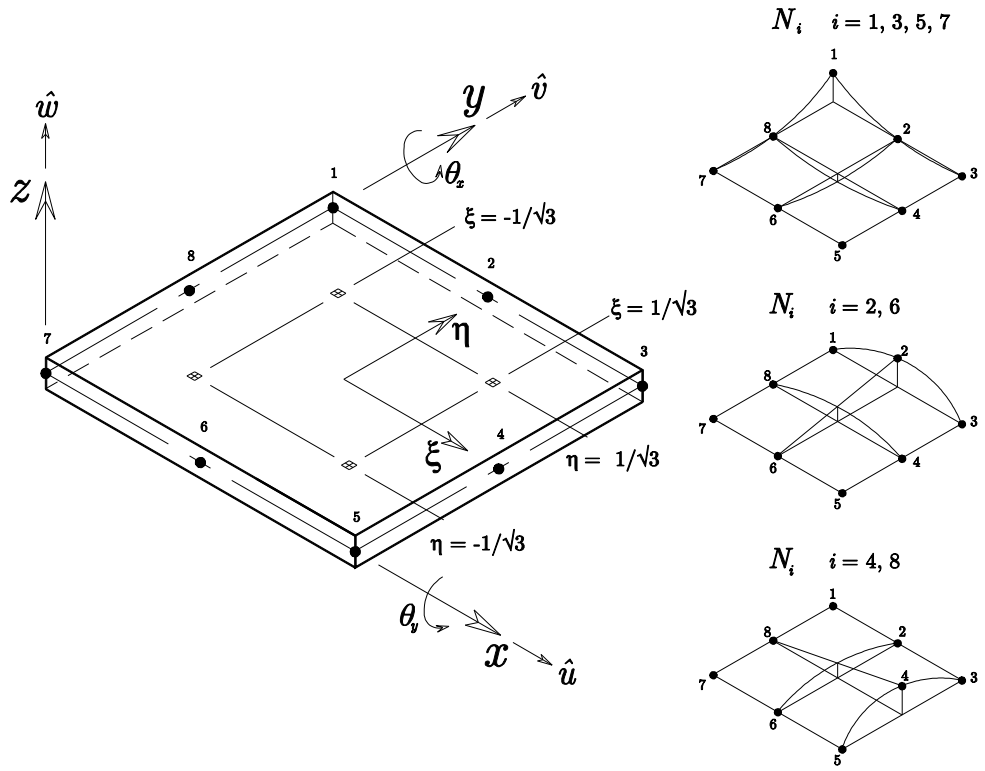


**Figure 3-6 Details of the eight node isoparametric master element.**

### *3.2.7.1 Nodal displacements of the master element*

The displacement components of all eight nodes of the master element, shown in Figure 3-6, are contained within the element nodal displacement vector $\boldsymbol{\delta}$ as

$$\boldsymbol{\delta} = \begin{Bmatrix} \boldsymbol{\delta}_1 \\ \boldsymbol{\delta}_2 \\ \vdots \\ \boldsymbol{\delta}_8 \end{Bmatrix} \tag{3.33}$$

where the mid-surface translations and normal rotations at the $i^{th}$ node of the master element, $\boldsymbol{\delta}_i$, are defined as

$$\boldsymbol{\delta}_i = \left[\hat{u}_i, \hat{v}_i, \hat{w}_i, \theta_{xi}, \theta_{yi}\right]^T \tag{3.34}$$

### *3.2.7.2 Interpolation of nodal quantities of the master element*

The master element is termed isoparametric since the shape functions are used to determine both the geometry and displacements (as well as other field variables) within the interpolation region defined by the element nodes.

The bi-dimensional, $C^0$, nodal shape functions, $N_i$, with reference to the master element nodes defined in Figure 3-6 are respectively

$$N_i = \frac{1}{4}\,(1+\xi_0)\;(1+\eta_0)\;(\xi_0+\eta_0-1)\;, \quad for \quad i=1,3,5,7$$

$$N_i = \frac{1}{4}\,(1+\xi^2)\;(1+\eta_0)\;, \quad for \quad i=2,6$$

$$N_i = \frac{1}{4}\,(1+\xi_0)\;(1+\eta^2)\;, \quad for \quad i=4,8 \qquad 3.35$$

*with*

$$\xi_0 = \xi\xi_i \quad and \quad \eta_0 = \eta\eta_i$$

Using these shape functions, the Cartesian coordinates of any point located within the element can be interpolated using the natural coordinates of the point $(\xi,\eta)$ and the element nodal coordinates $(x_i, y_i, z_i)$ as

$$x = \sum_{i=1}^{8} N_i x_i; \quad y = \sum_{i=1}^{8} N_i y_i; \quad z = \sum_{i=1}^{8} N_i z_i; \qquad 3.36$$

By taking advantage of the isoparametric formulation, the same shape functions are used to interpolate the translation and rotation components of the mid-surface displacement of any point, with natural coordinates $(\xi,\eta)$, from the nodal displacement defined in Equation 3.34 as

$$\begin{aligned} &\hat{u} = \sum_{i=1}^{8} N_i \hat{u}_i; \quad \hat{v} = \sum_{i=1}^{8} N_i \hat{v}_i; \quad \hat{w}_1 = \sum_{i=1}^{8} N_i \hat{w}_{1i} \\ &\theta_x = \sum_{i=1}^{8} N_i \theta_{xi}; \quad \theta_y = \sum_{i=1}^{8} N_i \theta_{yi} \end{aligned} \qquad 3.37$$

It is important to note that the same approach is followed to interpolate the magnitude of the initial deformation, $\hat{w}_0$, at any point within the element from the nodal deformations as

$$\hat{w}_0 = \sum_{i=1}^{n} N_i \hat{w}_{0i} \tag{3.38}$$

The interpolation of the mid-surface translations and normal rotations from the nodal displacement within the element described in Equation 3.37 can be written in compact form as

$$\hat{\mathbf{u}} = \mathbf{N}\boldsymbol{\delta} \tag{3.39}$$

where $\boldsymbol{\delta}$ represents the element nodal displacements, defined in Equation 3.33, and $\mathbf{N}$ is the element shape function matrix defined as

$$\mathbf{N} = \left[\mathbf{N}_1, \mathbf{N}_2, \mathbf{N}_3, \ldots, \mathbf{N}_8\right] \tag{3.40}$$

where $\mathbf{N}_i$ is the nodal shape function matrix of the $i^{th}$ node of the master element defined as

$$\mathbf{N}_i = N_i \mathbf{I}_5 \tag{3.41}$$

and $\mathbf{I}_5$ is a five by five identity matrix.

Using a similar approach, the variation of displacements $d\hat{\mathbf{u}}$, defined in Equation 3.15, is written in terms of the nodal virtual displacements $d\boldsymbol{\delta}$ as

$$d\hat{\mathbf{u}} = \mathbf{N} d\boldsymbol{\delta} \tag{3.42}$$

where $d\boldsymbol{\delta}$ represent the variation of the nodal displacements defined as

$$d\boldsymbol{\delta} = d\begin{Bmatrix} \boldsymbol{\delta}_1 \\ \boldsymbol{\delta}_2 \\ \vdots \\ \boldsymbol{\delta}_8 \end{Bmatrix} \tag{3.43}$$

Finally, the displacement gradients $\boldsymbol{\theta}$ defined in Equation 3.16 are written in terms of the nodal displacements $\boldsymbol{\delta}$ and Cartesian derivatives of the shape functions as

$$\boldsymbol{\theta} = \mathbf{G}\boldsymbol{\delta} \tag{3.44}$$

Where $\mathbf{G}$ is defined as

$$\mathbf{G} = \left[\mathbf{G}_1, \mathbf{G}_2, \cdots, \mathbf{G}_n\right] \tag{3.45}$$

with

$$\mathbf{G}_i = \begin{bmatrix} 0 & 0 & \dfrac{\partial N_i}{\partial x} & 0 & 0 \\ 0 & 0 & \dfrac{\partial N_i}{\partial y} & 0 & 0 \end{bmatrix} \tag{3.46}$$

It is important to note that $\mathbf{G}$ is a matrix defined purely in terms of the nodal coordinates. Similarly the variation of the gradient defined in Equation 3.19 can now be written in terms of virtual nodal displacements as

$$d\boldsymbol{\theta} = \mathbf{G}\, d\boldsymbol{\delta} \tag{3.47}$$

#### *3.2.7.3 Strain-displacement relationship of the master element*

The first term of the generalized Green's strain vector defined in Equation 3.11, $\hat{\boldsymbol{\varepsilon}}_0$, represents the linear strains in the panel. These strains are expressed in terms of the master element nodal displacements as

$$\hat{\boldsymbol{\varepsilon}}_0 = \mathbf{B}_0 \boldsymbol{\delta} \tag{3.48}$$

where $\mathbf{B}_0$ is the linear strain-displacement matrix defined as

$$\mathbf{B}_0 = \left[\mathbf{B}_{01}, \mathbf{B}_{02}, \cdots, \mathbf{B}_{08}\right] \tag{3.49}$$

with

$$\mathbf{B}_{0i} = \begin{bmatrix} \frac{\partial N_i}{\partial x} & 0 & 0 & 0 & 0 \\ 0 & \frac{\partial N_i}{\partial y} & 0 & 0 & 0 \\ \frac{\partial N_i}{\partial y} & \frac{\partial N_i}{\partial x} & 0 & 0 & 0 \\ 0 & 0 & 0 & -\frac{\partial N_i}{\partial x} & 0 \\ 0 & 0 & 0 & 0 & -\frac{\partial N_i}{\partial y} \\ 0 & 0 & 0 & -\frac{\partial N_i}{\partial y} & -\frac{\partial N_i}{\partial x} \\ 0 & 0 & \frac{\partial N_i}{\partial x} & -N_i & 0 \\ 0 & 0 & \frac{\partial N_i}{\partial y} & 0 & -N_i \end{bmatrix} \quad 3.50$$

or

$$\mathbf{B}_{0i} = \begin{bmatrix} \mathbf{B}_{0i}^{\ p} \\ \mathbf{B}_{0i}^{\ b} \\ \mathbf{B}_{0i}^{\ s} \end{bmatrix} \quad 3.51$$

where the sub-matrices $\mathbf{B}_0^{\ p}$, $\mathbf{B}_0^{\ b}$ and $\mathbf{B}_0^{\ s}$ represent the in-plane, bending and shear components of the linear strains respectively.

Similarly the initial, $\hat{\boldsymbol{\varepsilon}}_I$, and non-linear, $\hat{\boldsymbol{\varepsilon}}_{NL}$, components of the generalized strains can be expressed in terms of the master element nodal displacements as

$$\hat{\boldsymbol{\varepsilon}}_I = \mathbf{B}_I \boldsymbol{\delta}; \quad \hat{\boldsymbol{\varepsilon}}_{NL} = \frac{1}{2}\mathbf{B}_{NL}\boldsymbol{\delta} \quad 3.52$$

where $\mathbf{B}_I$ and $\mathbf{B}_{NL}$ are the initial and non-linear strain-displacement matrices of the master element defined as

$$\mathbf{B}_I = \left[\mathbf{B}_{I1}, \mathbf{B}_{I2}, \cdots, \mathbf{B}_{I8}\right] \quad 3.53$$

and

$$\mathbf{B}_{NL} = \left[\mathbf{B}_{NL1}, \mathbf{B}_{NL2}, \cdots, \mathbf{B}_{NL8}\right] \tag{3.54}$$

where $\mathbf{B}_I$ and $\mathbf{B}_{NL}$ are found by taking the variation of $\hat{\boldsymbol{\varepsilon}}_I$ and $\hat{\boldsymbol{\varepsilon}}_{NL}$ with respect to the nodal displacements (Zienkiewicz and Taylor, 1994).

Since both the initial and non-linear strains contribute only to the in-plane components of the generalized mid-surface strain vector, the initial and non-linear strain displacement sub-matrices of equations 3.53 and 3.54 can be defined as

$$\mathbf{B}_{Ii} = \begin{bmatrix} \mathbf{B}_{Ii}{}^{p} \\ 0 \\ 0 \end{bmatrix}; \quad \mathbf{B}_{NLi} = \begin{bmatrix} \mathbf{B}_{NLi}{}^{p} \\ 0 \\ 0 \end{bmatrix} \tag{3.55}$$

where $\mathbf{B}_{Ii}{}^{p}$ and $\mathbf{B}_{NLi}{}^{p}$ are found using the variation of strain defined in Equation 3.17 as

$$\mathbf{B}_{Ii}{}^{p} = \mathbf{A}_0\mathbf{G}_i = \begin{bmatrix} \sum_{k=1}^{8} \frac{\partial N_k}{\partial x}\hat{w}_{0k} & 0 \\ 0 & \sum_{k=1}^{8} \frac{\partial N_k}{\partial y}\hat{w}_{0k} \\ \sum_{k=1}^{8} \frac{\partial N_k}{\partial y}\hat{w}_{0k} & \sum_{k=1}^{8} \frac{\partial N_k}{\partial x}\hat{w}_{0k} \end{bmatrix} \mathbf{G}_i$$

$$\mathbf{B}_{NLi}{}^{p} = \mathbf{A}_1\mathbf{G}_i = \begin{bmatrix} \sum_{k=1}^{8} \frac{\partial N_k}{\partial x}\hat{w}_{1k} & 0 \\ 0 & \sum_{k=1}^{8} \frac{\partial N_k}{\partial y}\hat{w}_{1k} \\ \sum_{k=1}^{8} \frac{\partial N_k}{\partial y}\hat{w}_{1k} & \sum_{k=1}^{8} \frac{\partial N_k}{\partial x}\hat{w}_{1k} \end{bmatrix} \mathbf{G}_i \tag{3.56}$$

Substituting Equations 3.48 and 3.52 into Equation 3.11 the generalized Green's strain vector at any point within the element is now defined in terms of nodal displacements $\boldsymbol{\delta}$ and the displacement gradients as

$$\hat{\boldsymbol{\varepsilon}} = \left[\mathbf{B}_0 + \mathbf{B}_I + \frac{1}{2}\mathbf{B}_{NL}\right]\boldsymbol{\delta} \tag{3.57}$$

It can be observed from Equations 3.57 and 3.56 that the strains are quadratically dependent upon the nodal displacements $\boldsymbol{\delta}$.

Similarly, the variation of strain can be expressed in terms of the virtual nodal displacement, $d\boldsymbol{\delta}$, by substituting Equations 3.42 and 3.47 into 3.13 and 3.17 respectively yields the strain variations

$$\begin{aligned} d\hat{\boldsymbol{\varepsilon}}_0 &= \mathbf{B}_0 d\boldsymbol{\delta} \\ d\hat{\boldsymbol{\varepsilon}}_I &= \mathbf{B}_I d\boldsymbol{\delta} \\ d\hat{\boldsymbol{\varepsilon}}_{NL} &= \mathbf{B}_{NL} d\boldsymbol{\delta} \end{aligned} \qquad 3.58$$

or

$$d\hat{\boldsymbol{\varepsilon}} = \mathbf{B} d\boldsymbol{\delta} \qquad 3.59$$

in which

$$\mathbf{B} = \mathbf{B}_0 + \mathbf{B}_I + \mathbf{B}_{NL} \qquad 3.60$$

## 3.3 Formulation of the slave element

The stiffener is idealised as a beam, i.e. a structural member whose length to cross-sectional dimensions is very large and that under load undergoes not only twisting and stretching along its length, but also bending about an axis transverse to its length.

Similarly to the shallow-shell, the displacement field in a beam is not normally described using a three dimensional theory but using a simpler, one-dimensional theory instead.

The two more commonly used theories to model the kinematic behaviour of beams are Euler-Bernoulli beam theory (EBT), that neglects the transverse shear strain, and Timoshenko beam theory (TBT), which assumes a linear variation of the transverse shear strain along the beam cross section. As mentioned in Section 3.2.1, transverse shear strains are important in the analysis of composite laminates and therefore TBT was adopted in this work.

### 3.3.1 **Displacement field in a beam**

The three dimensional Cartesian displacement vector $\mathbf{u}_{st} = \left[u', v', w'\right]^T$ of any material point within the stiffener $\mathbf{x}_{st} = x', y', z'$ can be expressed using the generalised displacement vector $\mathbf{u}_{st}$ presented in Equation 3.61

$$\mathbf{u}_{st} = \begin{Bmatrix} u' \\ \hat{w}_1 \\ \theta_{x'} \\ \theta_{y'} \end{Bmatrix} \tag{3.61}$$

where $u'$, $\hat{w}_1$ are the centroidal translations and $\theta_{x'}$, $\theta_{y'}$ the centroidal rotations defined in Figure 3-7. Using expression 3.61 the three dimensional displacement field in a beam is defined in the beam coordinate system $x' - y'$ as

$$\begin{aligned} u_{st} &= u' - z\theta_{x'} \\ v_{st} &= -z\theta_{y'} \\ w_{st} &= \hat{w}_0 + \hat{w}_1 + y'\theta_{y'} \end{aligned} \tag{3.62}$$

Here, $\hat{w}_0$ is the stress-free, centroidal deformation in the $z$ direction of the beam.

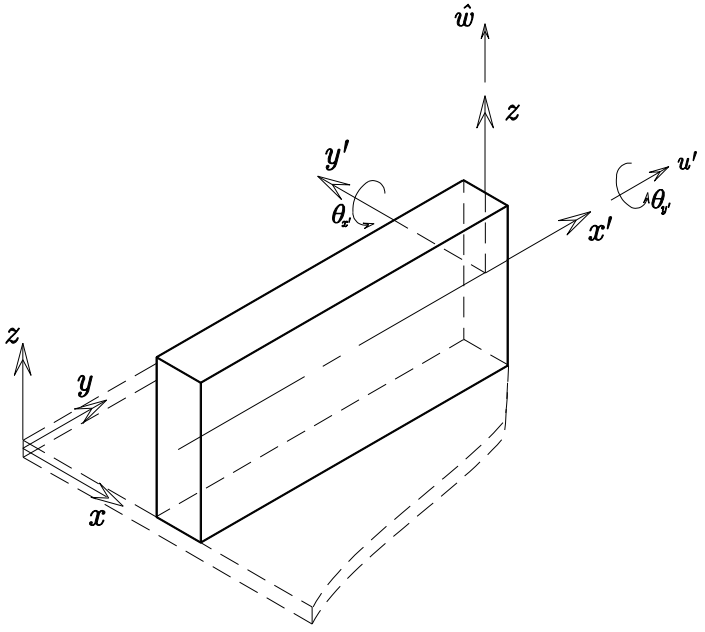


**Figure 3-7 Coordinate system and degrees of freedom of the beam.**

### 3.3.2 Strain curvature relations of the beam

The non-linear strain vector of the beam defined in the $x'-y'$ coordinate system and expressed using the beam degrees of freedom is given by

$$\boldsymbol{\varepsilon}_{st} = \begin{Bmatrix} \varepsilon_{x'} \\ \gamma_{x'y'} \\ \gamma_{x'z} \end{Bmatrix} = \begin{Bmatrix} \dfrac{du'}{dx'} - z\dfrac{d\theta_{x'}}{dx'} \\ \dfrac{d\hat{w}_1}{dx'} - y'\dfrac{d\theta_{y'}}{dx'} - \theta_{x'} \\ -z\dfrac{d\theta_{y'}}{dx'} \end{Bmatrix} + \begin{Bmatrix} \frac{1}{2}\left(\dfrac{d\hat{w}}{dx}'\right)^2 \\ 0 \\ 0 \end{Bmatrix} - \begin{Bmatrix} \frac{1}{2}\left(\dfrac{d\hat{w}_0}{dx'}\right)^2 \\ 0 \\ 0 \end{Bmatrix} \tag{3.63}$$

By separating the bending strains from the direct normal strains and by re-arranging the last two column vectors in Equation 3.63 the strains in the beam can be expressed as

$$\boldsymbol{\varepsilon}_{st} = \mathbf{H}\hat{\boldsymbol{\varepsilon}}_{st} \tag{3.64}$$

where

$$\mathbf{H} = \begin{bmatrix} 1 & z & 0 & 0 \\ 0 & 0 & 1 & y' \\ 0 & 0 & 0 & z \end{bmatrix} \tag{3.65}$$

and $\hat{\boldsymbol{\varepsilon}}_{st}$ is the generalised strain vector of the beam defined as

$$\hat{\boldsymbol{\varepsilon}}_{st} = \begin{Bmatrix} \varepsilon_{x'} \\ k_{x'} \\ \gamma_{x'y'} \\ \gamma_{x'z} \end{Bmatrix} = \underbrace{\begin{Bmatrix} \dfrac{du'}{dx'} \\ -\dfrac{d\theta_{x'}}{dx'} \\ \dfrac{d\hat{w}_1}{dx'} - \theta_{x'} \\ -\dfrac{d\theta_{y'}}{dx'} \end{Bmatrix}}_{Linear} + \underbrace{\begin{Bmatrix} \dfrac{d\hat{w}_0}{dx'}\dfrac{d\hat{w}_1}{dx'} \\ 0 \\ 0 \\ 0 \end{Bmatrix}}_{Initial} + \underbrace{\begin{Bmatrix} \frac{1}{2}\left(\dfrac{d\hat{w}_1}{dx'}\right)^2 \\ 0 \\ 0 \\ 0 \end{Bmatrix}}_{Non-linear} \tag{3.66}$$

It should be appreciated that the generalized strain vector presented in Equation 3.66 is analogous to that of the shell defined in Equation 3.10. Consequently the generalized strain vector of the beam can also be subdivided as

$$\hat{\boldsymbol{\varepsilon}}_{st} = \hat{\boldsymbol{\varepsilon}}_{0st} + \hat{\boldsymbol{\varepsilon}}_{Ist} + \hat{\boldsymbol{\varepsilon}}_{NLst} \tag{3.67}$$

Where, $\hat{\boldsymbol{\varepsilon}}_{0st}$ , $\hat{\boldsymbol{\varepsilon}}_{Ist}$ and $\hat{\boldsymbol{\varepsilon}}_{NLst}$ are the linear, initial and non-linear components of the strain-displacement relation of the stiffening beam respectively.

### 3.3.3 **Variation of strain in the beam**

The variation of strain in the beam $d\hat{\boldsymbol{\varepsilon}}_{st}$ due to the virtual displacement $d\mathbf{u}'$ is defined in a similar way to the variation of the strain in the shell. Here the variation in the generalized beam strain is defined as

$$d\hat{\boldsymbol{\varepsilon}}_{st} = d\hat{\boldsymbol{\varepsilon}}_{0st} + d\hat{\boldsymbol{\varepsilon}}_{Ist} + d\hat{\boldsymbol{\varepsilon}}_{NLst} \tag{3.68}$$

since $\hat{\boldsymbol{\varepsilon}}_{0st}$ is a linear function of the centroidal displacements $\mathbf{u}'$ its variation is expressed as

$$d\hat{\boldsymbol{\varepsilon}}_{0st} = \mathbf{L}_{st} d\mathbf{u}' \tag{3.69}$$

where

$$\mathbf{L}_{st} = \begin{bmatrix} \dfrac{d}{dx'} & 0 & 0 & 0 \\ 0 & 0 & \dfrac{d}{dx'} & 0 \\ 0 & \dfrac{d}{dx'} & -1 & 0 \\ 0 & 0 & 0 & \dfrac{d}{dx'} \end{bmatrix} \tag{3.70}$$

and

$$d\mathbf{u}' = d\begin{Bmatrix} u' \\ \hat{w}_1 \\ \theta_{x'} \\ \theta_{y'} \end{Bmatrix} \tag{3.71}$$

In order to obtain the variation of the non-linear, $\hat{\boldsymbol{\varepsilon}}_{NLst}$, and initial strains, $\hat{\boldsymbol{\varepsilon}}_{Ist}$, defined in the second and third columns of Equation 3.66, the gradient of the lateral deformation, $\hat{w}_1$, and initial deformations, $\hat{w}_0$, of the beam as

$$\boldsymbol{\theta}_{st} = \frac{d\hat{w}_k}{dx'}, \quad with\ k = 0,1 \tag{3.72}$$

Using this expression, and noting that both vectors contribute only to the axial strains of the beam, their respective variation is obtained in terms of the virtual gradient as

$$\begin{aligned} d\hat{\boldsymbol{\varepsilon}}_{I\,st}{}^{a} &= \mathbf{A}_{0\,st}\, d\boldsymbol{\theta} \\ d\hat{\boldsymbol{\varepsilon}}_{NL\,st}{}^{a} &= \mathbf{A}_{1\,st}\, d\boldsymbol{\theta} \end{aligned} \tag{3.73}$$

where

$$\mathbf{A}_k = \frac{d\hat{w}_k}{dx'}, \quad with\ k = 0,1 \tag{3.74}$$

and

$$d\boldsymbol{\theta} = d\left(\frac{d\hat{w}_1}{dx'}\right) \tag{3.75}$$

### 3.3.4 Stress-strain relations of a beam

In this Section the stress-strain relation for isotropic and laminated stiffening beam cross-sections shown in Figure 3-8 are presented.

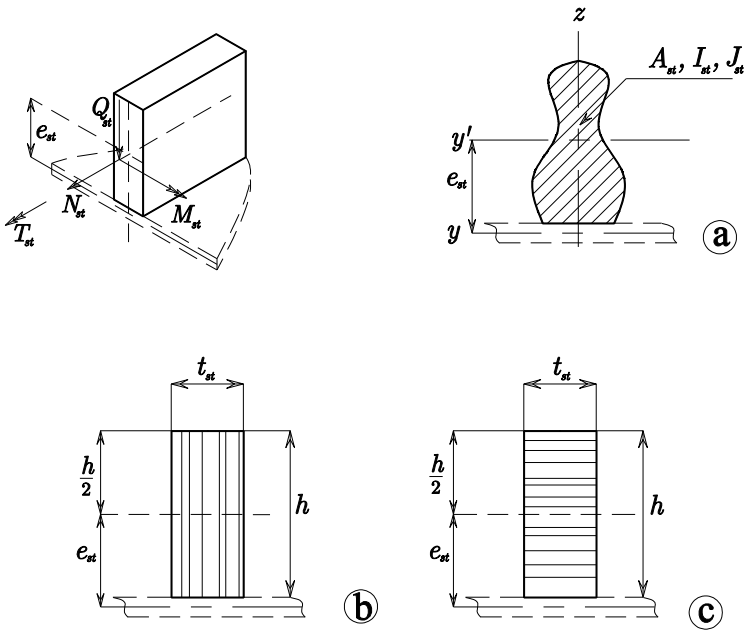


**Figure 3-8 Definition of stress components and stiffener cross section dimensions.**

### 3.3.4.1 Isotropic stiffening beams

The generalised stresses in an isotropic stiffening beam of arbitrary cross section shown in diagram **a** of Figure 3-8, are expressed in terms of the normal and shear strains as suggested by Mukhopadhyay and Satsangi (1984) as

$$\boldsymbol{\zeta}_{st} = \bar{\mathbf{D}}_{st}\boldsymbol{\varepsilon}_{st} \tag{3.76}$$

where

$$\bar{\mathbf{D}}_{st} = \begin{bmatrix} E & 0 & 0 \\ 0 & G & 0 \\ 0 & 0 & G \end{bmatrix} \tag{3.77}$$

where the beam stresses $\boldsymbol{\zeta}_{st}$ are defined as

$$\boldsymbol{\zeta}_{st} = \begin{Bmatrix} \sigma_{x'} \\ \gamma_{x'y'} \\ \gamma_{z'x'} \end{Bmatrix} \tag{3.78}$$

Combining Equation 3.64 and 3.76, and integrating the stresses over the cross section of the beam, the generalized stress vector of the beam is obtained as

$$\boldsymbol{\zeta}_{st} = \hat{\mathbf{D}}_{st}\hat{\boldsymbol{\varepsilon}}_{st} \tag{3.79}$$

where the generalized centroidal stresses in the beam, $\boldsymbol{\zeta}_{st}$, are defined as

$$\boldsymbol{\zeta}_{st} = \begin{Bmatrix} N_{st} \\ M_{st} \\ T_{st} \\ Q_{st} \end{Bmatrix} \tag{3.80}$$

and the rigidity matrix, $\hat{\mathbf{D}}_{st}$, of the isotropic stiffening beam of arbitrary cross section, is defined as

$$\hat{\mathbf{D}}_{st} = \iint_{A_{st}} \mathbf{H}^T \bar{\mathbf{D}} \mathbf{H}\, dy'\, dz = \iint_{A_{st}} \begin{bmatrix} E & Ez & 0 & 0 \\ Ez & Ez^2 & 0 & 0 \\ 0 & 0 & G & -Gy' \\ 0 & 0 & -Gy' & G\ y'^2 + z^2 \end{bmatrix} dy'\, dz \qquad 3.81$$

If the expression $\iint_{A_{st}} -Gy'\, dy'\, dz$ is assumed to be zero, as proposed by Mukhopadhyay and Satsangi (1984), then the integration of Equation 3.81 yields

$$\hat{\mathbf{D}}_{st} = \begin{bmatrix} EA_{st} & E(A_{st}e_{st}) & 0 & 0 \\ E(A_{st}e_{st}) & EI_{st} & 0 & 0 \\ 0 & 0 & GA_{st}k_{st} & 0 \\ 0 & 0 & 0 & GJ_{st} \end{bmatrix} \qquad 3.82$$

where $e_{st}$, $A_{st}$, $I_{st}$, $J_{st}$ represent the eccentricity, area, second moment of area and polar moment of inertia of the stiffening beam cross section, whilst $E$, $G$ and $k_{st}$ are the modulus of elasticity, shear modulus and the shear correction factor respectively.

It is important to note that the second moment of area of the stiffener is calculated with respect to the panel mid-surface using the parallel axis theorem.

#### *3.3.4.2 Laminated stiffening beams*

Since the derivation of the stress-strain relationship and the rigidity matrix, $\hat{\mathbf{D}}_{st}$, of laminated stiffening beams is very extensive and since it has been discussed in detail by other authors (Chattopadhyay *et al.*, 1993, Ray and Satsangi, 1996, Prusty and Satsangi, 2001b), only the final rigidity matrices, $\hat{\mathbf{D}}_{st}$, are presented in this Section. For all the mathematical details, the reader is advised to refer to the cited literature.

According to Chattopadhyay *et al.* (1993), the rigidity matrix of a laminated beam of rectangular cross section of vertical lamination, as shown in diagram **b** of Figure 3-8, is defined as

$$\hat{\mathbf{D}}_{st} = \begin{bmatrix} \bar{A}_{11}h & \bar{A}_{11}h\,ecc & \bar{A}_{13}h & -\bar{B}_{13}h \\ \bar{A}_{11}h\,ecc & \bar{A}_{11}\left(\frac{h}{12}+e_{st}^{\,2}\right) & \bar{A}_{13}h\,e_{st} & -\bar{B}_{13}h\,e_{st} \\ \bar{A}_{13}h & \bar{A}_{13}h\,e_{st} & \bar{A}_{13}hk_{st} & -\bar{B}_{33}h \\ -\bar{B}_{13}h & -\bar{B}_{13}h\,e_{st} & -\bar{B}_{33}h & \frac{1}{6}\,Q_{44}+Q_{66}\;\;ht_{st}^{\,3} \end{bmatrix} \qquad 3.83$$

Similarly, the rigidity matrix of a laminated beam of rectangular cross-section with a horizontal lamination, as shown in diagram **c** of Figure 3-8, is defined as

$$\hat{\mathbf{D}}_{st} = \begin{bmatrix} \bar{A}_{22}t_{st} & \bar{B}_{22}t_{st} & 0 & \bar{B}_{23}t_{st} \\ \bar{B}_{22}t_{st} & \bar{D}_{22}t_{st} & 0 & \bar{D}_{23}t_{st} \\ 0 & 0 & \bar{S}_{11}t_{st}k_{st} & 0 \\ \bar{B}_{23}t_{st} & \bar{D}_{23}t_{st} & 0 & \frac{1}{6}\,Q_{55}+Q_{66}\;\;ht_{st}^{\,3} \end{bmatrix} \qquad 3.84$$

where $h$ and $t_{st}$ represent the stiffener height and thickness respectively. The in-plane ($\bar{A}_{ij}$), bending ($\bar{D}_{ij}$)and bending-stretching ($\bar{B}_{ij}$) constitutive coefficients as well as the compliances ($Q_{ij}$) of the beam's laminate are calculated as described in Section 3.2.6.2.

It must be noted that the rigidity matrix for other laminated open or closed cross-sections can be formulated, as suggested by Chattopadhyay *et al.* (1993), by dividing the cross section of the stiffener into horizontal and vertical components. The rigidities of each component are then calculated separately using Equation 3.83 or 3.84 to then be combined by considering their locations with respect to the panel mid-surface.

For further details the reader is referred to the works of Prusty and Satsangi (2001b) for open „T' sections and Ray and Satsangi (1996) for closed hat sections.

### 3.3.5 Formulation of the finite element equations of the slave element

A one dimensional, isoparametric element, having three nodes and four degrees of freedom per node is used in the present investigation to formulate the equilibrium equations of the stiffening beam.

A diagram that represents the interpolation region of the element, as well as the elements global and natural coordinate systems is presented in Figure 3-9.

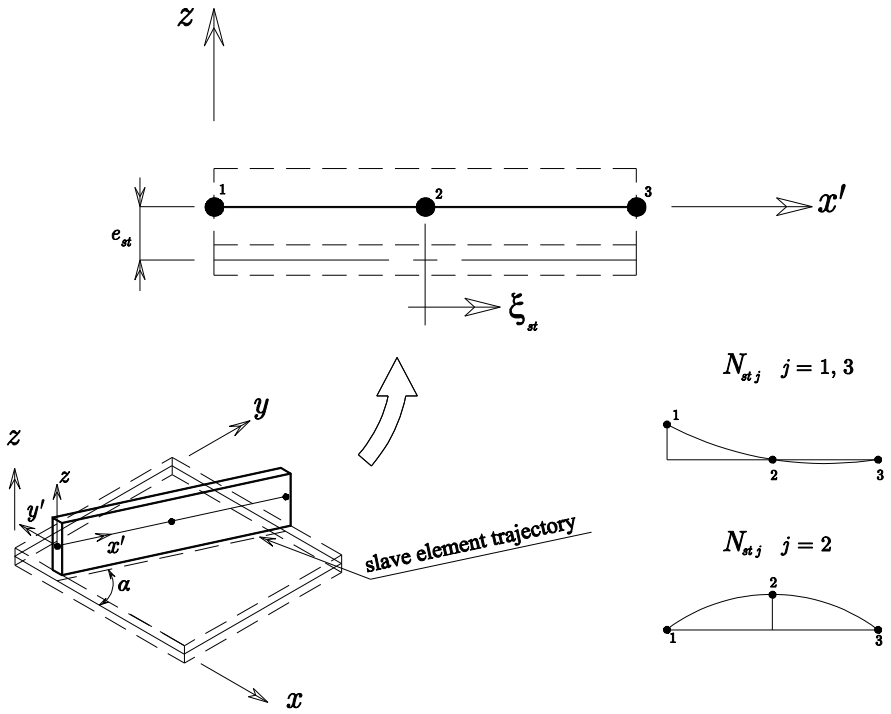


**Figure 3-9 Details of the three node isoparametric slave element.**

### *3.3.5.1 Nodal displacements of the slave element*

The nodal displacement components of all three nodes of the slave element, shown in Figure 3-9, are contained within the element nodal displacement vector $\boldsymbol{\delta}_{st}$ as

$$\boldsymbol{\delta}_{st} = \begin{Bmatrix} \boldsymbol{\delta}_{st\,1} \\ \boldsymbol{\delta}_{st\,2} \\ \boldsymbol{\delta}_{st\,3} \end{Bmatrix} \tag{3.85}$$

Where the centroidal translations and normal rotations at the $j^{th}$ node of the master element, $\boldsymbol{\delta}_i$, are defined in the skew axes system $x'-y'$, as

$$\boldsymbol{\delta}_{st\,j} = \left[ u'_j, \hat{w}_{1i}, \theta_{x'i}, \theta_{y'i} \right]^T \tag{3.86}$$

In order to obtain the unique set of nodal unknowns required to describe the master-slave element system, the displacement field of the beam element is described using the

nodal unknowns of the master element $\hat{\mathbf{u}}$ by introducing the coordinate transformation suggested by Thompson *et al.* (1988) as

$$\mathbf{u}' = \mathbf{\Lambda}\hat{\mathbf{u}} \tag{3.87}$$

where

$$\mathbf{\Lambda} = \begin{bmatrix} \mathbf{\Lambda}_j & 0 & 0 \\ 0 & \mathbf{\Lambda}_j & 0 \\ 0 & 0 & \mathbf{\Lambda}_j \end{bmatrix} \tag{3.88}$$

and

$$\mathbf{\Lambda}_j = \begin{bmatrix} \cos\alpha & \sin\alpha & 0 & 0 & 0 \\ 0 & 0 & 1 & 0 & 0 \\ 0 & 0 & 0 & \cos\alpha & \sin\alpha \\ 0 & 0 & 0 & -\sin\alpha & \cos\alpha \end{bmatrix} \tag{3.89}$$

The angle $\alpha$ defines the orientation of the slave element $x'$ axis (stiffener trajectory) with respect to the master element $x$ axis as shown in Figure 3-9.

#### *3.3.5.2 Interpolation of nodal quantities of the slave element*

The interpolation functions of the isoparametric beam element with reference to the slave element node numbering defined in Figure 3-9, are respectively

$$N_{st1} = \frac{-\xi'(1-\xi')}{2} \quad N_{st2} = \frac{(1-\xi')}{2} \quad N_{st3} = \frac{\xi'(1+\xi')}{2} \tag{3.90}$$

Using these shape functions, the Cartesian coordinates of any point located within the element can be interpolated using the natural coordinates of the point ($\xi'$) and the element nodal coordinates ($x'_j$) as

$$x' = \sum_{j=1}^{3} N_{st\,j} x'_j \tag{3.91}$$

Since the nodes of the slave element are located within the interpolation region of the master element, it is possible to interpolate the nodal displacements, and any other nodal quantity, of the slave element from the master element nodal displacements.

In this work the interpolation expression suggested by Ray and Satsangi (1996) is adopted to interpolate the slave element displacements $\boldsymbol{\delta}_{st}$ as

$$\boldsymbol{\delta}_{st} = \boldsymbol{\Lambda}\mathbf{T}\boldsymbol{\delta} \tag{3.92}$$

Where $\boldsymbol{\Lambda}$ is the orientation matrix, defined in Equation 3.88, and $\mathbf{T}$ represents the interpolation matrix of the slave element unknowns, from the master element nodal displacements , $\boldsymbol{\delta}$ , defined as

$$\mathbf{T} = \begin{bmatrix} \mathbf{T}_{1,1} & \cdots & \mathbf{T}_{1,8} \\ \vdots & \ddots & \vdots \\ \mathbf{T}_{3,1} & \cdots & \mathbf{T}_{3,8} \end{bmatrix} \tag{3.93}$$

and

$$\mathbf{T}_{ji} = N_{ji}\mathbf{I}_5 \tag{3.94}$$

where $\mathbf{I}_5$ is a five by five identity matrix and $N_{ji}$ is shape functions of the $i^{th}$ node of the master element, defined in Equation 3.35, used to interpolate the displacements of the $j^{th}$ node of the slave element.

Using a similar approach, the variation of displacements $d\mathbf{u}'$, defined in Equation 3.71 are written in terms of the nodal virtual displacements of the master element $d\boldsymbol{\delta}$, defined in Equation 3.43, as

$$d\mathbf{u}' = \boldsymbol{\Lambda}\mathbf{T}d\boldsymbol{\delta} \tag{3.95}$$

Finally, the displacement gradients $\boldsymbol{\theta}_{st}$ defined in Equation 3.72 are written in terms of the nodal displacements $\boldsymbol{\delta}$ and Cartesian derivatives of the shape functions as

$$\boldsymbol{\theta} = \mathbf{G}\boldsymbol{\Lambda}\mathbf{T}\boldsymbol{\delta} \tag{3.96}$$

Where $\mathbf{G}$ is defined as

$$\mathbf{G} = \left[\mathbf{G}_1, \mathbf{G}_2, \mathbf{G}_3\right] \tag{3.97}$$

with

$$\mathbf{G}_j = \left\{0, \frac{dN_j}{dx'}, 0, 0\right\} \tag{3.98}$$

As in the case of the master element, here it is important to note that $\mathbf{G}$ is a matrix defined purely in terms of the nodal coordinates of the slave element. The variation of the gradient defined in Equation 3.75 can now be written in terms of virtual nodal displacements of the master element as

$$d\boldsymbol{\theta} = \mathbf{G}\boldsymbol{\Lambda}\mathbf{T}d\boldsymbol{\delta} \tag{3.99}$$

#### *3.3.5.3 Strain-displacement relationship of the slave element*

The first term of the generalised strain vector defined in Equation 3.67, $\hat{\boldsymbol{\varepsilon}}_{0st}$, represents the linear strains in the stiffener. Using Equation 3.92, these strains are expressed in terms of the master element nodal displacements as

$$\hat{\boldsymbol{\varepsilon}}_{0st} = \mathbf{B}_{0st}\boldsymbol{\Lambda}\mathbf{T}\boldsymbol{\delta} \tag{3.100}$$

Where $\mathbf{B}_{0st}$ is the linear strain-displacement matrix of the slave element defined as

$$\mathbf{B}_{0st} = \left[\mathbf{B}_{0st1}, \mathbf{B}_{0st1}, \mathbf{B}_{0st1}\right] \tag{3.101}$$

with

$$\mathbf{B}_{0st\,j} = \begin{bmatrix} \frac{\partial N_j}{\partial x'} & 0 & 0 & 0 \\ 0 & 0 & -\frac{\partial N_j}{\partial x'} & 0 \\ 0 & \frac{\partial N_j}{\partial x'} & -N_j & 0 \\ 0 & 0 & 0 & -\frac{\partial N_j}{\partial x'} \end{bmatrix} \tag{3.102}$$

Similarly the initial, $\hat{\boldsymbol{\varepsilon}}_{Ist}$, and non-linear , $\hat{\boldsymbol{\varepsilon}}_{NLst}$, components of the generalised strains can be expressed in terms of the master element nodal displacements as

$$\hat{\boldsymbol{\varepsilon}}_{Ist} = \mathbf{B}_{Ist}\boldsymbol{\Lambda}\mathbf{T}\boldsymbol{\delta}; \quad \hat{\boldsymbol{\varepsilon}}_{NLst} = \frac{1}{2}\mathbf{B}_{NLst}\boldsymbol{\Lambda}\mathbf{T}\boldsymbol{\delta} \tag{3.103}$$

Where $\mathbf{B}_{Ist}$ and $\mathbf{B}_{NLst}$ are the initial and non-linear strain-displacement matrices of the slave element defined as

$$\mathbf{B}_{Ist} = \left[\mathbf{B}_{Ist1}, \mathbf{B}_{Ist2}, \mathbf{B}_{Ist3}\right] \tag{3.104}$$

and

$$\mathbf{B}_{NLst} = \left[\mathbf{B}_{NLst1}, \mathbf{B}_{NLst2}, \mathbf{B}_{NLst3}\right] \tag{3.105}$$

where $\mathbf{B}_{Ist}$ and $\mathbf{B}_{NLst}$ are found by taking the variation of $\hat{\boldsymbol{\varepsilon}}_{Ist}$ and $\hat{\boldsymbol{\varepsilon}}_{NLst}$ with respect to the nodal displacements. Since both the initial and non-linear strains contribute only to the axial component of the generalised centroidal strain vector, the initial and non-linear strain displacement sub-matrices of Equations 3.53 and 3.54 can be defined as

$$\mathbf{B}_{Ist\,j} = \begin{bmatrix} \mathbf{B}_{Ist\,j}{}^{a} \\ 0 \\ 0 \\ 0 \end{bmatrix}; \quad \mathbf{B}_{NLst\,j} = \begin{bmatrix} \mathbf{B}_{NLst\,j}{}^{a} \\ 0 \\ 0 \\ 0 \end{bmatrix} \tag{3.106}$$

where $\mathbf{B}_{Ist\,j}{}^{a}$ and $\mathbf{B}_{NLst\,j}{}^{a}$ are found using the variation of strain defined in Equation 3.73 as

$$\begin{aligned} \mathbf{B}_{Ij}{}^{a} &= \mathbf{A}_0 \mathbf{G}_j = \left(\sum_{k=1}^{3} \left(\frac{dN_k}{dx'}\right) \hat{w}_{0k}\right) \mathbf{G}_j \\ \mathbf{B}_{NLj}{}^{a} &= \mathbf{A}_1 \mathbf{G}_j = \left(\sum_{k=1}^{3} \left(\frac{dN_k}{dx'}\right) \hat{w}_{1k}\right) \mathbf{G}_j \end{aligned} \tag{3.107}$$

Substituting Equations 3.100 and 3.103 into Equation 3.67 the generalised strain vector at any point within the slave element is now defined in terms of nodal displacements of the master element $\boldsymbol{\delta}$ as

$$\hat{\boldsymbol{\varepsilon}}_{st} = \left[\mathbf{B}_{0st} + \mathbf{B}_{Ist} + \frac{1}{2}\mathbf{B}_{NLst}\right] \boldsymbol{\Lambda}\mathbf{T}\boldsymbol{\delta} \tag{3.108}$$

It can be observed from Equation 3.108 that the strains are quadratically dependent upon the nodal displacements $\boldsymbol{\delta}$. In a similar fashion, the variation of strain in the slave element can be expressed in terms of the virtual nodal displacement of the master element, $d\boldsymbol{\delta}$, by substituting Equations 3.95 and 3.99 into 3.69 and 3.73 respectively yields the strain variations

$$d\hat{\boldsymbol{\varepsilon}} = \mathbf{B}_{st}\boldsymbol{\Lambda}\mathbf{T}d\boldsymbol{\delta} \tag{3.109}$$

where

$$\mathbf{B}_{st} = \mathbf{B}_{0st} + \mathbf{B}_{Ist} + \mathbf{B}_{NLst} \tag{3.110}$$

# Chapter 4. Derivation and solution of non-linear equations

## 4.1 Introduction

In the previous Chapter the discrete finite element expressions that define the displacement, strains and stresses as a function of the nodal quantities within their respective interpolation regions were derived for both the master and slave elements.

In this Chapter the non-linear equilibrium expressions are derived and discretised. Available solution techniques are discussed and the most suitable to solve the non-linear problem in hand is selected.

The elemental and global finite element expressions required to solve the non-linear problem are derived. A method to include panel initial deformations in the arbitrarily stiffened finite element model is developed.

The techniques required to represent the boundary conditions as well as the loads acting on the stiffened panel are discussed. A new method to account for uniform in-plane compressive load acting on the cross sectional area of stiffeners at the edges of the master element is formulated for both concentrically and eccentrically stiffened elements.

## 4.2 Virtual work equilibrium equations

The virtual work equilibrium expression, for a continuum under the action of conservative body forces and surface tractions, in a Total Lagrangian frame of reference, is defined by Pica and Wood (1980) as

$$\int_V d\boldsymbol{\varepsilon}^T \boldsymbol{\zeta}\, dv = \int_V \rho d\mathbf{u}^T \mathbf{q} dv + \int_a d\mathbf{u}^T \mathbf{p}\, da \qquad 4.1$$

The left hand expression represents the internal virtual work, $dW_{int}$, integrated over the undeformed volume at the reference configuration where $\boldsymbol{\zeta}$ represents the second Piola-Kirchhoff stresses and $d\boldsymbol{\varepsilon}$ represents the virtual Green's strains due to the virtual displacements $d\mathbf{u}$. The expression on the right side of Equation 4.1 represents the external virtual work $dW_{ext}$ containing the body forces and surface tractions. Here, the mass density is represented by $\rho$, whilst the body forces per unit mass and the surface tractions acting over the undeformed area $a$ are represented by $\mathbf{q}$ and $\mathbf{p}$ respectively.

Substituting the generalized strain, $\hat{\boldsymbol{\varepsilon}}$, and the mid-surface stress resultant, $\boldsymbol{\zeta}$, into the left side integral, $dW_{int}$ can be re-written as an area integral giving

$$dW_{int} = \int_A d\hat{\boldsymbol{\varepsilon}}^T \boldsymbol{\zeta}\, dA \tag{4.2}$$

In which the second Piola-Kirchhoff stress resultant vector $\boldsymbol{\zeta}$ and the generalised Green's strain vector $\hat{\boldsymbol{\varepsilon}}$ are given by Equations 3.8 and 3.11 respectively.

As previously mentioned, the right side integrals in Equation 4.1 represent the external virtual work, $dW_{ext}$, and can be separated into virtual work done by body forces $dW_{ext}{}^{b}$ and by surface tractions $dW_{ext}{}^{t}$ as

$$dW_{ext} = dW_{ext}{}^{b} + dW_{ext}{}^{t} \tag{4.3}$$

As the magnitude of the body forces acting in the panels is normally of several orders of magnitude smaller than the surface tractions they have not been included in this investigation (i.e. $dW_{ext}{}^{b} = 0$).

The virtual work done by the surface tractions $dW_{ext}{}^{t}$ is expressed in terms of mid surface quantities as

$$dW_{ext}{}^{t} = \int_{a_s} d\hat{\mathbf{u}}^T \hat{\mathbf{P}}\, da + \int_s d\hat{\mathbf{u}}^T \hat{\mathbf{P}}_e\, ds \tag{4.4}$$

Where $d\hat{\mathbf{u}}$ is the mid-surface virtual displacement vector and $\hat{\mathbf{P}}$ and $\hat{\mathbf{P}}_e$ are the generalised surface and edge tractions evaluated over the plate surfaces $a_s$, and the plate edges $s$ respectively.

Finally, by substituting Equations 4.2 and 4.4 into Equation 4.1 an expression that represents the balance of internal and external virtual work in the shallow-shell, written entirely in terms of mid-surface quantities, is obtained as

$$\int_A d\hat{\boldsymbol{\varepsilon}}^T \boldsymbol{\zeta}\, dA = \int_{a_s} d\hat{\mathbf{u}}^T \hat{\mathbf{P}}\, da + \int_s d\hat{\mathbf{u}}^T \hat{\mathbf{P}}_e\, ds \qquad 4.5$$

This virtual work expression is discretised, substituting the strain-displacement and constitutive expressions derived in the previous chapter for $d\hat{\mathbf{u}}$ and $d\hat{\boldsymbol{\varepsilon}}$ respectively giving

$$d\boldsymbol{\delta}^T \left[ \int_A \mathbf{B}^T \boldsymbol{\zeta}\, da - \mathbf{R}_{ext} \right] = 0 \qquad 4.6$$

Where the equivalent nodal vector $\mathbf{R}_{ext}$ due to the external body forces and tractions is

$$\mathbf{R}_{ext} = \int_{a_s} \mathbf{N}^T \hat{\mathbf{P}}\, da + \int_{a_e} \mathbf{N}^T \hat{\mathbf{P}}_e\, ds \qquad 4.7$$

The load vector $\mathbf{R}_{ext}$ may also contain nodal point loads. Since the nodal virtual displacements $d\boldsymbol{\delta}$ are arbitrary, the element non-linear equilibrium equations become,

$$\boldsymbol{\psi}_{\boldsymbol{\delta}} = \mathbf{R}_{int} - \mathbf{R}_{ext} \qquad 4.8$$

where $\boldsymbol{\psi}_{\boldsymbol{\delta}}$ represents the difference between the external and internal forces. The internal forces, $\mathbf{R}_{int}$, are calculated as

$$\mathbf{R}_{int} = \int_A \mathbf{B}^T \boldsymbol{\zeta}\, da \qquad 4.9$$

## 4.3 Solution to non-linear equilibrium equations

Numerical solution techniques for non-linear problems such as the one expressed in Equation 4.8 are normally classified as incremental, iterative, or incremental-iterative techniques.

In an incremental solution the non-linear load-displacement path is obtained by applying the external loading as a sequence of sufficiently small increments so that the structure can be assumed to respond linearly within each increment. The major advantage of incremental methods is their simplicity. In this regard, these schemes are particularly attractive for the analysis of structures exhibiting moderate non-linearity.

However, since the equilibrium between external loads and internal forces is not evaluated in purely incremental methods; the calculated response curve can drift from the true response. This drift can accumulate and lead to gross and undetectable errors and even solution instabilities.

In contrast to a purely incremental solution, a purely iterative solution is intended to correct, in an iterative fashion, the imbalances between the linear approximation and the actual non-linear response or to reduce the drift in the solution to a tolerable level (McGuire *et al.*, 2000).

In this investigation, the non-linear equilibrium equations 4.8 are solved using the Newton-Raphson method. To illustrate the discussion a graphical representation of the method is presented in Figure 4-1 for a single degree of freedom system.

In this method the non-linear equilibrium equations are expanded in a Taylor's series and truncated to only two terms. If an initial estimate $\boldsymbol{\delta}^i$ for the total displacement vector gives a residual (unbalanced) force such that

$$\boldsymbol{\psi}\ \boldsymbol{\delta}^i \neq 0 \qquad 4.10$$

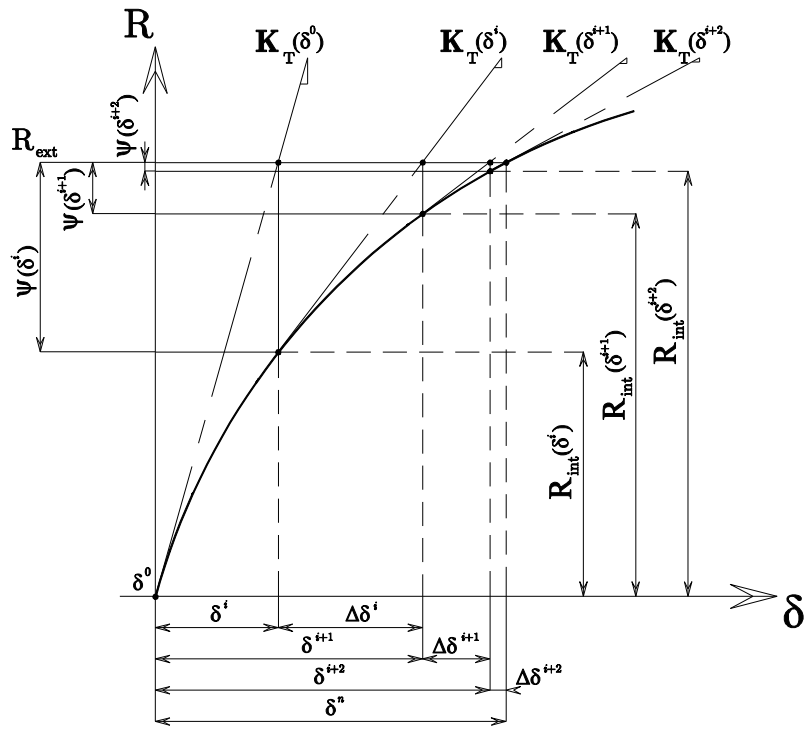


**Figure 4-1 Graphical representation of the Newton-Raphson method.**

Then, an improved value $\boldsymbol{\delta}^{i+1}$ is obtained by equating to zero the linearised Taylor's series expansion of $\boldsymbol{\psi}_{\boldsymbol{\delta}^{i+1}}$ in the neighbourhood of $\boldsymbol{\delta}^i$ as

$$\boldsymbol{\psi}_{\boldsymbol{\delta}^{i+1}} \approx \boldsymbol{\psi}_{\boldsymbol{\delta}^i} + \mathbf{K}_T \Delta\boldsymbol{\delta}^i = 0 \tag{4.11}$$

Where $\mathbf{K}_T$ is the tangent stiffness matrix evaluated at $\boldsymbol{\delta}^i$ and given by

$$\mathbf{K}_T = d\boldsymbol{\psi}_{\boldsymbol{\delta}^i} \tag{4.12}$$

Equation 4.11 is the linear incremental equilibrium equation which gives a linearised approximation to the relation between the residual forces and incremental displacement, $\Delta\boldsymbol{\delta}^i$, at a point $\boldsymbol{\delta}^i$ on the equilibrium path. The improved solution is then found as,

$$\boldsymbol{\delta}^{i+1} = \boldsymbol{\delta}^i + \Delta\boldsymbol{\delta}^i \tag{4.13}$$

Equations 4.11 and 4.13 represent the Newton-Raphson solution to the non-linear Equations 4.8. The terms $\boldsymbol{\psi}_{\boldsymbol{\delta}^i}$ and $\Delta\boldsymbol{\delta}^i$ give a measure of the convergence of the solution.

By successively solving the corrected linearised equations for displacements produced by the corrected forces of the previous cycle and correcting the node forces each time using the nonlinear equations, an iterative scheme is established.

Nevertheless, for a solution method to be reliable and adoptable, both economy in computer cost and accuracy of the obtained results must be considered. The major computational expense of the Newton-Raphson method is the calculation of the tangent stiffness matrix and its factorization (Geradin *et al.*, 1981).

In some structural problems however, the tangent stiffness matrix, $\mathbf{K}_T$, may be quite stable. Consequently, several authors (Bathe and Gracewski, 1981, McGuire *et al.*, 2000, Kao, 1974) have suggested that updating this matrix in each cycle of the Newton-Raphson iteration is no longer necessary and therefore computing time can thus be reduced considerably. This modification to the full Newton-Raphson iteration is known as the modified Newton-Raphson iteration.

Since the Newton-Raphson method requires repeated calculations and inversions of the tangent stiffness matrix, $\mathbf{K}_\mathbf{T}$, a modified Newton-Raphson method is also employed whereby $\mathbf{K}_\mathbf{T}$ is calculated once only on the second iteration of each load increment.

As a result of the modified Newton-Raphson iteration, the use of the original tangent stiffness matrix not only accelerates the convergence but also prevents divergence of the solution for slowly stiffening problems, such as the post-buckling of stiffened plates.

Although the modified iteration could theoretically function with the tangent stiffness matrix being formed and factorized only for the first cycle of the iteration, practically it is recommended (Kao, 1974) that the stiffness matrix is updated and factorized after 3-5 iterations cycles to improve the efficiency of the solution.

According to Kao (Kao, 1974), the solution obtained by both the full Newton-Raphson iteration and its modified form may be taken as an exact solution because examination of convergence criteria are included. It should be noted, however, that the use of this technique may be inadequate for the analysis of structures that exhibit extreme deformations or large internal tensile forces (McGuire *et al.*, 2000).

A drawback of using a purely iterative technique on its own is that it can only provide a single point solution. To overcome this limitation a more flexible technique that combines the advantages of both iterative and incremental schemes is required. In an incremental-iterative solution the applied load, $\mathbf{R}$, is subdivided into a number of incremental load steps, for each one of which an iterative process aimed at satisfying the requirement of equilibrium to within a specified tolerance is performed.

The full or modified Newton-Raphson iteration procedure works well provided the load level is below the critical load or limit point. At a limit point, the Newton-Raphson fails to converge as the stiffness of the structure is zero or negative. To overcome this limitation, common to the snap-back and snap-through analysis of deep shells under transverse load, it is recommended that the Newton-Raphson method is constrained by using a suitable displacement control scheme as suggested by Riks (1979) and Crisfield (1981).

However, since this behaviour is not expected in the analysis of flat stiffened panels under transverse load or in the post-buckling analysis of stiffened panels under in-plane load, this investigation uses an incremental-iterative solution procedure, that combines Euler incrementation with either a full or modified Newton-Raphson iteration.

### 4.3.1 **Tangent stiffness matrix**

The tangent stiffness matrix given in Equation 4.12 may be written as

$$\mathbf{K_T} = d\ \mathbf{R}_{int} - \mathbf{R}_{ext} = d\left(\int_A \mathbf{B}^T \boldsymbol{\zeta}\, da - \mathbf{R}_{ext}\right) \tag{4.14}$$

For conservative loading, the partial derivative of the external load vector with respect to the nodal displacements is equal to zero. Hence, Equation 4.14 is reduced to

$$\mathbf{K_T} = d\left(\int_A \mathbf{B}^T \boldsymbol{\zeta}\, da\right) \tag{4.15}$$

or

$$\mathbf{K}_T = \int_A d\mathbf{B}^T\, \boldsymbol{\zeta}\, da + \int_A \mathbf{B}^T\ d\boldsymbol{\zeta}\ da \tag{4.16}$$

In the first integral, the variation $\mathbf{B}$ is defined as

$$d\mathbf{B} = d\left[\mathbf{B}_0 + \mathbf{B}_I + \mathbf{B}_{NL}\right] \tag{4.17}$$

Noting that both $\mathbf{B}_0$ and $\mathbf{B}_I$ are not a function of the nodal displacements $\boldsymbol{\delta}$, Equation 4.17 is reduced to

$$d\mathbf{B} = d\mathbf{B}_{NL} \tag{4.18}$$

by substituting Equation 3.55 into 4.18

$$d\mathbf{B}_{NL} = d\mathbf{B}_{NL}{}^{p} = d\mathbf{A}_1\mathbf{G} \tag{4.19}$$

Using this expression, the first integral of Equation 4.16 can be re-arranged into

$$\int_A d\mathbf{B}^{T}\boldsymbol{\zeta}\, da = \int_A d\mathbf{A}_1\mathbf{G}^{T}\boldsymbol{\zeta}\, da = \int_A \mathbf{G}^{T}\mathbf{d}\mathbf{A}_1{}^{T}\boldsymbol{\zeta}\, da \tag{4.20}$$

Finally using the special property of the matrix $\mathbf{A}_1$, defined by Zienkiewicz and Taylor (Zienkiewicz and Taylor, 1994) as

$$d\mathbf{A}_1{}^{T}\boldsymbol{\zeta} = \begin{bmatrix} N_x & N_{xy} \\ N_{xy} & N_y \end{bmatrix}\mathbf{G} \tag{4.21}$$

the first integral in Equation 4.16 becomes the initial stress stiffness matrix depending on the stress level within the element

$$\mathbf{K}_\sigma = \int_A \mathbf{G}^{T}\begin{bmatrix} N_x & N_{xy} \\ N_{xy} & N_y \end{bmatrix}\mathbf{G}\, da \tag{4.22}$$

In the second integral expression of Equation 4.16 the stress resultants $\boldsymbol{\zeta}$ are a linear functions of the strains $\hat{\boldsymbol{\varepsilon}}$. Hence, the variation of the stress may be written as,

$$d\boldsymbol{\zeta} = \hat{\mathbf{D}}\, d\hat{\boldsymbol{\varepsilon}} \tag{4.23}$$

Substituting for $d\hat{\boldsymbol{\varepsilon}}$ from Equation 3.59 gives $d\boldsymbol{\zeta}$ in terms of the variation of $\boldsymbol{\delta}$ as

$$d\boldsymbol{\zeta} = \hat{\mathbf{D}}\mathbf{B} \tag{4.24}$$

Hence the second integral becomes

$$\int_A \left(\mathbf{B}_0 + \mathbf{B}_I + \mathbf{B}_{NL}\right)^T \hat{\mathbf{D}} \left(\mathbf{B}_0 + \mathbf{B}_I + \mathbf{B}_{NL}\right) da \tag{4.25}$$

or

$$\begin{aligned} \mathbf{K}_0 &= \int_A \mathbf{B}_0{}^T \hat{\mathbf{D}} \mathbf{B}_0 da \\ \mathbf{K}_{NL} &= \int_A \left(\mathbf{B}_I + \mathbf{B}_{NL}\right)^T \hat{\mathbf{D}} \left(\mathbf{B}_I + \mathbf{B}_{NL}\right) da \end{aligned} \tag{4.26}$$

where $\mathbf{K}_0$ and $\mathbf{K}_{NL}$ represent the small displacement and the large displacement stiffness matrices respectively.

Finally, combining Equations 4.26 and 4.22 the tangent stiffness matrix is found as

$$\mathbf{K}_T = \mathbf{K}_0 + \mathbf{K}_{NL} + \mathbf{K}_\sigma \tag{4.27}$$

The tangent stiffness matrix of the slave element, $\mathbf{K}_{Tst}$, is defined in a similar fashion as

$$\mathbf{K}_{Tst} = \mathbf{K}_{0st} + \mathbf{K}_{NLst} + \mathbf{K}_{\sigma st} \tag{4.28}$$

where the initial stress stiffness, linear and non-linear stiffness matrices of the slave element expressed as function of the master element degrees of freedom are defined as

$$\begin{aligned} \mathbf{K}_{0st} &= \mathbf{T}^T \mathbf{\Lambda}^T \left( \int_l \mathbf{B}_{0st}{}^T \hat{\mathbf{D}}_{st} \mathbf{B}_{0st} ds \right) \mathbf{\Lambda} \mathbf{T} \\ \mathbf{K}_{NLst} &= \mathbf{T}^T \mathbf{\Lambda}^T \left( \int_A \left(\mathbf{B}_{Ist} + \mathbf{B}_{NLst}\right)^T \hat{\mathbf{D}}_{st} \left(\mathbf{B}_{Ist} + \mathbf{B}_{NLst}\right) ds \right) \mathbf{\Lambda} \mathbf{T} \\ \mathbf{K}_{\sigma st} &= \mathbf{T}^T \mathbf{\Lambda}^T \left( \int_l \mathbf{G}_{st}{}^T N_{st} \mathbf{G}_{st} ds \right) \mathbf{\Lambda} \mathbf{T} \end{aligned} \tag{4.29}$$

Finally the tangent stiffness matrix of the stiffened element, i.e. the combined master-slave element, is obtained as

$$\mathbf{K}_{T\,total} = \mathbf{K}_T + \sum_{i=1}^{n} \mathbf{K}_{Tst\,i} \tag{4.30}$$

where $n$ represents the total number of slave elements for which trajectories cross the master element interpolation region.

### 4.3.2 Secant stiffness matrix

To evaluate the residual nodal force vector $\boldsymbol{\psi}_{\boldsymbol{\delta}}$ of Equation 4.8 the equivalent nodal forces due to the stress resultant vector $\boldsymbol{\zeta}$ may be written for a typical element as

$$\mathbf{P}_i = \int_A \mathbf{B}^T \boldsymbol{\zeta}\, da \tag{4.31}$$

or, expressing the stresses using the constitutive relations given in Equation 3.22

$$\mathbf{P}_i = \int_A \mathbf{B}^T \hat{\mathbf{D}} \hat{\boldsymbol{\varepsilon}}\, da \tag{4.32}$$

Substituting $\mathbf{B}$ with Equation 3.60 and expressing $\hat{\boldsymbol{\varepsilon}}$ as function of the nodal displacements using Equation 3.57 yields

$$\mathbf{P}_i = \mathbf{K}_S \boldsymbol{\delta} \tag{4.33}$$

where $\mathbf{K}_S$ is the secant stiffness matrix of the master element defined as

$$\mathbf{K}_S = \int_A \left(\mathbf{B_0} + \mathbf{B_L}\right)^T \hat{\mathbf{D}} \left(\mathbf{B_0} + \frac{1}{2}\mathbf{B_L}\right) dA \tag{4.34}$$

Similarly, the secant stiffness matrix of the slave element, $\mathbf{K}_{S\,st}$, expressed as function of the master element degrees of freedom is defined as

$$\mathbf{K}_{S\,st} = \mathbf{T}^T \boldsymbol{\Lambda}^T \left( \int_l \left(\mathbf{B}_{0st} + \mathbf{B}_{Lst}\right)^T \hat{\mathbf{D}}_{st} \left(\mathbf{B}_{0st} + \frac{1}{2}\mathbf{B}_{Lst}\right) ds \right) \boldsymbol{\Lambda}\mathbf{T} \tag{4.35}$$

Finally the secant stiffness matrix of the stiffened element, i.e. the combined master-slave element, is obtained as

$$\mathbf{K}_{S\,total} = \mathbf{K}_S + \sum_{i=1}^{n} \mathbf{K}_{S\,st\,i} \tag{4.36}$$

where $n$ represents the total number of slave elements for which trajectories cross the master element interpolation region.

### 4.3.3 **Panel initial deformations**

The panel initial deformation, $\hat{w}_0$, required for the non-linear buckling analysis of unstiffened and stiffened panels are calculated in this investigation by conducting a preliminary Eigen-value buckling analysis. The analysis has two functions: first it determines a critical buckling load (Eigen-value) and secondly, and most importantly, it defines the buckled shape of the panel (Eigen-vector).

The linear buckling analysis has been discussed in detail by other authors (Mukhopadhyay and Mukherjee, 1990, Ray, 1997, Prusty and Satsangi, 2001a), and therefore only the final global matrices are presented in this Section. For all the mathematical details, the reader is advised to refer to the cited literature. The Eigen value problem is defined as

$$\mathbf{K}_{0total} - \lambda \mathbf{K}_{\sigma total} \ \boldsymbol{\delta}_v = 0 \qquad 4.37$$

were $\lambda$ and $\boldsymbol{\delta}_v$ represent the Eigen-value and Eigen-vector respectively whilst $\mathbf{K}_{0total}$ and $\mathbf{K}_{\sigma total}$ represents the linear and geometrical stiffness matrices respectively defined in Section 4.3.1.

A major difference with respect to previous investigations (Mukhopadhyay and Mukherjee, 1990, Ray, 1997, Prusty and Satsangi, 2001a) is that in the present work a linear static analysis was conducted in order to calculate, and not to assume, the in-plane stresses required to evaluate the geometrical stiffness matrix.

Equation 4.37 is solved using the simultaneous iteration technique presented by Corr and Jennings (1976). Once the solution is obtained, the Eigen-vector, $\boldsymbol{\delta}_v$, is normalised as

$$\left\| \boldsymbol{\delta}_v \right\| = \frac{1}{\hat{w}_{ref}} \boldsymbol{\delta}_v \qquad 4.38$$

where $\hat{w}_{ref}$ represents the maximum out of plane deformation of the panel.

Finally the initial deformation vector, $\boldsymbol{\delta}_{ini}$, is obtained by multiplying the normalised Eigen-vector by the initial deformation factor, $f_{ini}$,defined by the user as a percentage of the panel thickness, as

$$\boldsymbol{\delta}_{ini} = \left\|\boldsymbol{\delta}_0\right\| f_{ini} \tag{4.39}$$

It is important to note that this vector contains only the initial deformations of the master element.

In order to calculate the initial deformations of the slave element, $\boldsymbol{\delta}_{ini\,st}$, it is suggested that the master element initial deformations are transformed using the expression defined in Equation 3.92, as

$$\boldsymbol{\delta}_{ini\,st} = \boldsymbol{\Lambda}\mathbf{T}\boldsymbol{\delta}_{ini} \tag{4.40}$$

## 4.4 Loads

Stiffened panels on a ship are normally subjected to two types of loadings: in-plane and/or transverse loads.

Transverse loading, as shown in diagram **a** of Figure 4-2, is created by hydrostatic pressure acting on the submerged plating below the water line.

In-plane loads (diagram **b** of Figure 4-2) on the other hand are created by the bending of the hull girder. Depending on the direction of the hull girder bending, these forces will be either tensile or compressive.

Both loads cases must be accurately represented in the finite element model in order to be of practical use for designers of marine structures.

As part of the non-linear incremental-iterative solution method discussed in Section 4.2, these loads are applied in a stepwise fashion, where each load step represents a fraction of the final load.

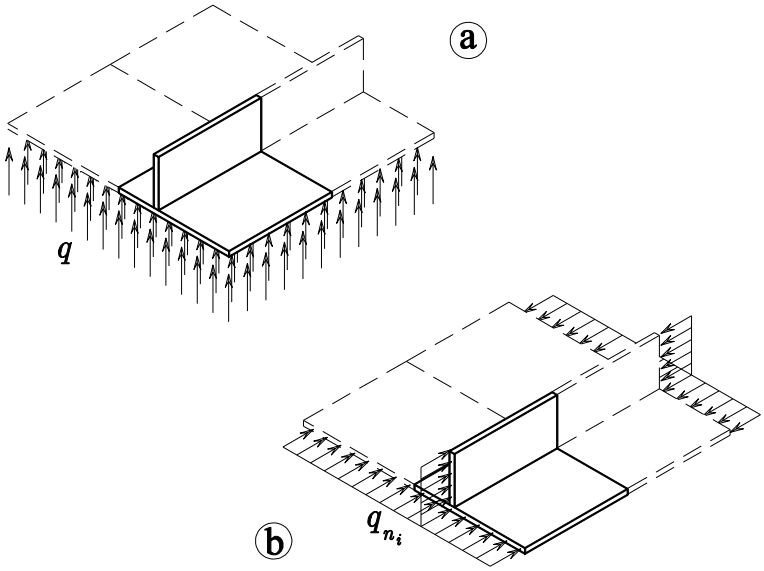


**Figure 4-2 Loads in a ship stiffened panel**

### 4.4.1 **Transverse Loads**

Transverse loads are applied using a consistent load vector for the element. Here the interpolation functions are used to obtain the loads at each node of the element.

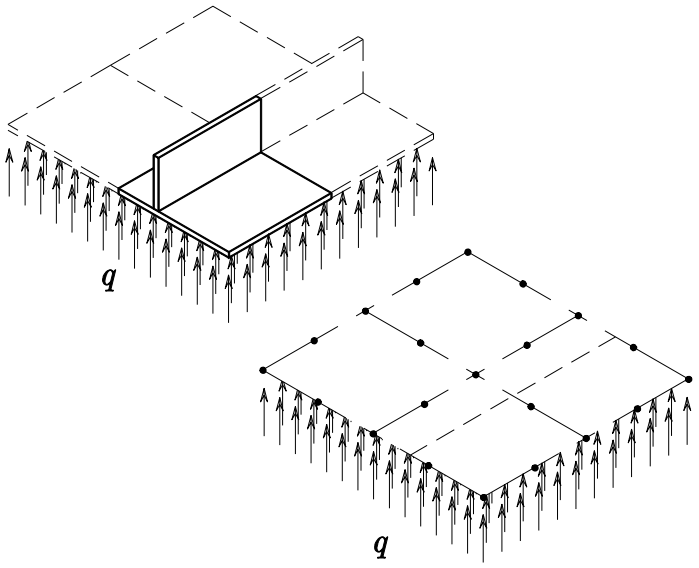


**Figure 4-3 Transverse loads in the stiffened element**

The consistent load vector for the stiffened shallow shell element due to a uniformly distributed load $q$ is given by

$$\mathbf{p}_e = \int_A \mathbf{N}^T q dA \qquad 4.41$$

The direction of the distributed load $q$ is given by the normal of the element. Where the orientation of the element normal is defined using the right hand rule.

### 4.4.2 In-plane loads

In finite element models, in-plane tensile and compressive loads are normally applied as either a distributed linear load or as a constant edge displacement along the edges of the panel.

As discussed in Section 2.2.3, previous investigations on stiffened panels under in-plane loads have assumed a uniform stress field to obtain linear buckling loads. However that approach is not applicable for non-linear buckling calculations as the in-plane stress field is non-uniform. Furthermore, this non-uniformity changes along the non-linear response path.

Consequently, in this Section a new and original procedure for correctly modelling in-plane loads is now discussed for concentrically and eccentrically stiffened panels.

#### *4.4.2.1 Concentric Stiffeners*

When a concentrically stiffened panel is loaded in compression, as shown in diagram **a** of Figure 4-4, both the stiffener and plate cross sectional areas are able to receive load.

However, in a finite element model created using arbitrarily stiffened elements, such as the one shown in diagram **b** of Figure 4-4, the stiffener cross sectional area, $A_{st}$, is not physically represented in the model.

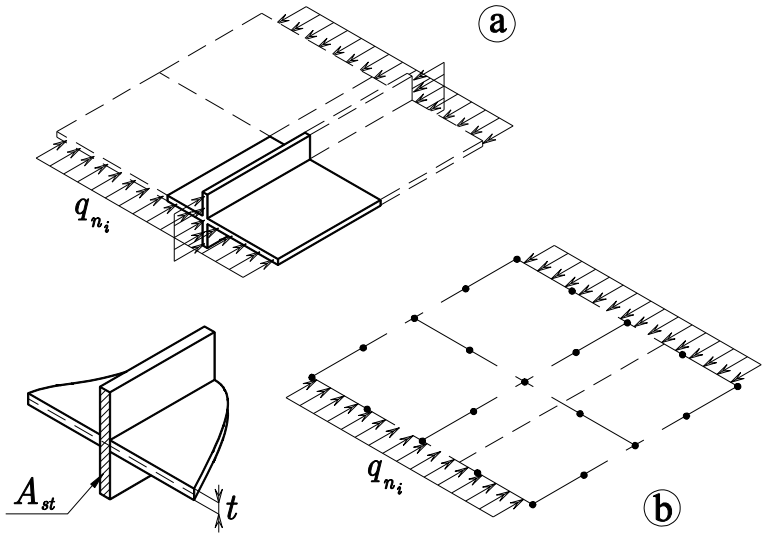


**Figure 4-4 Edge load for concentrically stiffened elements.**

Consequently if a uniform in-plane load is to be applied to the entire edge of the panel (plate and stiffener), a fraction of the total force acting on the edge of the panel will be missing. This absence causes the in-plane deformations to be erroneous and, since an incorrect displacement field generates an incorrect in-plane stress field, this modelling issue will affect not only the strength calculations but also the stability calculations that are dependent on the in-plane stress field.

In order to address this previously unreported modelling issue, an equivalent concentrated force method is proposed in this investigation. The first step of the method is to determine the magnitude of the missing stiffener load, $F_{st}$. Here it is suggested that this force is calculated as:

$$F_{st} = \frac{q_{n_i} A_{st}}{t} \qquad 4.42$$

Where $q_{n_i}$ is the normal force per unit length applied to the $i^{th}$ edge of the panel, $A_{st}$ is the stiffener cross sectional area and $t$ is the thickness of the panel.

The second step requires determining how this load is to be applied to the edge nodes of the stiffened element. It is evident that, since the stiffness of the stiffener element is distributed over the plate element according to the position of its nodes, the force has to be distributed following a similar consideration.

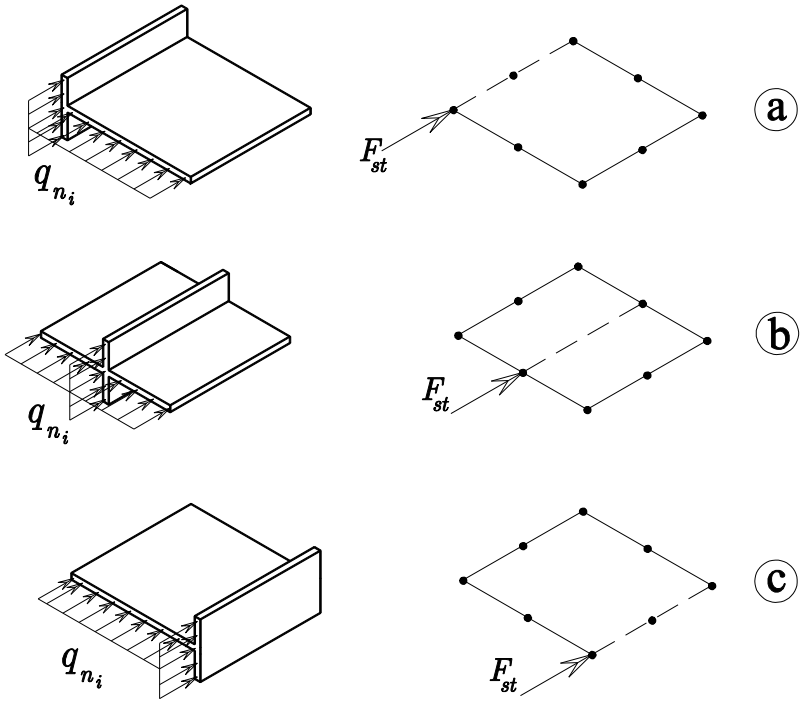


**Figure 4-5 Stiffener load application for case 1.**

The first and simplest scenario, designated as case 1, is when the location of the end node of a stiffener coincides with the location of any of nodes lying on the edge of the shallow shell element.

In such a configuration it is suggested that the extra load due to the stiffener, $F_{st}$, is assigned directly to the corresponding degree of freedom of the coinciding node as shown in Figure 4-5. It must be noted that the suggested procedure is also valid for users of general purpose finite element codes attempting to model stiffened panels under in-plane loads by placing beam elements along the edges of shell elements as shown in diagrams **a** and **c** of Figure 4-5.

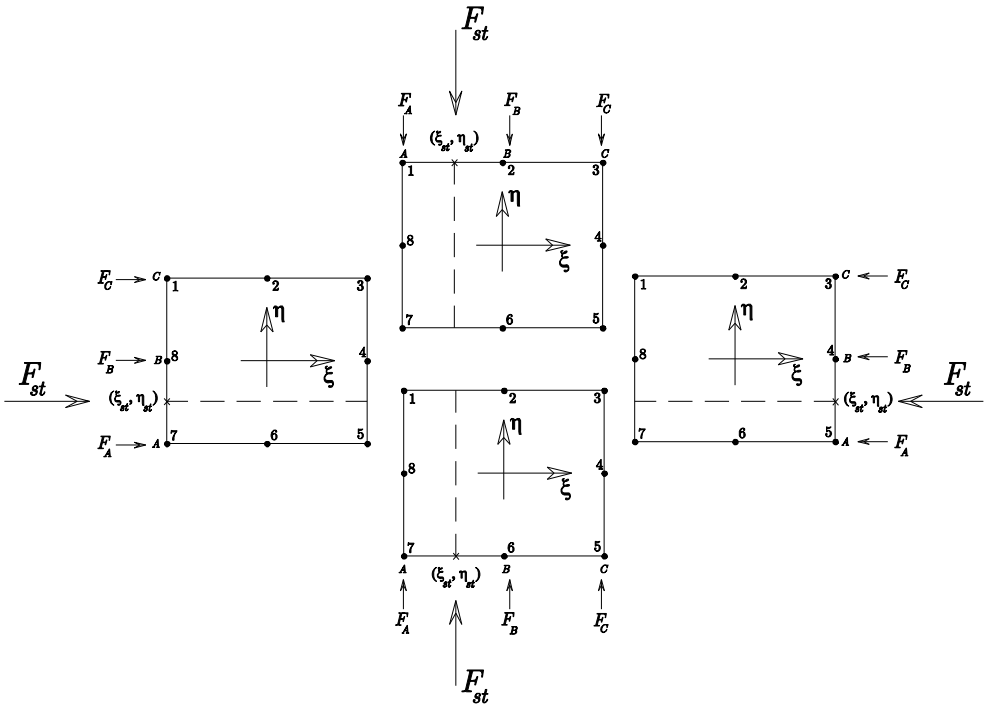


**Figure 4-6 Stiffener load application for case 2.**

The second and more complex scenario, designated as case 2, is shown in Figure 4-6. In this case the end node of a stiffener does not coincide with the location of any of the nodes lying on the edge of the shallow shell element and therefore the load must be distributed among all the edge nodes. Since the stiffness of the stiffener element is distributed over the shallow shell element using the shape functions of the shallow shell element (see Section 3.2.7.2), it is suggested that the extra load is distributed along the edge node in a similar fashion:

$$\begin{aligned} F_A &= N_{A\,\xi_{st},\eta_{st}}\, F_{st} \\ F_B &= N_{B\,\xi_{st},\eta_{st}}\, F_{st} \\ F_C &= N_{C\,\xi_{st},\eta_{st}}\, F_{st} \end{aligned} \qquad 4.43$$

Here, $F_{st}$ is the stiffener load calculated using Equation 4.42, and $N_A, N_B$ and $N_C$ are the shape functions, defined in Equation 3.35, of nodes A, B and C respectively evaluated where the end point of the stiffener, $\xi_{st}, \eta_{st}$ , touches the edge of the shallow shell element as represented in Figure 4-6.

#### 4.4.2.2 Eccentric Stiffeners

When the stiffener is eccentric the problem becomes more complicated. In the concentric case both plate and stiffener share a common neutral surface for bending. However, when a panel is reinforced by placing stiffeners at only one side of the plate, separation exists between the plane of bending of the stiffener and the plane of bending of the plate. This offset between bending planes is responsible for coupling terms in the stiffness matrix of the arbitrary orientated stiffened element that link in-plane displacements with out of the plane displacements.

Moreover, in an eccentrically stiffened panel the force applied to the stiffener is applied at a distance from the middle surface of the shell element as shown in Figure 4-7.

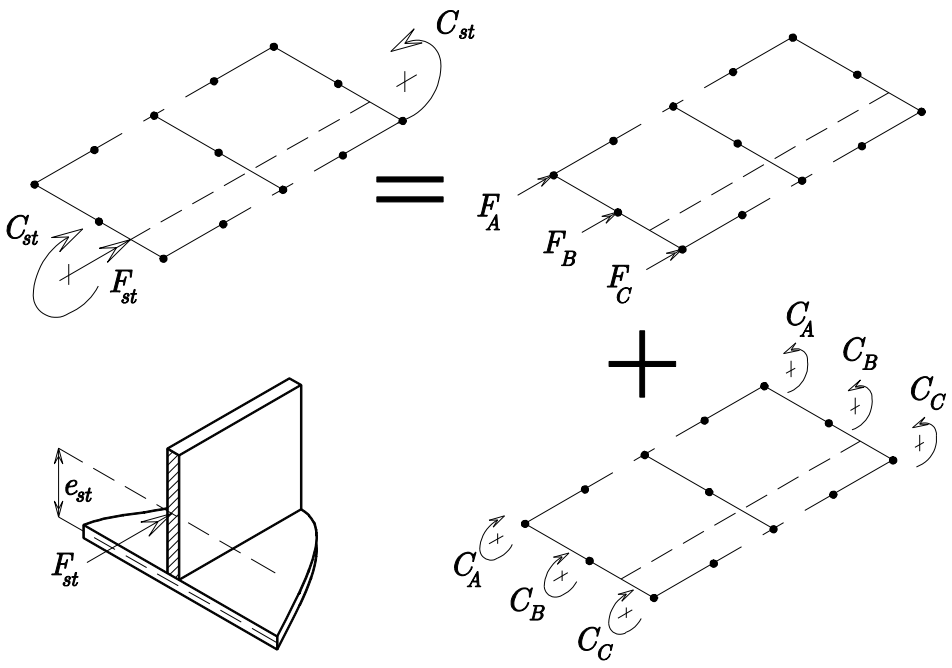


**Figure 4-7 Extra stiffener moment for eccentrically stiffened panels.**

Therefore, if the stiffener load is neglected, not only non-uniform in-plane displacements but also artificial out of plane displacements are generated due to the now coupled terms in the stiffness matrix of the arbitrarily stiffened shallow shell element.

To overcome this unrealistic behaviour it is suggested that, in addition to a concentrated load, a couple is also applied to the loaded edge of the panel. The magnitude of this couple, $C_{st}$, is determined by

$$C_{st} = F_{st} e_{st} \tag{4.44}$$

Where $F_{st}$ is the magnitude of the extra load due to the stiffener calculated using Equation 4.42 and $e_{st}$ is the eccentricity of the stiffener.

The application of this moment to the corner and mid-side nodes of the shallow shell element follows the same principles discussed for case 1 of Section 4.4.2.1. However, when the stiffener end does not coincide with the location of a shallow shell element edge node (case 2), it is suggested that the magnitude of each nodal couple be calculated as

$$\begin{aligned} C_A &= F_A e_{st} \\ C_B &= F_B e_{st} \\ C_C &= F_C e_{st} \end{aligned} \tag{4.45}$$

where $F_A$, $F_B$ and $F_C$ are the distributed nodal forces calculated using Equation 4.43.

It is crucial to note that the displacement boundary conditions on the unloaded side of the panel will not generate the reaction couple necessary to maintain static equilibrium. It is therefore necessary to also apply the couple $C_{st}$ to the unloaded edge of the panel following the procedure discussed above.

The application of this new method is discussed and validated for both concentric and eccentric stiffening configurations in Sections 6.3.1, 6.3.2 and 6.3.3.

### 4.4.3 **Load vector assembly**

The global load vector $\mathbf{R}_{ext}$ is obtained by assembling the equivalent nodal loads $\mathbf{R}_e$ at element level. For concentrated loads the load value is applied to the corresponding degree of freedom of the particular node.

## 4.5 Boundary conditions and nodal constraints

Once all the elemental tangent stiffness matrices have been assembled into the global stiffness matrix, $\mathbf{K}_T$, it is necessary to apply the essential boundary conditions before the linearised equilibrium equations can be solved for the unknown nodal incremental displacements. The physical reason for this is that without supports the structure will float away if the slightest external load is applied. Mathematically the tangent stiffness matrix $\mathbf{K}_T$ is singular and cannot be inverted so long rigid-body motions are still possible.

Consequently, the singularity of $\mathbf{K}_T$ must therefore be removed in order to solve for the unknown incremental displacements. In this investigation the boundary conditions are introduced using the penalty method (Cook *et al.*, 1989). In this scheme any or all structural nodal degree of freedom can be constrained by incorporating a very large diagonal stiffness coefficient, known as the penalty number, to $\mathbf{K}_T$.

Moreover, using the penalty method it is possible to prescribe a single or multiple nonzero nodal degrees of freedom. In this case, in addition to having a very large diagonal stiffness coefficient added to $\mathbf{K}_T$, a large load is added to the corresponding component of the external load vector $\mathbf{R}$. The magnitude of this load is equal to the product of the penalty number and the magnitude of the prescribed nonzero degree of freedom. This feature of the penalty method allows the modelling of uniform edge shortening in non-linear buckling problems.

It is important to note that, although the global secant stiffness $\mathbf{K}_S$ does not need to be inverted, it also must be constrained using the previously mentioned scheme in order to correctly evaluate the internal forces in the finite element model.

The nodal constraints used in this investigation to represent the essential simply supported boundary conditions, described graphically in Figure 4-8, are listed in Table 4-1, whilst the clamped boundary conditions, described graphically in Figure 4-9, are listed in Table 4-2.

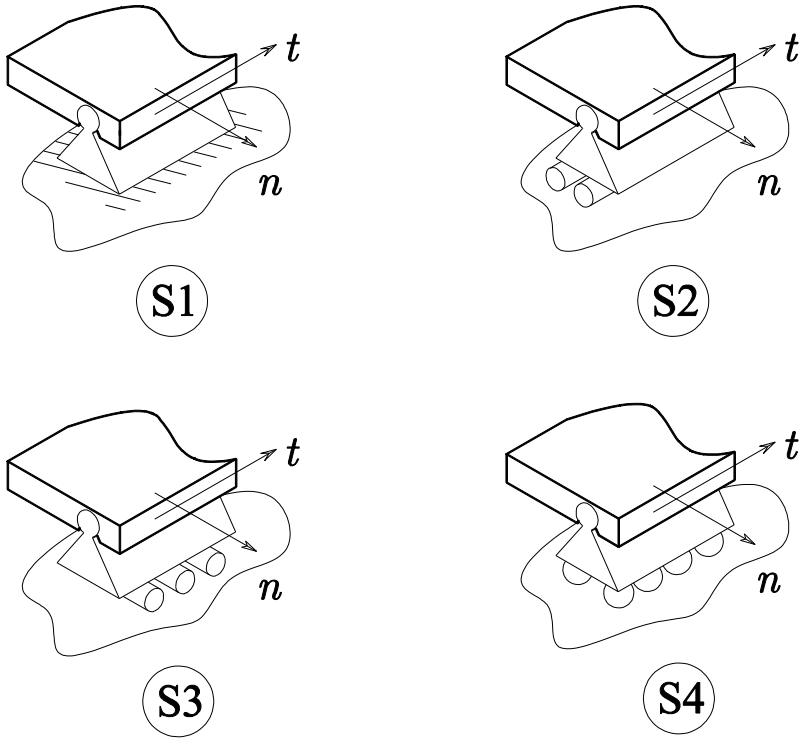


**Figure 4-8 Simply supported boundary conditions along the edge of the panel.**

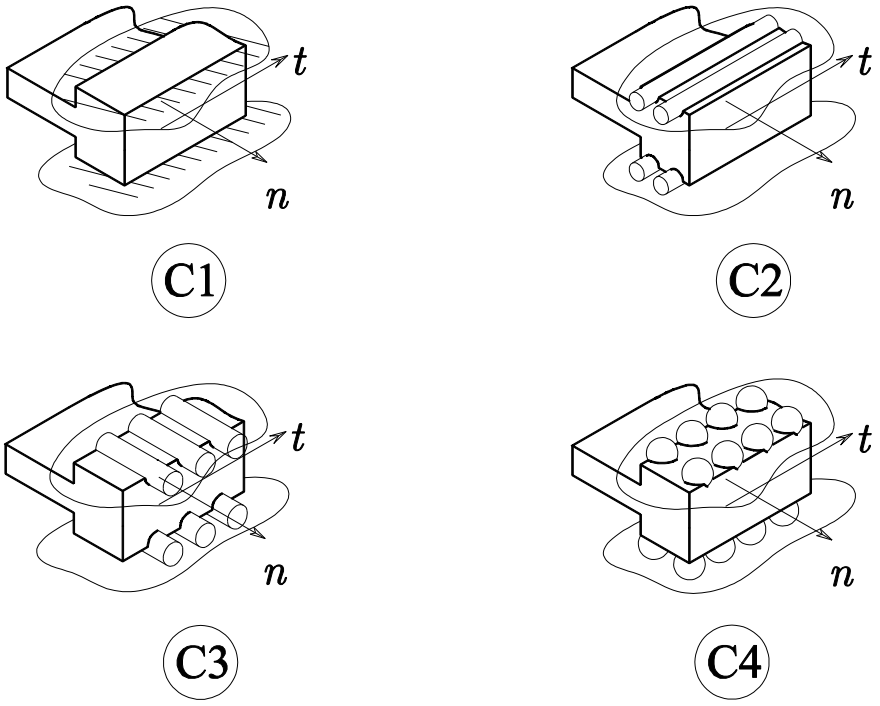


**Figure 4-9 Clamped boundary conditions along the edge of the panel.**

**Table 4-1 Nodal constrains used to represent simply supported boundary conditions.**

| S1 | S2 | S3 | S4 |
|---|---|---|---|
| $w = 0$ | $w = 0$ | $w = 0$ | $w = 0$ |
| $\frac{dw}{dt} = 0$ | $\frac{dw}{dt} = 0$ | $\frac{dw}{dt} = 0$ | $\frac{dw}{dt} = 0$ |
| $u_n = 0$ | $u_t = 0$ | $u_n = 0$ | |
| $u_t = 0$ | | | |

**Table 4-2 Nodal constrains used to represent clamped boundary conditions.**

| C1 | C2 | C3 | C4 |
|---|---|---|---|
| $w = 0$ | $w = 0$ | $w = 0$ | $w = 0$ |
| $\frac{dw}{dn} = 0$ | $\frac{dw}{dn} = 0$ | $\frac{dw}{dn} = 0$ | $\frac{dw}{dn} = 0$ |
| $\frac{dw}{dt} = 0$ | $\frac{dw}{dt} = 0$ | $\frac{dw}{dt} = 0$ | $\frac{dw}{dt} = 0$ |
| $u_n = 0$ | $u_t = 0$ | $u_n = 0$ | |
| $u_t = 0$ | | | |

This notation is analogous to that suggested by Almroth's (1966) where the subscripts $n$ and $t$ denote the directions in the plane of the panel normal and tangential to the edge under consideration as defined in Figure 4-10.

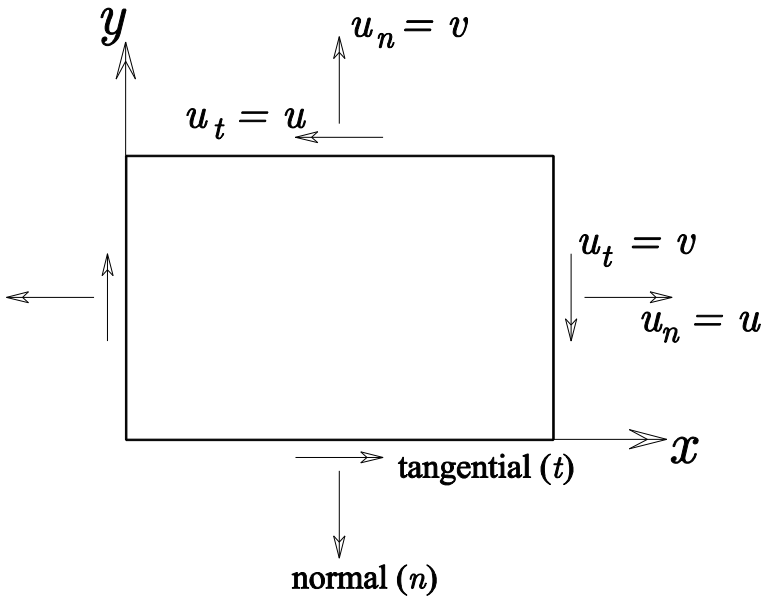


**Figure 4-10 Normal and tangential directions along the edges of the panel.**

## 4.6 Convergence criteria and convergence tolerance

As stated by Bathe and Cimento (1980), the solution results should be checked at the end of each iteration, to assess whether it has converged within a preset tolerance(s), whether more iteration is necessary or whether the iteration process is diverging. If the convergence tolerance is too loose, inaccurate results are obtained, and if the tolerance is too tight, excessive computational effort is spent obtaining needless accuracy.

Although convergence criteria based on stress and energy considerations exist, most authors (Crisfield, 1979, Bergan, 1972) recommend the use of convergence criteria based on either a residual force criterion or a displacement criterion.

### 4.6.1 Residual force criterion

The residual force convergence criterion is normally based on a comparison between the current unbalanced or residual forces within the structure and the external loads. The total residual force convergence criterion is defined as

$$conv_0 = \frac{\sqrt{\boldsymbol{\psi}^T \boldsymbol{\psi}}}{\sqrt{\mathbf{R}_{ext}{}^T \mathbf{R}_{ext}}} \tag{4.46}$$

where $\boldsymbol{\psi}$ is the internal-external force imbalance vector and $\mathbf{R}_{ext}$ is the external force vector. As the geometrically non-linear analysis of stiffened plate involves mixed loads, i.e. forces and moments, this expression must be modified appropriately. The most commonly used approach is to scale both the internal/applied force imbalance and the applied external force. Here an obvious choice for the scaling is

$$\underline{\mathbf{S}} = diag\ \mathbf{K}_t^{-1} \tag{4.47}$$

Which yields,

$$conv_0 = \frac{\sqrt{\boldsymbol{\psi}^T \underline{\mathbf{S}} \boldsymbol{\psi}}}{\sqrt{\mathbf{R}_{ext}{}^T \underline{\mathbf{S}} \mathbf{R}_{ext}}} \tag{4.48}$$

### 4.6.2 **Displacement criteria**

Given that the deformations in each iteration are the base of any equilibrium requirement, it has been suggested (McGuire *et al.*, 2000) to adopt a convergence criterion based on these calculated values.

Such criterion should verify that the change in the last iterative displacement, measured in an appropriate norm, does not exceed a given tolerance. To obtain such displacement criterion a non-dimensional iterative displacement vector is first defined as:

$$\Delta u^i = \left\{ \frac{\Delta u_1}{r_{1\,ref}}, \frac{\Delta u_2}{r_{2\,ref}}, \ldots, \frac{\Delta u_k}{r_{k\,ref}}, \ldots, \frac{\Delta u_m}{r_{m\,ref}} \right\}^i \tag{4.49}$$

Where $m$ is the total number of degrees of freedom, and $\Delta u_k{}^i$ is the incremental change in the $k^{th}$ degree of freedom during the $i^{th}$ iteration. Every degree of freedom is scaled by a reference displacement quantity $r_{k\,ref}$, which represents the largest degree of freedom of the corresponding type. In other words, the translational degrees of freedom are scaled by the largest translation, and the rotational degrees of freedom are scaled by the largest rotation. As suggested by Bergan and Clough (1972), three different convergence criteria can be established by using three alternative norms for measuring the size of the $\Delta u^i$.

$$conv_1 = \frac{1}{N} \sum_{k=1}^{m} \left| \frac{\Delta u_k}{r_{k\,ref}} \right| \tag{4.50}$$

$$conv_2 = \left[ \frac{1}{N} \sum_{k=1}^{m} \left| \frac{\Delta u_k}{r_{k\,ref}} \right|^2 \right]^{\frac{1}{2}} \tag{4.51}$$

$$conv_3 = \max_k \left| \frac{\Delta u_k}{r_{k\,ref}} \right| \tag{4.52}$$

Where equations 4.50, 4.51 and 4.52 represent respectively the absolute Euclidian, modified Euclidean and maximum norms of the non-dimensional iterative displacement

vector. Both, the absolute and the Euclidean norm are modified by dividing them by $N$ to obtain quantities that are independent of the total number of degrees of freedom.

### 4.6.3 **Convergence tolerance**

For any of the previously mentioned criterion, the following expression can be used,

$$conv_i < \gamma \tag{4.53}$$

where $\gamma$ represents the convergence tolerance defined by the user.

Normally the tolerance value is chosen between $10^{-2}$ and $10^{-6}$ depending on the type of structural problem in hand.

Stiffening (hardening) problems, such as the large deflection of a transversely loaded stiffened panel, require a tight force tolerance since a small error in the equilibrium state (force vector norm), can be correlated to a large error in the displacement variables (Bathe and Cimento, 1980).

On the other hand, softening problems, such as the non-linear buckling response of in-plane loaded imperfect stiffened panels requires a tight displacement tolerance since a small error in the displacement configuration (displacement vector norm) can be correlated to a large error in the equilibrium of force values (Bathe and Cimento, 1980).

## 4.7 Computer code implementation

In order to study the geometrically non-linear response of stiffened panels, the formulation was coded into a FORTRAN 90 computer program named NLSPAN (Non-Linear Stiffened Panel ANalysis) using the Intel Visual Fortran compiler.

The development of this computer code was aimed only at validating the proposed arbitrarily stiffened element formulation and is not expected to have the extensive analysis and modelling capabilities of commercially available Finite Element packages. Consequently, only a general overview of this code is included in this section.

Following common finite element programming practice, the computer code was divided into three main modules, namely a pre-processor, a non-linear solver and a post-processor.

In the pre-processor module, the details of the given structure such as geometry, initial deformations, boundary conditions, material properties, loading, stiffener location and properties, lamination in the panel skin and the stiffener are defined using a single or multiple (batch) input file(s). Using this information the panel domain is first discretised using the master elements.

Once the master element mesh is defined, the stiffener trajectory is used to intercept the master element mesh lines. This procedure defines the virtual slave element mesh, i.e. location of the slave elements within the master elements.

The non-linear solver module, described in the flow chart presented in Figure 4-11 is then used to generate and solve the non-linear equilibrium equations described in Section 4.2 using the Newton-Raphson procedure described in Section 4.3.

For each load increment an external load vector is calculated first as described in Section 4.4.

Next the global tangent stiffness is computed by assembling first the linearised equation of the master elements and then augmenting them with the stiffness contribution of the slave elements as described in Equation 4.30.

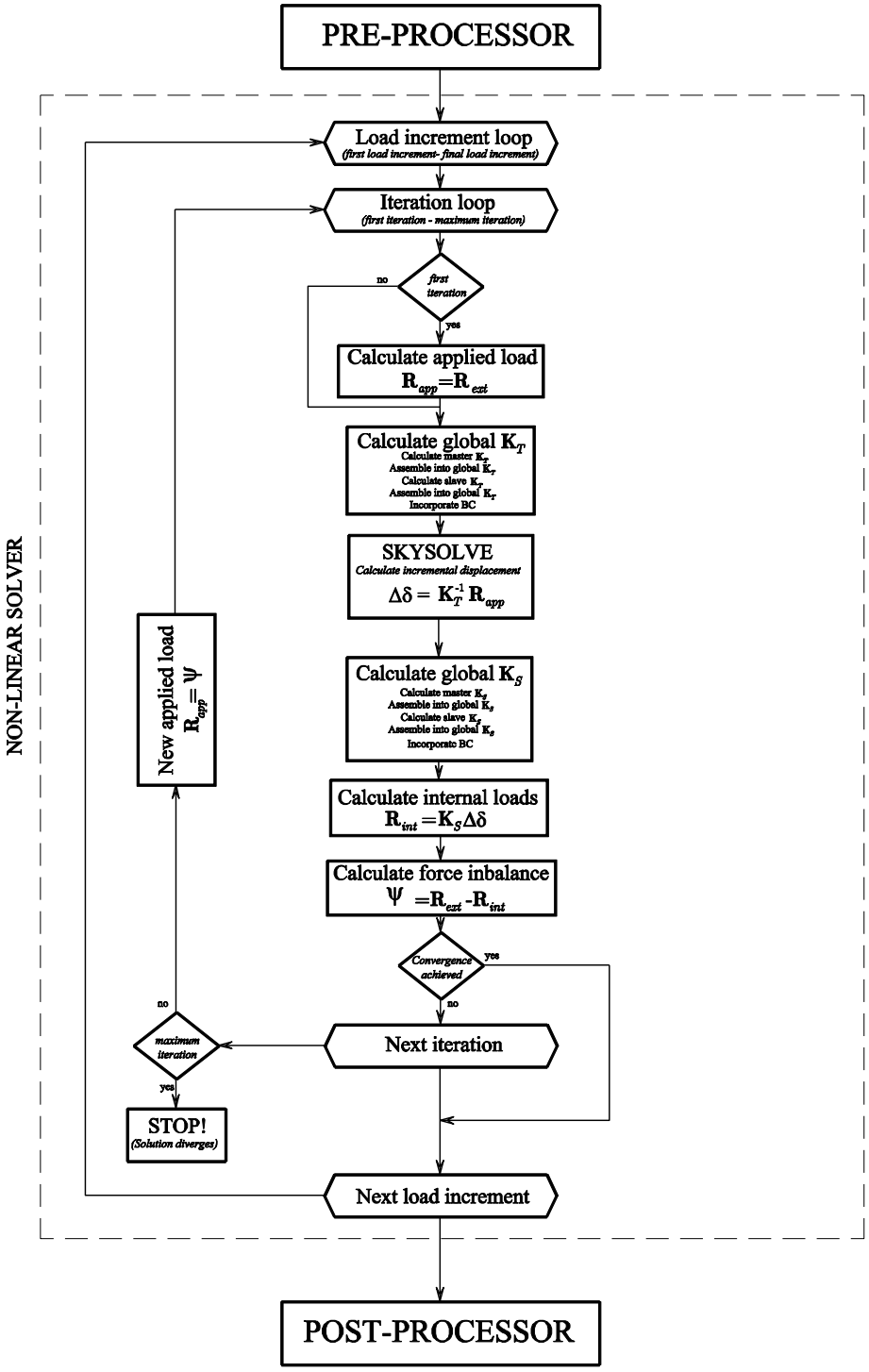


**Figure 4-11 General flow chart of NLSPAN non-linear solver.**

For numerical efficiency the global tangent stiffness matrix is assembled and stored as a one-dimensional array using a sky-line storage scheme (Akin, 1994). Then, the nodal constraints used to represent the boundary conditions described in Section 4.5 are incorporated to the global tangent stiffness matrix.

Next, the set of linearised equilibrium equations are solved for each iterative load increment using SKYSOLVE, a Gauss-Choleski algorithm coded in FORTRAN77 capable of solving a set of linear equations which coefficients stored using a skyline storage scheme (Akin, 1994).

The internal force of the structure is calculated next by solving Equation 4.31. This requires the evaluation of the product of global secant stiffness matrix and the incremental displacement vector.

The convergence of the iterative solution process in evaluated by calculating the convergence criteria, discussed in Section 4.6, and comparing them against a predefined convergence tolerance.

If convergence is not achieved the process is repeated using the inbalance of internal and applied forces as the new iterative load. If convergence is achieved the next load increment is analysed.

Once the solution for every incremental load is obtained, all nodal results obtained in the non-linear solver are recorded to file in the post-processor module.

# Chapter 5. Large deflection analysis validation

## 5.1 Introduction

In the previous Chapters, the development of a finite element formulation has been presented for the large deflection analysis of arbitrarily stiffened and unstiffened panels under transverse and in-plane loads. In this Chapter, the performance, accuracy and applicability of NLSPAN for the analysis of stiffened and unstiffened panels under transverse loading is validated through a series of numerical examples.

A wide range of stiffened and unstiffened panels were modelled using NLSPAN. The results obtained were compared with those available in the open literature and those obtained using ANSYS commercial finite element package (2004).

As discussed in Chapter 3, the finite element model of a stiffened panel, generated using arbitrarily stiffened elements, normally includes both stiffened and unstiffened element. Consequently the validation work was divided into two Sections:

1. Analysis of unstiffened panels under transverse load (Section 5.2)
2. Analysis of stiffened panels under transverse load (Section 5.3)

The validation of unstiffened panels not only ensures that the master element is capable of representing the behaviour of a unstiffened panel but also gives guidance on the mesh density required in the subsequent validation of NLSPAN stiffened panel analysis capability.

The validation work of NLSPAN's stiffened panel analysis capability was focused to verify the capability of the proposed formulation in representing panels where the stiffener was placed at truly arbitrary orientations.

Both the unstiffened and stiffened test cases include isotropic and composite laminated panels with different boundary conditions.

An illustration that summarizes important details of the investigated panel (panel dimensions, coordinate system, material properties and finite element mesh) has been provided in each validation problem. The boundary conditions are detailed in each illustration according to the notation defined in Table 4-1 and Table 4-2 of Section 4.4.2. The illustration also defines, using the letter $w$, the point where the out of the plane deflection is measured.

The non-dimensional results of each validation problem are presented in both graphical and tabular form in order to facilitate the study of the difference between the presented data sets. The non-dimensional quantities defined in order to present the validation results are listed in Table 5-1.

**Table 5-1 Non-dimensional quantities for panels under transverse load.**

| | |
|---|---|
| $w/t$ | Non-dimensional out of the plane deflection ( $w$ ) |
| $\sigma_x a^2 / Et^2$ | Non-dimensional normal stress |
| $\frac{qa^4}{Et^4}$ | Non-dimensional transverse load ( $q$ ) of the isotropic panels |
| $\frac{qa^4}{E_{22}t^4}$ | Non-dimensional transverse load ( $q$ ) of the composite laminated panels |

## 5.2 Unstiffened panels under transverse load

Several problems available in the open literature were chosen to benchmark the performance of the proposed formulation in modelling the geometrically non-linear response of unstiffened plates under transverse loads.

In Sections 5.2.1 and 5.2.2 large deflection results for isotropic panels with both clamped and simply supported boundary conditions obtained using the present formulation are presented and compared with analytical and numerical results available in the open literature.

Laminated composite panels under transverse loads are investigated in Sections 5.2.3, 5.2.4 and 5.2.5. Analysed problems consider different lamination schemes; boundary conditions as well as different panel length to thickness ratios.

### 5.2.1 Clamped isotropic square unstiffened panel

The first problem to be considered is the large deflection of a clamped unstiffened panel under transverse load. Levy (1942) presented a double Fourier series solution for the large deflection of clamped panels having C1 boundary conditions on all edges. This analytical solution is quoted as having a possible error of less than 2% (Pica *et al.*, 1980). For that reason it has been adopted by several authors as a benchmark problem for new geometrically non-linear finite element formulations (Pica *et al.*, 1980, Rao *et al.*, 1993, Chattopadhyay *et al.*, 1995).

In order to obtain the non-linear response path, and by taking advantage of symmetry, only a quarter of the domain was discretised in NLSPAN. It is important to note that, for comparison purposes, the same plate dimensions and mesh density used by other authors were adopted in the NLSPAN model (Pica *et al.*, 1980, Rao *et al.*, 1993, Chattopadhyay *et al.*, 1995). These dimensions, as well as the finite element mesh, and the material properties are detailed in Figure 5-1.

The non-dimensional plate centre deflection and plate centre stress results, obtained at different non-dimensional load steps using a force convergence tolerance of 1%, are presented in Table 5-2 and Table 5-3 respectively.

The results obtained with the proposed formulation (NLSPAN) have been compared with Levy's analytical results as well as with the finite element results of Pica *et al.* (1980), Rao *et al.* (1993) and Chattopadhyay *et al.* (1995).

The centre deflection results shown in Table 5-2 compare well with Levy's analytical solution, having an average absolute error of 1.3%. Moreover, the current results are slightly better than those of Pica *et al.* (1.4%), Chattopadhyay *et al.* (1.4%) and Rao *et al.* (1.4%).

A similar trend exists in the non-dimensional central stress results shown in Table 5-3, the current formulation shows an average absolute error of 2.0% compared with Levy's analytical solution, and again performs better than Rao *et al.* (2.1%), Pica *et al.* (2.2%), and Chattopadhyay *et al.* (4.0%).

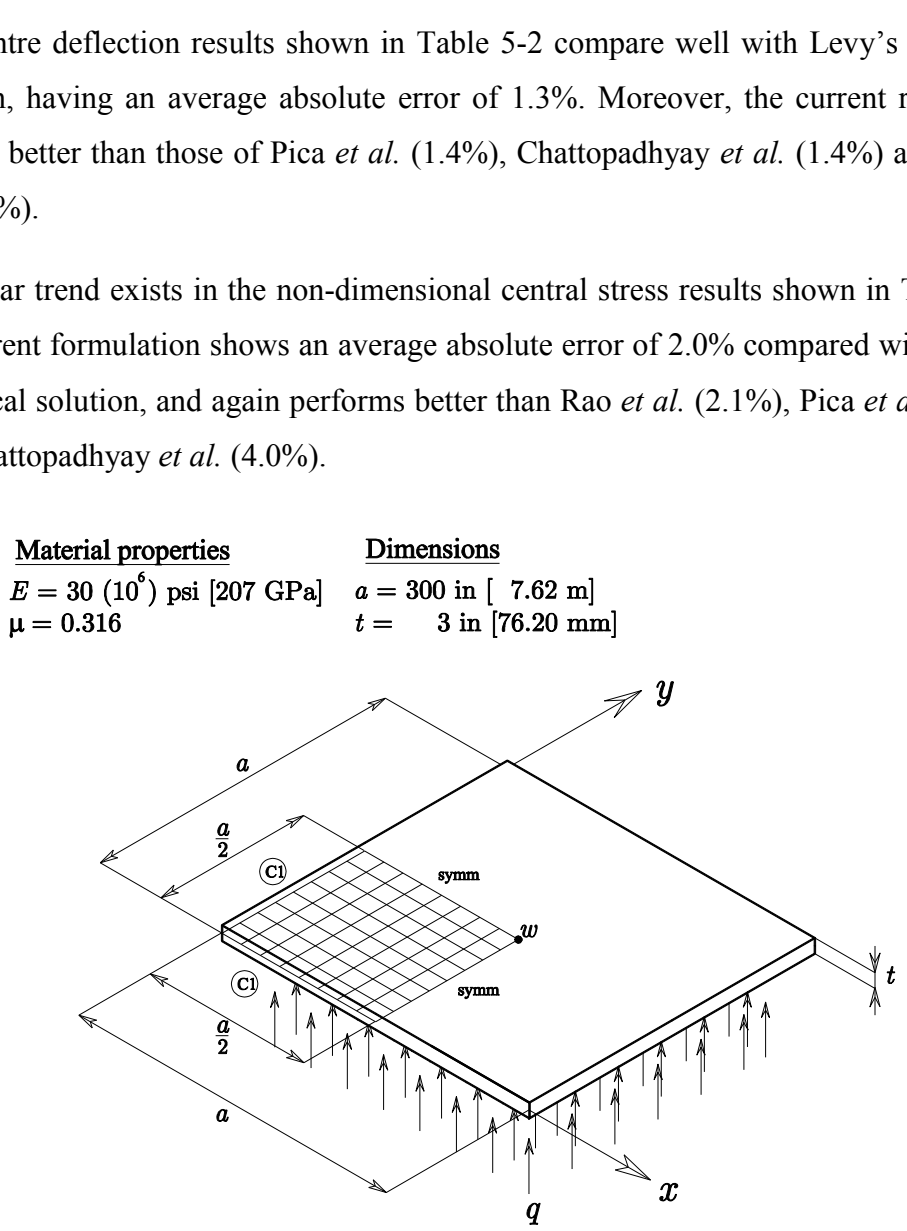


**Figure 5-1 Details of the isotropic clamped square panel.**

**Table 5-2 Non-dimensional out of the plane deflection of a clamped square panel.**

| $\frac{qa^4}{Et^4}$ | $w/t$ | | | | | | | | |
|---|---|---|---|---|---|---|---|---|---|
| | **Levy (exact)** | **Pica et al. (QS)** | | **Rao et al.** | | **Chattopadhyay et al.** | | **NLSPAN** | |
| 17.79 | 0.237 | 0.235 | (0.8%) | 0.235 | (1.0%) | 0.236 | (0.4%) | 0.235 | (0.8%) |
| 38.39 | 0.471 | 0.467 | (0.8%) | 0.466 | (1.1%) | 0.468 | (0.6%) | 0.470 | (0.3%) |
| 63.40 | 0.695 | 0.689 | (0.9%) | 0.686 | (1.3%) | 0.690 | (0.7%) | 0.691 | (0.6%) |
| 95.00 | 0.912 | 0.900 | (1.3%) | 0.899 | (1.5%) | 0.902 | (1.1%) | 0.903 | (1.0%) |
| 134.90 | 1.121 | 1.104 | (1.5%) | 1.103 | (1.7%) | 1.105 | (1.4%) | 1.107 | (1.2%) |
| 184.00 | 1.323 | 1.299 | (1.8%) | 1.298 | (1.9%) | 1.301 | (1.7%) | 1.302 | (1.6%) |
| 245.00 | 1.521 | 1.491 | (2.0%) | 1.489 | (2.1%) | 1.493 | (1.9%) | 1.494 | (1.8%) |
| 318.00 | 1.714 | 1.677 | (2.1%) | 1.675 | (2.3%) | 1.679 | (2.1%) | 1.680 | (2.0%) |
| 402.00 | 1.902 | 1.868 | (1.8%) | 1.853 | (2.6%) | 1.856 | (2.4%) | 1.857 | (2.3%) |

Note: Figures in brackets denote the absolute percentage error

**Table 5-3 Non-dimensional central stress of a clamped square panel.**

| $\frac{qa^4}{Et^4}$ | $\sigma_x a^2/Et^2$ | | | | | | | | |
|---|---|---|---|---|---|---|---|---|---|
| | **Levy (exact)** | **Pica et al. (QS)** | | **Rao et al.** | | **Chattopadhyay et al.** | | **NLSPAN** | |
| 17.79 | 2.640 | 2.657 | (0.6%) | 2.628 | (0.5%) | 2.680 | (1.5%) | 2.575 | (2.4%) |
| 38.39 | 5.220 | 5.514 | (5.6%) | 5.481 | (5.0%) | 5.590 | (7.1%) | 5.389 | (3.2%) |
| 63.40 | 8.030 | 8.353 | (4.0%) | 7.823 | (2.6%) | 8.502 | (5.9%) | 8.164 | (1.7%) |
| 95.00 | 11.070 | 11.115 | (0.4%) | 11.133 | (0.6%) | 11.347 | (2.5%) | 10.898 | (1.6%) |
| 134.90 | 13.330 | 13.817 | (3.7%) | 13.869 | (4.0%) | 14.137 | (6.1%) | 13.590 | (2.0%) |
| 184.00 | 15.890 | 16.461 | (3.6%) | 16.548 | (4.1%) | 16.873 | (6.2%) | 16.227 | (2.1%) |
| 245.00 | 19.240 | 19.160 | (0.4%) | 19.274 | (0.2%) | 19.659 | (2.2%) | 18.936 | (1.6%) |
| 318.00 | 21.880 | 21.902 | (0.1%) | 22.040 | (0.7%) | 22.488 | (2.8%) | 21.692 | (0.9%) |
| 402.00 | 25.120 | 24.805 | (1.3%) | 24.822 | (1.2%) | 24.660 | (1.8%) | 24.466 | (2.6%) |

Note: Figures in brackets denote the absolute percentage error

### 5.2.2 **Simply supported isotropic square unstiffened panel**

In this Section, Rushton's (Rushton, 1970) finite difference dynamic relaxation solution for the large deflection of simply supported plates having S1 boundary conditions on all edges was used to benchmark the proposed formulation. This analytical solution is quoted as having a possible error of less than 0.5% (Pica *et al.*, 1980).

For comparison purposes the same plate dimensions, mesh density and material properties used by other authors (Pica *et al.*, 1980, Chattopadhyay *et al.*, 1995) were used in this example. A summary of the problem parameters and boundary conditions is presented in Figure 5-2.

Results for centre deflection and centre stress, obtained at different non-dimensional load steps using a force convergence tolerance of 1%, are presented in Table 5-4 and Table 5-5 respectively. The results obtained with the proposed formulation (NLSPAN) have been compared with Rushton's, (1970) analytical results as well as with the finite element results of Pica *et al.* (1980), Rao *et al.* (1993) and Chattopadhyay *et al.* (1995). It must be noted that Rao *et al.* (1993) did not benchmark their formulation against Rushton's solution.

The deflection results shown in Table 5-4 compare well with Rushton's analytical solution having an average absolute error of 1.0%. The current deflection results do not compare as well as to those of Pica *et al.* (0.9%) but are better than those of Chattopadhyay *et al.* (1.3%).

However, in Table 5-5, it can be seen that the current formulation clearly outperformed the other finite element formulations for the stress calculation. Indeed, NLSPAN centre results show only 1.0% averaged absolute error compared to Rushton's analytical solution whilst Pica *et al.* and Chattopadhyay *et al.* averaged absolute error are 1.9% and 4.4% respectively.

| Material properties | Dimensions |
|---|---|
| $E = 30\ (10^6)$ psi [207 GPa] | $a = 300$ in [ 7.62 m] |
| $\mu = 0.316$ | $t =$ 3 in [76.20 mm] |

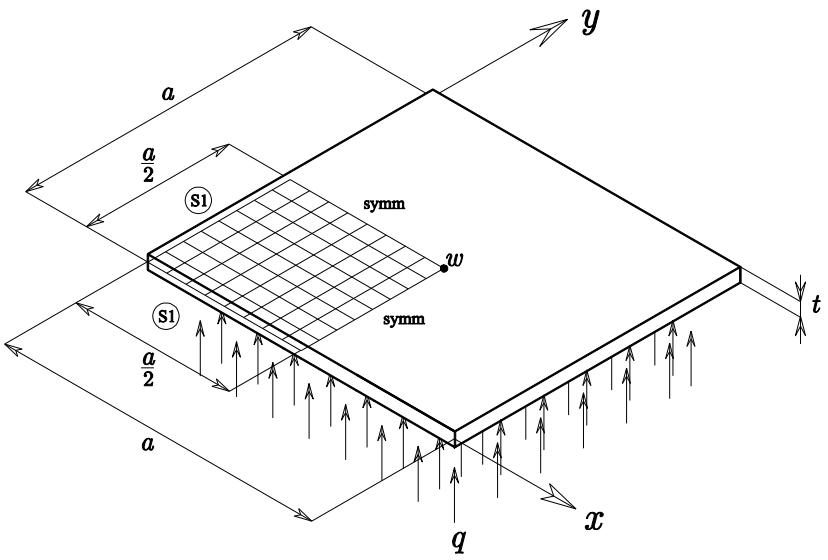


**Figure 5-2 Details of the isotropic simply supported square plate.**

**Table 5-4 Non-dimensional out of the plane deflection of a simply supported square panel.**

| $\frac{qa^4}{Et^4}$ | $w/t$ | | | | | |
|---|---|---|---|---|---|---|
| | Rushton (exact) | Pica et al. (QS) | | Chattopadhyay et al. | | NLSPAN | |
| 9.16 | 0.335 | 0.348 | (3.8%) | 0.344 | (2.6%) | 0.347 | (3.5%) |
| 36.60 | 0.818 | 0.818 | (0.0%) | 0.809 | (1.1%) | 0.815 | (0.4%) |
| 146.50 | 1.470 | 1.466 | (0.3%) | 1.454 | (1.1%) | 1.463 | (0.5%) |
| 586.00 | 2.400 | 2.393 | (0.3%) | 2.375 | (1.1%) | 2.389 | (0.5%) |
| 2344.00 | 3.830 | 3.812 | (0.5%) | 3.785 | (1.2%) | 3.808 | (0.6%) |
| 9377.00 | 6.070 | 6.052 | (0.3%) | 6.009 | (1.0%) | 6.046 | (0.4%) |

Note: Figures in brackets denote the absolute percentage error

**Table 5-5 Non-dimensional central stress of a simply supported square panel.**

| $\frac{qa^4}{Et^4}$ | $\sigma_x a^2 / Et^2$ | | | | | | |
|---|---|---|---|---|---|---|---|
| | Rushton (exact) | Pica et al. (QS) | | Chattopadhyay et al. | | NLSPAN | |
| 9.16 | 2.460 | 2.621 | (6.6%) | 2.665 | (8.3%) | 2.616 | (6.3%) |
| 36.60 | 6.900 | 7.003 | (1.5%) | 7.156 | (3.7%) | 6.979 | (1.1%) |
| 146.50 | 14.500 | 14.644 | (1.0%) | 15.034 | (3.7%) | 14.625 | (0.9%) |
| 586.00 | 30.000 | 30.183 | (0.6%) | 31.011 | (3.4%) | 30.151 | (0.5%) |
| 2344.00 | 65.200 | 65.673 | (0.7%) | 67.480 | (3.5%) | 65.607 | (0.6%) |
| 9377.00 | 148.300 | 149.660 | (0.9%) | 153.780 | (3.7%) | 149.433 | (0.8%) |

Note: Figures in brackets denote the absolute percentage error

### 5.2.3 Simply supported unidirectional laminated square unstiffened panel

The benchmark problem presented in this Section, investigates the correlation between results obtained with current formulation and both experimental and finite element results for a simply supported unidirectional laminated plate under transverse loads.

The experiment was conducted by Zaghloul and Kennedy (1975) on a 12 in (304.8 mm) long and 0.138 in (3.5 mm) thick, square simply supported specimen. The specimen was loaded by applying a monotonically increasing uniform pressure of up to 2.0 psi (13.7 kPa).

The finite element results were presented by Zhang and Kim (2006) using two different displacement-based elements, RDKQ-NL20 and RDKQ-NL24, and by Argyris and Tenek (1994) using a 3-node multilayered triangular facet element based on the natural mode method. Elements RDKQ-NL20 and RDKQ-NL24 were developed by Zhang and Kim using the linear displacement interpolation functions of the standard 4-node quadrilateral isoparametric plane element and the in-plane displacement functions of a quadrilateral plane element with drilling degrees of freedom respectively.

For comparison purposes the mesh density used by Zhang and Kim (10x10) was adopted in the present work. A summary of the plate dimension, material properties and lamination details is presented in Figure 5-3.

Table 5-6 compares the centre deflection results obtained at different load steps with the proposed formulation (NLSPAN), using a force convergence tolerance of 1%, with the experimental results of Zaghloul and Kennedy as well as with the finite element results of Argyris and Tenek (1994) and Zhang and Kim (2006). It must be noted that the Zaghloul and Kennedy experimental results as well as Argyris and Tenek finite element results were tabulated by Zhang and Kim from a graph presented by Argyris and Tenek (1994).

The deflection results shown in Table 5-6 present an excellent correlation with Zaghloul and Kennedy experimental results having an average absolute error of 1.6% which is close to the accuracy of Argyris and Tenek formulation (1.4%). Meanwhile, Zhang and Kim elements, RDKQ-NL20 and RDKQ-NL24, showed limited accuracy with average errors of 4% and 11.6% respectively.

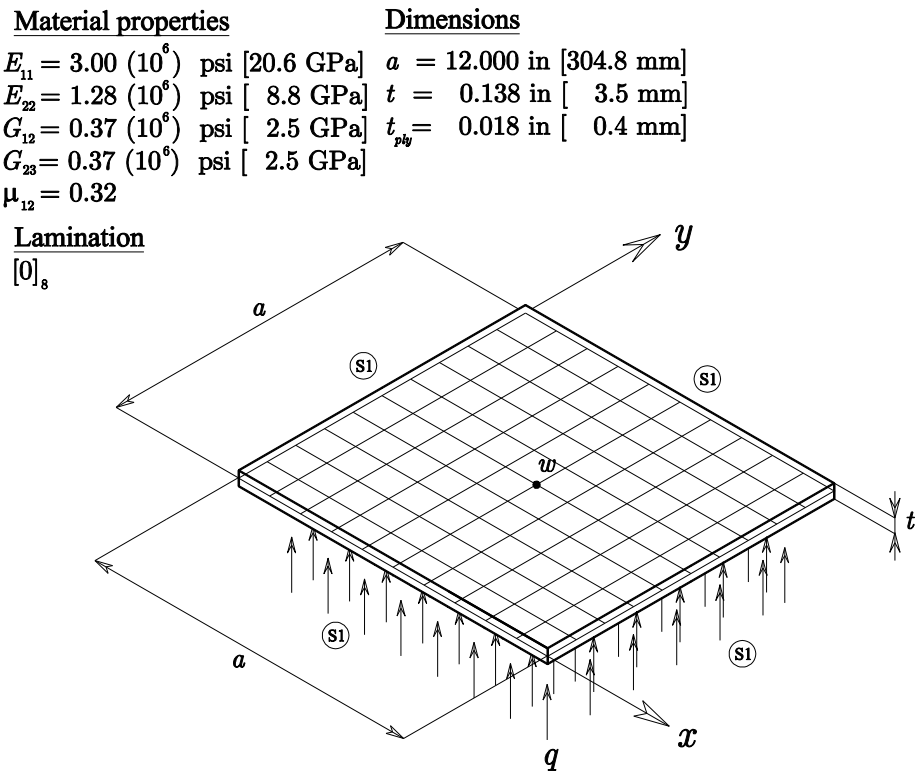


**Figure 5-3 Details of the unidirectional laminated, simply supported square panel.**

**Table 5-6 Non-dimensional out of the plane deflection of an 8-ply unidirectional simply supported panel under distributed load.**

| $\frac{qa^4}{E_{22}t^4}$ | $w/t$ | | | | | | | |
|---|---|---|---|---|---|---|---|---|
| | Zaghloul and Kennedy (experimental) | Zhang and Kim (RDKQ-NL24) | | Zhang and Kim (RDKQ-NL20) | | Argyris and Tenek | | NLSPAN | |
| 17.9 | 0.587 | 0.516 | (12.1%) | 0.564 | (3.8%) | 0.609 | (3.7%) | 0.590 | (0.6%) |
| 35.7 | 1.014 | 0.874 | (13.9%) | 0.951 | (6.2%) | 1.022 | (0.7%) | 0.998 | (1.6%) |
| 53.6 | 1.283 | 1.141 | (11.1%) | 1.238 | (3.5%) | 1.283 | (0.0%) | 1.292 | (0.7%) |
| 71.5 | 1.558 | 1.354 | (13.1%) | 1.466 | (5.9%) | 1.558 | (0.0%) | 1.524 | (2.2%) |
| 89.3 | 1.667 | 1.535 | (7.9%) | 1.657 | (0.6%) | 1.710 | (2.6%) | 1.717 | (3.0%) |

Note: Figures in brackets denote the absolute percentage error

### 5.2.4 Clamped symmetric bidirectional laminated square unstiffened panel

In this Section the correlation between results obtained with current formulation and both experimental and finite element results for a clamped 4-ply symmetric bidirectional laminated square plate under transverse loads is investigated.

This experiment was also conducted by Zaghloul and Kennedy (1975) on a 12 in (304.8 mm) long specimen but with a total thickness of 0.096 in (3.5 mm). The rotation and translation of the edges of the specimen were constrained whilst the loading was applied uniformly, increasing monotonically to a final pressure of 2.0 psi (13.7 kPa).

The finite element results were presented by Zhang and Kim (2006) using two different displacement-based 4-node quadrilateral elements, RDKQ-NL20 and RDKQ-NL24, and by Putcha and Reddy (1986) using a refined shear flexible laminated element. A summary of the plate dimension, material properties and lamination details is presented in Figure 5-4.

In line with the works of Putcha and Reddy and Zhang and Kim the plate was discretised using a quarter symmetry model and a 4x4 mesh density. The non-linear solution was obtained using a force convergence tolerance of 1%.

Table 5-7 presents the non-dimensional results obtained using the current formulation as well as those of Zaghloul and Kennedy and Putcha and Reddy which were tabulated by Zhang and Kim from a graph presented by Putcha and Reddy (1986). The results of Zhang and Kim for the RDKQ-NL20 and the RDKQ-NL24 elements are shown in a single column in Table 5-7 as they are quoted to have the same results (Zhang and Kim, 2006).

All finite element results presented in Table 5-7 show an overly stiff behaviour that underestimates the plate deflections. Both Putcha and Reddy and Zhang and Kim results had an average error of 20% whilst the current formulation shows a slightly lesser average error (17%). The difference between the numerical and experimental results is attributed to possible difference in the support conditions used in the experiment, i.e. the exact nature of the clamped boundary conditions used in the test may not be properly represented by the ones used in the finite element analysis (Reddy, 2006).

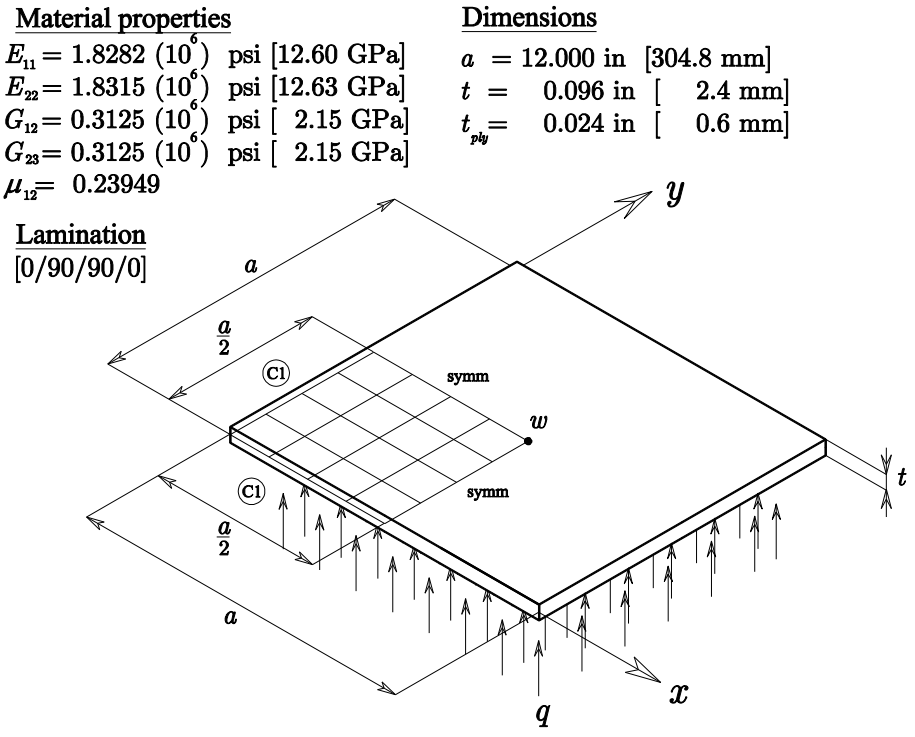


**Figure 5-4 Details of the symmetric bidirectional laminated square plate.**

**Table 5-7 Non-dimensional out of the plane deflection of a 4-ply symmetric bidirectional clamped plate under distributed load.**

| $\frac{qa^4}{E_{22}t^4}$ | $w/t$ | | | | | |
|---|---|---|---|---|---|---|
| | Zaghloul and Kennedy (experimental) | Zhang and Kim | | Putcha and Reddy | | NLSPAN | |
| 53.3 | 0.813 | 0.638 | (22%) | 0.646 | (21%) | 0.675 | (17%) |
| 106.6 | 1.271 | 1.000 | (21%) | 1.000 | (21%) | 1.043 | (18%) |
| 160.0 | 1.542 | 1.254 | (19%) | 1.240 | (20%) | 1.290 | (16%) |
| 213.3 | 1.813 | 1.451 | (20%) | 1.458 | (20%) | 1.478 | (18%) |
| 266.6 | 1.948 | 1.614 | (17%) | 1.563 | (20%) | 1.633 | (16%) |

Note: Figures in brackets denote the absolute percentage error

### 5.2.5 Simply supported symmetric bidirectional laminated square unstiffened panels with different a/t ratios

A simply supported 4-layer symmetric bidirectional laminated square plate with various length to thickness ratios ($a/t$) and subjected to a uniformly distributed load, is studied here.

This problem was solved analytically by Gorgi (1986) using double Fourier series and was used by Kant and Kommineni (1992) and Zhang and Kim (2006) to study the performance of their finite element formulations for different length to thickness ratios. A summary of the plate dimension, mesh density, material properties and lamination details is presented in Figure 5-5.

Kant and Kommineni used a $C^0$ element based on a Higher order Shear Deformation (HOST). The finite element results presented by Zhang and Kim were obtained using the same displacement-based 4-node quadrilateral elements, RDKQ-NL20 and RDKQ-NL24, mentioned in sections 5.2.3 and 5.2.4.

Non-dimensional deflection results obtained using a force convergence tolerance of 1% for models with length to thickness ratios ($a/t$) of 40, 20 and 10 are presented in Table 5-8, Table 5-9 and Table 5-10 respectively.

Both Gorgi and Kant and Kommineni results were tabulated by Zhang and Kim (Zhang and Kim, 2006) from a graph presented by Kant and Kommineni (1992).

The current formulation shows the best results for the thick plate model ($a / t = 10$) with an average error of 0.6% compared to 1.6% of Kant and Kommineni HOST element, and 1.3% and 1.6% for Zhang and Kim RDKQ-NL20 and RDKQ-NL24 elements respectively.

The largest error average (2.3%) in results obtained by the current formulation was found to occur for a length to thickness ratio of 20. This error is similar to that obtained by Zhang and Kim using the RDKQ-NL24 element. The best results for this length to thickness ratio, only 0.3% error, were obtained using the Kant and Kommineni HOST element. Zhang and Kim RDKQ-NL20 element had only a slightly worse performance with an average error of 0.5%.

For the largest length to thickness ratio ($a / t = 40$) Kant and Kommineni HOST element outperformed all the other finite element formulation with an apparent perfect performance. In this study the average error of the current formulation (1.6%) is reasonably low and sits between that of the RDKQ-NL20 element (1.2%) and the RDKQ-NL24 element (1.9%).

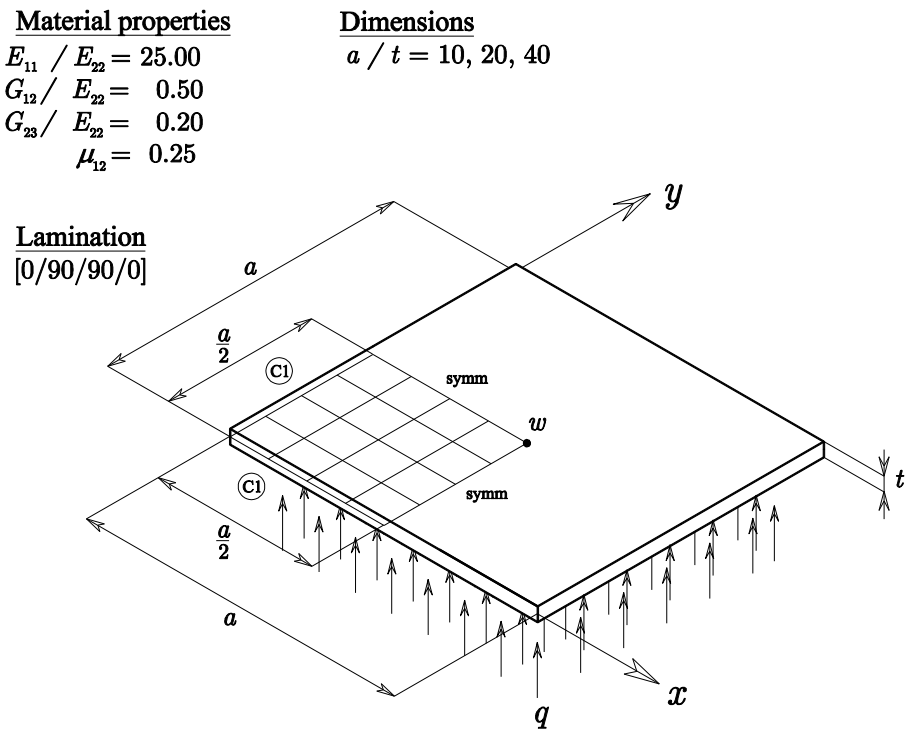


**Figure 5-5 Details of the symmetric bidirectional laminated square panel with different a/t ratios.**

**Table 5-8 Non-dimensional out of the plane deflection of a simply supported square composite panel with a/t=40.**

| $\frac{qa^4}{E_{22}t^4}$ | $w/t$ | | | | | | | |
|---|---|---|---|---|---|---|---|---|
| | Gorgi (analytical) | Kant and Kommineni (HOST) | | Zhang and Kim (RDKQ-NL20) | | Zhang and Kim (RDKQ-NL20) | | NLSPAN | |
| 50 | 0.293 | 0.293 | (0.0%) | 0.291 | (0.6%) | 0.294 | (0.4%) | 0.288 | (1.8%) |
| 100 | 0.464 | 0.464 | (0.0%) | 0.461 | (0.7%) | 0.467 | (0.7%) | 0.457 | (1.5%) |
| 150 | 0.582 | 0.582 | (0.0%) | 0.577 | (0.8%) | 0.587 | (0.8%) | 0.572 | (1.7%) |
| 200 | 0.644 | 0.644 | (0.0%) | 0.667 | (3.5%) | 0.679 | (5.4%) | 0.660 | (2.5%) |
| 250 | 0.738 | 0.738 | (0.0%) | 0.740 | (0.3%) | 0.754 | (2.2%) | 0.733 | (0.7%) |

Note: Figures in brackets denote the absolute percentage error

**Table 5-9 Non-dimensional out of the plane deflection of a simply supported square composite panel with a/t=20.**

| $\frac{qa^4}{E_{22}t^4}$ | $w/t$ | | | | | | | |
|---|---|---|---|---|---|---|---|---|
| | **Gorgi (analytical)** | **Kant and Kommineni (HOST)** | | **Zhang and Kim (RDKQ-NL20)** | | **Zhang and Kim (RDKQ-NL20)** | | **NLSPAN** | |
| 50 | 0.320 | 0.320 | (0.0%) | 0.323 | (0.9%) | 0.327 | (2.2%) | 0.306 | (4.5%) |
| 100 | 0.486 | 0.493 | (1.4%) | 0.487 | (0.2%) | 0.495 | (1.8%) | 0.473 | (2.7%) |
| 150 | 0.592 | 0.592 | (0.0%) | 0.597 | (0.9%) | 0.608 | (2.7%) | 0.584 | (1.3%) |
| 200 | 0.680 | 0.680 | (0.0%) | 0.682 | (0.2%) | 0.695 | (2.2%) | 0.670 | (1.5%) |
| 250 | 0.752 | 0.752 | (0.0%) | 0.751 | (0.1%) | 0.766 | (1.9%) | 0.740 | (1.6%) |

Note: Figures in brackets denote the absolute percentage error

**Table 5-10 Non-dimensional out of the plane deflection of a simply supported square composite panel with a/t=10**

| $\frac{qa^4}{E_{22}t^4}$ | $w/t$ | | | | | | | |
|---|---|---|---|---|---|---|---|---|
| | **Gorgi (analytical)** | **Kant and Kommineni (HOST)** | | **Zhang and Kim (RDKQ-NL20)** | | **Zhang and Kim (RDKQ-NL20)** | | **NLSPAN** | |
| 50 | 0.356 | 0.360 | (1.1%) | 0.363 | (2.0%) | 0.370 | (4.0%) | 0.353 | (0.9%) |
| 100 | 0.510 | 0.520 | (2.0%) | 0.514 | (0.8%) | 0.525 | (2.9%) | 0.509 | (0.2%) |
| 150 | 0.610 | 0.624 | (2.3%) | 0.616 | (1.0%) | 0.629 | (3.1%) | 0.612 | (0.4%) |
| 200 | 0.689 | 0.696 | (1.0%) | 0.695 | (0.9%) | 0.710 | (3.0%) | 0.691 | (0.3%) |
| 250 | 0.747 | 0.760 | (1.7%) | 0.761 | (1.8%) | 0.777 | (4.0%) | 0.756 | (1.2%) |

Note: Figures in brackets denote the absolute percentage error

## 5.3 Stiffened panels under transverse load

The large deflection response of isotropic and laminated stiffened panels under the action of transverse loads is studied in this Section. Four different validation problems are analysed and discussed.

The first two problems (Sections 5.3.1 and 5.3.2 respectively) investigate the performance of the current formulation in modelling the large deflection response of isotropic and composite laminated cross stiffened panels under uniformly distributed loads.

The third problem (Section 5.3.3) investigates the performance of NLSPAN in analysing a diagonally stiffened panel with both concentric and eccentric stiffeners.

Finally, the fourth problem (Section 5.3.4) demonstrates that the present formulation is capable of modelling stiffener placed arbitrarily within the panel. Again, in this new validation problem both eccentrically and concentrically stiffened panels are considered.

### 5.3.1 Cross stiffened isotropic panel

A simply supported isotropic square panel stiffened by two central stiffeners was analysed using the proposed formulation.

In analysing this problem both Chattopadhyay *et al.* (1995) and Liao and Reddy (1989) took advantage of the symmetry of the panel by discretizing only a quarter of the structure with a 2x2 mesh. Although numerically efficient, such a model does not strictly use arbitrarily orientated stiffened elements as it places both stiffeners along the edges of the stiffened elements and therefore could be analysed in any commercially available package by combining shell and beam elements.

Consequently, in this study, two different models have been investigated. First, and for comparison purposes, the structure was discretised using the same quarter symmetry model used by Chattopadhyay *et al.* and Liao and Reddy. In the second model the entire panel was discretised using a 5x4 mesh, as shown in Figure 5-6. This new model places one stiffener along the edge of the stiffened elements but also places the other stiffener across the middle of the stiffened elements.

This stiffened panel was previously studied by Liao and Reddy (1990) and by Chattopadhyay *et al.* (1995) using the finite element method. A summary of the stiffened panel dimension, mesh densities, lamination details and material properties is presented in Figure 5-6.

It must be noted that the comparison results were obtained by digitizing the data presented by Chattopadhyay *et al.* (1995) in graphical form.

Figure 5-7 presents a comparison of the results of the non-dimensional central deflection of the quarter symmetry model for different non-dimensional transverse load levels obtained by the present method with those of Chattopadhyay *et al.* and Liao and Reddy.

The centre deflection results were found to agree very well with those of Liao and Reddy, whilst the results of Chattopadhyay *et al.* diverge slightly at higher load levels. Since the results of the quarter symmetry model were found to agree well with published results it was decided to use them to gauge the accuracy of the 5x4 model, i.e. the model with truly arbitrarily orientated stiffeners.

Table 5-11 presents a comparison between the deflection results of the two cross stiffened NLSPAN models. An excellent correlation exists between the two set of results.

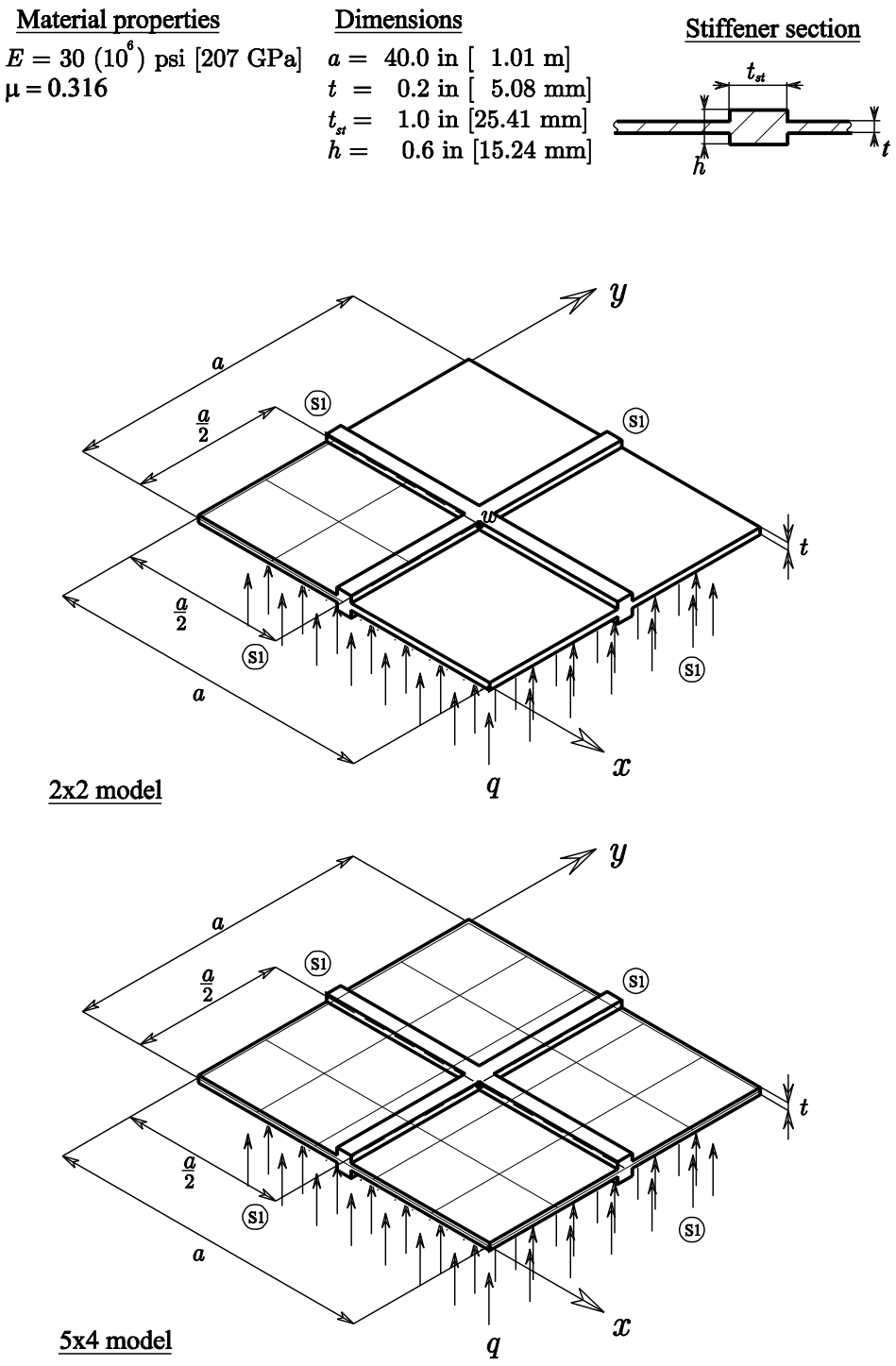


**Figure 5-6 Details of the cross stiffened isotropic panel.**

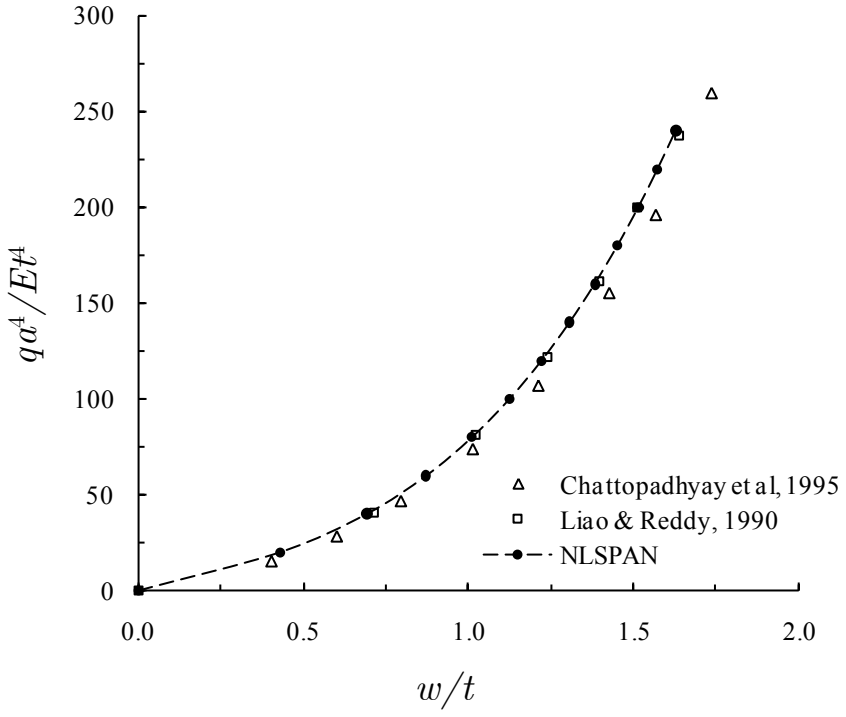


**Figure 5-7 Non-dimensional load-deflection results for a cross stiffened isotropic panel.**

**Table 5-11 Comparison of the out of the plane deflection results for the two NLSPAN cross stiffened models.**

| $\frac{qa^4}{Et^4}$ | $w/t$ | | |
|---|---|---|---|
| | NLSPAN (2x2) | NLSPAN (5x4) | |
| 20 | 0.443 | 0.429 | (3.3%) |
| 40 | 0.706 | 0.692 | (2.0%) |
| 60 | 0.884 | 0.873 | (1.4%) |
| 80 | 1.021 | 1.011 | (1.0%) |
| 100 | 1.133 | 1.125 | (0.7%) |
| 120 | 1.229 | 1.222 | (0.6%) |
| 140 | 1.313 | 1.307 | (0.4%) |
| 160 | 1.388 | 1.383 | (0.3%) |
| 180 | 1.456 | 1.452 | (0.2%) |
| 200 | 1.518 | 1.515 | (0.2%) |
| 220 | 1.576 | 1.574 | (0.1%) |
| 240 | 1.629 | 1.629 | (0.1%) |

Note: Figures in brackets denote the absolute percentage differences

### 5.3.2 **Cross stiffened composite panel**

A simply supported cross stiffened composite plate, as shown in Figure 5-8, was analysed for cross-ply and angle ply lamination schemes. Results for this example were previously reported by Chattopadhyay *et al*. (1995) and Liao and Reddy (1990).

The full stiffened plate was modelled in NLSPAN since, as stated by Reddy (1997), the non-linear response of a quarter symmetry for anti-symmetric angle ply laminated model do not agree, in general, with those of the corresponding full-plate model.

As for the cross stiffened isotropic panel study, two different meshes were considered here. Firstly a 4x4 full mesh is used to validate the results obtained using the current formulation against those of Chattopadhyay *et al.* and Liao and Reddy and secondly a 5x4 mesh is used to test the performance of the arbitrarily stiffened element when the stiffener is not placed along mesh lines of the model.

It must be noted that the comparison results were obtained by digitizing the data presented by Chattopadhyay *et al.* (1995) in graphical form.

In Figure 5-9 the non-dimensional results of the central deflections of the 4x4 cross ply laminated stiffened panel model are compared with those by Chattopadhyay *et al.* and Liao and Reddy. Excellent agreement was found at all load levels.

Figure 5-10 presents the non-dimensional results of the central deflections of the 4x4 angle ply laminated stiffened panel model. In this figure the results obtained using NLSPAN were compared with those by Chattopadhyay *et al.* and Liao and Reddy. The results compare well with those obtained by Chattopadhyay *et al*, however there is discrepancy for the angle ply lamination where the results of Liao and Reddy overestimate the deflection values.

The divergence increases with the intensity of the transverse load. This discrepancy can be explained by the modelling approach adopted by Liao and Reddy. These authors used a quarter-symmetry model to represent the stiffened plate. As previously mentioned, this approach gives the same non-linear results as the full plate model for anti-symmetric cross-ply laminates but not for anti-symmetric angle ply laminates.

Since the results of the 4x4 model were found to agree well with published results it was decided to use them to gauge the accuracy of the 5x4 model, i.e. the model with truly arbitrarily orientated stiffeners.

Table 5-12 presents a comparison between the deflection results of the two cross stiffened NLSPAN models. An excellent correlation exists between the two modelling approaches, with an average absolute difference between both set of results of only 1.6% and 0.8% for the cross ply and angle ply models respectively.

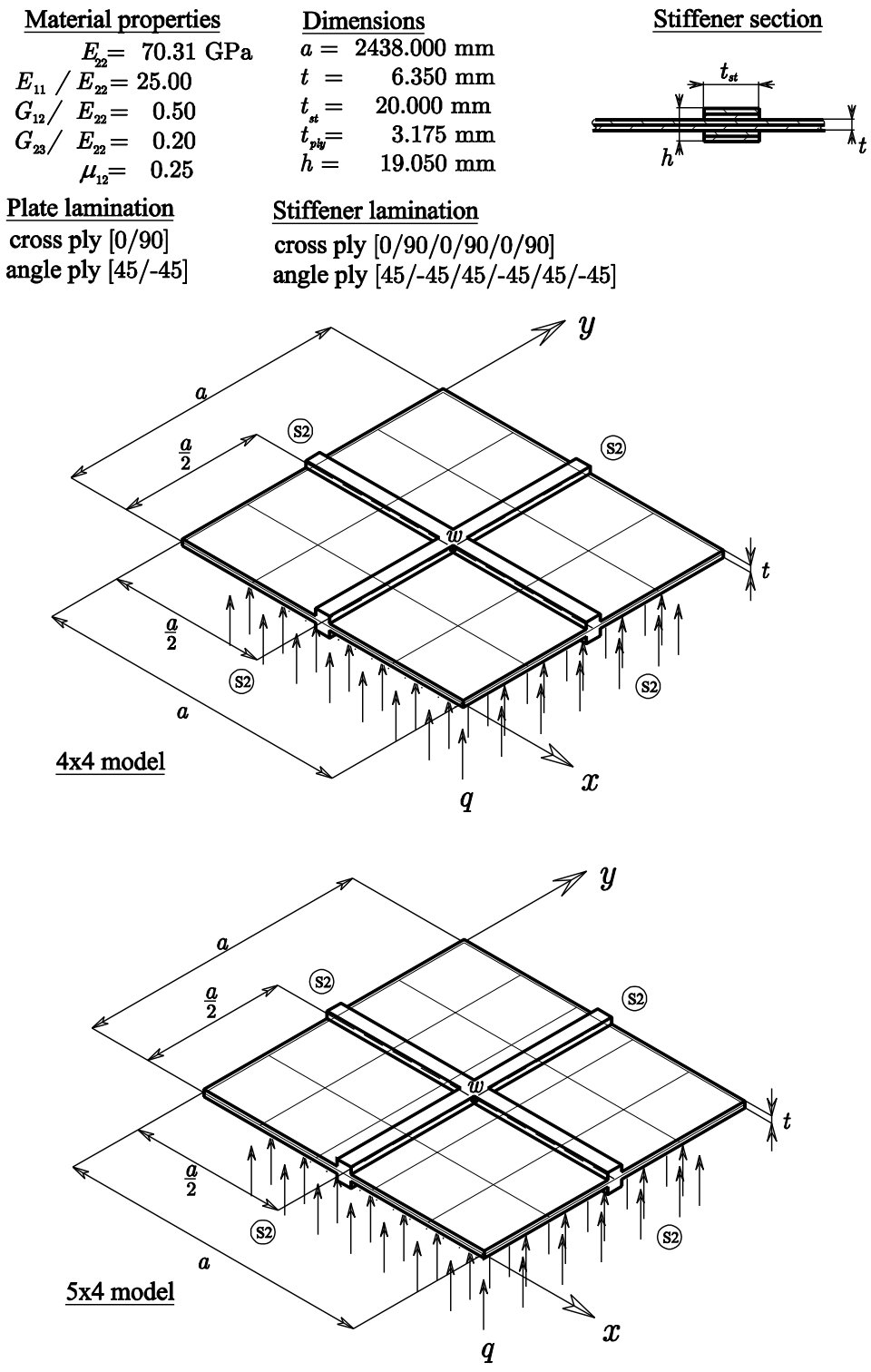


**Figure 5-8 Details of the cross stiffened laminated panel.**

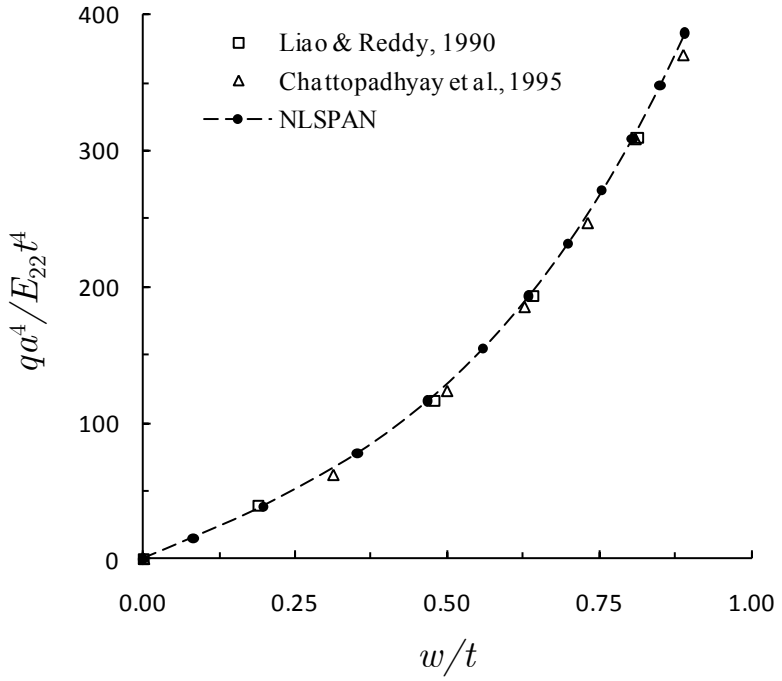


**Figure 5-9 Non-dimensional load-deflection response of the cross ply laminated stiffened panel.**

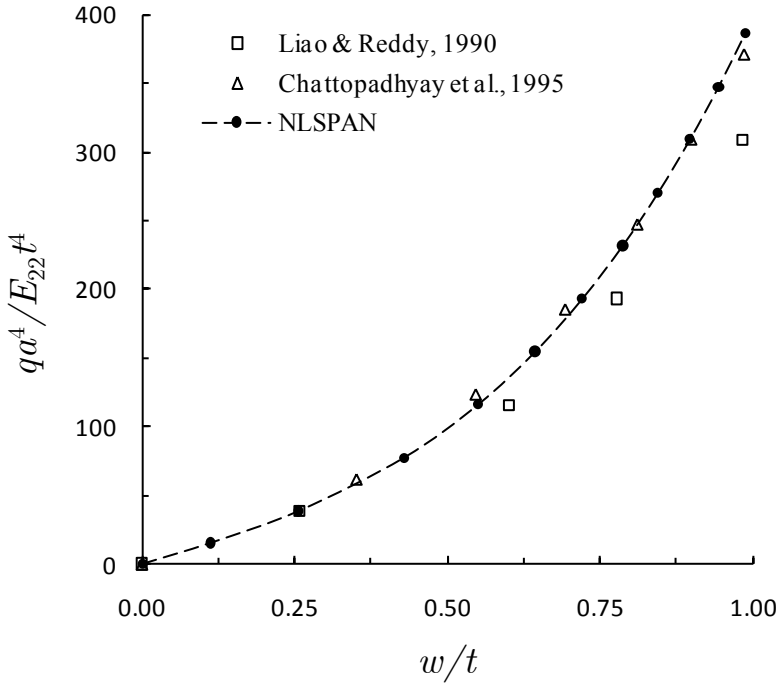


**Figure 5-10 Non-dimensional load-deflection response of the angle ply laminated stiffened panel.**

**Table 5-12 Comparison of the out of the plane deflection results for the two NLSPAN cross stiffened laminated models.**

| $\frac{qa^4}{E_{22}t^4}$ | $w/t$ | | | | | |
|---|---|---|---|---|---|---|
| | Cross Ply | | | Angle Ply | | |
| | NLSPAN (4x4) | NLSPAN (5x4) | | NLSPAN (4x4) | NLSPAN (5x4) | |
| 15.5 | 0.082 | 0.084 | (2.9%) | 0.112 | 0.116 | (2.7%) |
| 38.6 | 0.197 | 0.203 | (2.7%) | 0.256 | 0.262 | (2.1%) |
| 77.3 | 0.352 | 0.360 | (2.2%) | 0.428 | 0.434 | (1.3%) |
| 115.9 | 0.468 | 0.477 | (1.8%) | 0.549 | 0.554 | (0.9%) |
| 154.5 | 0.559 | 0.568 | (1.6%) | 0.643 | 0.647 | (0.6%) |
| 193.2 | 0.635 | 0.643 | (1.4%) | 0.721 | 0.724 | (0.4%) |
| 231.8 | 0.699 | 0.707 | (1.2%) | 0.787 | 0.789 | (0.3%) |
| 270.4 | 0.755 | 0.763 | (1.1%) | 0.845 | 0.847 | (0.2%) |
| 309.0 | 0.805 | 0.813 | (1.0%) | 0.897 | 0.898 | (0.2%) |
| 347.7 | 0.850 | 0.858 | (0.9%) | 0.944 | 0.945 | (0.1%) |
| 386.3 | 0.891 | 0.899 | (0.9%) | 0.987 | 0.988 | (0.0%) |

Note: Figures in brackets denote the absolute percentage differences

### 5.3.3 **Square panel with diagonal stiffeners**

The large deflections of a simply supported square plate with two stiffeners along the diagonals of the plate were analysed, for both concentric and eccentric stiffeners.

This panel was analysed by Samanta and Mukhopadhyay (1999), who modelled the stiffened panel using quarter-symmetry and 8x8 triangular mesh. Samanta and Mukhopadhyay presented load-deflection results for only two load levels: an initial load of 6.897 kPa and a final load equal to 200 times the initial load.

Such limited data set does not allow a proper comparison of results. Therefore, in this investigation the full non-linear response path of this stiffened panel was calculated using the general purpose finite element analysis package ANSYS, where the stiffened panels (eccentric and concentric) were modelled with an 8x8 irregular mesh and quarter-symmetry.

| Material properties | Dimensions |
|---|---|
| $E = 117.25$ Gpa | $a =$ 25.400 mm |
| $\mu =$ 0.30 | $t =$ 0.254 mm |
| | $t_{st} =$ 0.254 mm |
| | $h =$ 1.270 mm |

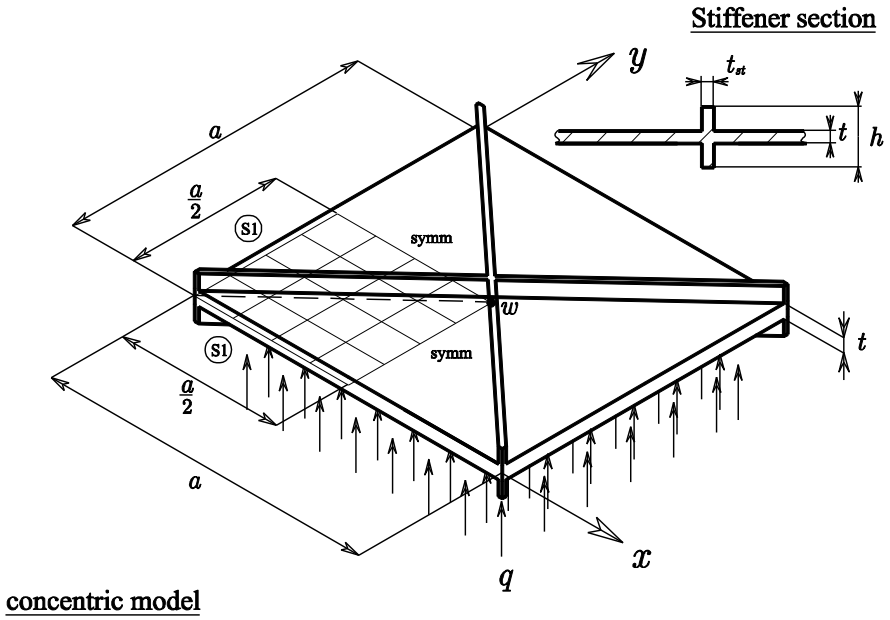


concentric model

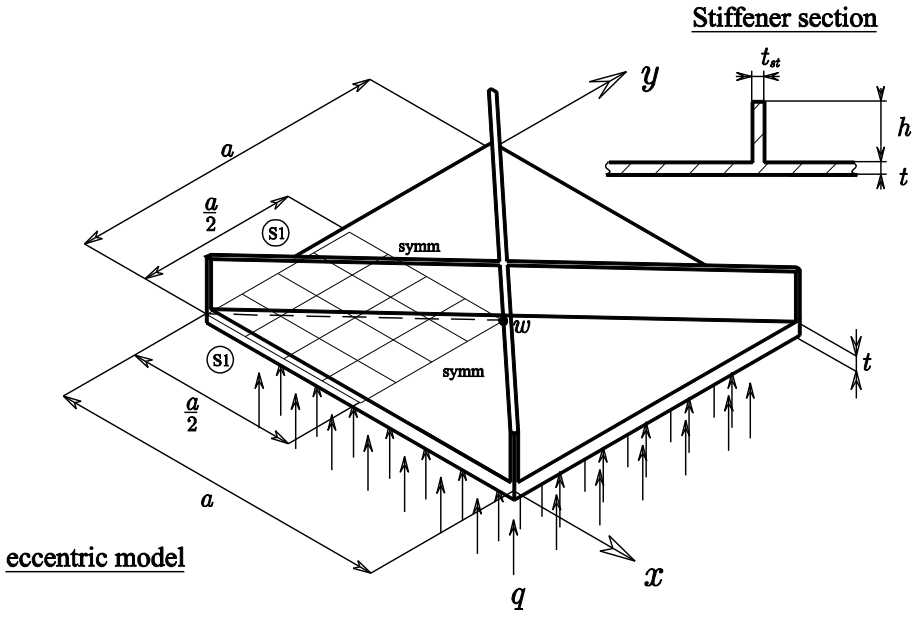


eccentric model

**Figure 5-11 Details of the square panel with diagonal stiffeners.**

The ANSYS models, shown in Figure 5-12, were generated using SHELL93, 8-node, shell elements together with BEAM189, 3-node, beam elements to represent the skin and the stiffener. It is important to note that, in ANSYS, the mesh quality was limited by the position and orientation of the stiffener which limits the flexibility of the panel mesh.

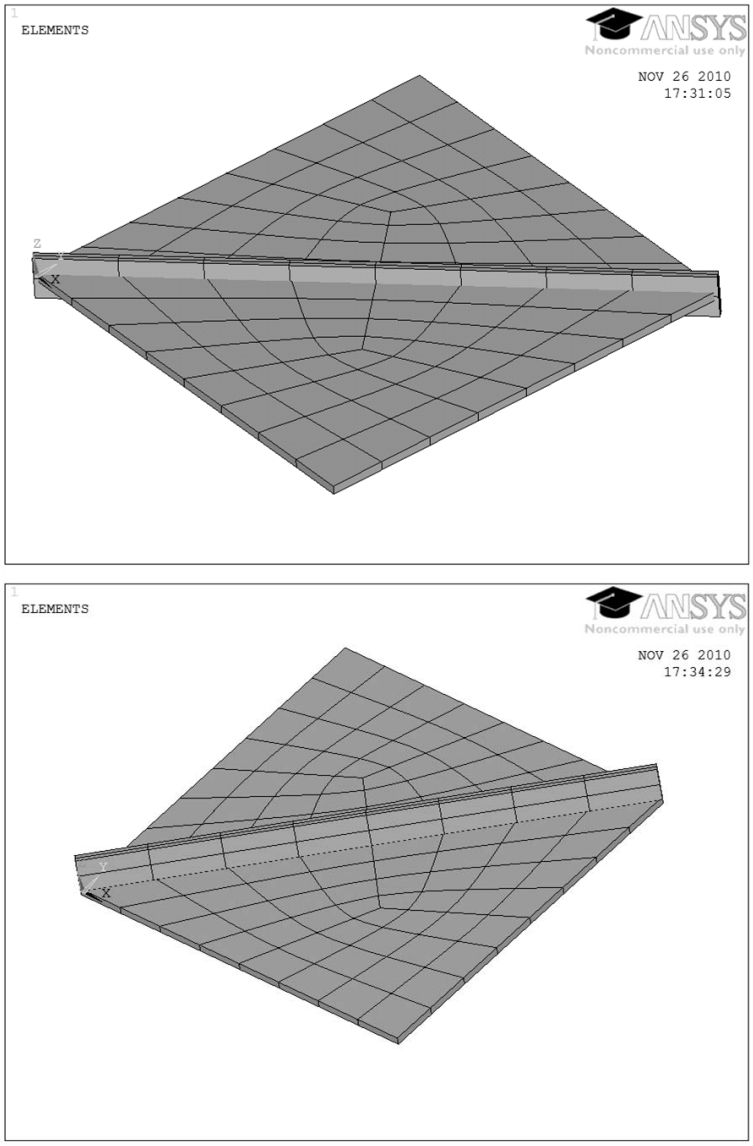


**Figure 5-12 ANSYS finite element models of the diagonally stiffened panel.**

The load-deflection results obtained using NLSPAN, with a quarter-symmetry model and a 4x4 square mesh, and ANSYS are tabulated in Table 5-13 and presented graphically in Figure 5-13. The eccentrically stiffened panel shows, as expected, stiffer load-deflection behaviour than the concentrically stiffened panel.

Furthermore, ANSYS and NLSPAN results were found to be in close agreement with each other in both cases. The average absolute difference in the concentrically and eccentrically stiffened panel results was 0.1% and 2.1% respectively.

Table 5-14 presents the comparison of the results of Samanta and Mukhopadhyay, ANSYS and NLSPAN for a load level equal to 200 times the initial load. Relative to the results obtained in ANSYS, the performance of both elements is similar for the concentric case were the result of Samanta and Mukhopadhyay show a slighty better performance (0.4%) than the result obtained in this study using NLSPAN. In the concentric case the result obtained using NLSPAN show significantly less variation (0.1%) than that obtained by Samanta and Mukhopadhyay (1.0%).

**Table 5-13 Comparison of the out of the plane deflection results for the diagonally stiffened models.**

| $\frac{qa^4}{Et^4}$ | $w/t$ | | | | | |
|---|---|---|---|---|---|---|
| | Eccentric | | | Concentric | | |
| | ANSYS | NLSPAN | | ANSYS | NLSPAN | |
| 29.4 | 0.157 | 0.151 | (4.2%) | 0.444 | 0.447 | (0.5%) |
| 58.8 | 0.306 | 0.294 | (4.0%) | 0.745 | 0.743 | (0.2%) |
| 88.2 | 0.444 | 0.427 | (3.7%) | 0.945 | 0.952 | (0.7%) |
| 117.6 | 0.570 | 0.551 | (3.4%) | 1.114 | 1.114 | (0.0%) |
| 147.1 | 0.684 | 0.664 | (3.0%) | 1.246 | 1.247 | (0.0%) |
| 176.5 | 0.790 | 0.768 | (2.8%) | 1.360 | 1.361 | (0.0%) |
| 205.9 | 0.886 | 0.864 | (2.6%) | 1.461 | 1.460 | (0.0%) |
| 235.3 | 0.975 | 0.952 | (2.3%) | 1.550 | 1.550 | (0.0%) |
| 264.7 | 1.058 | 1.035 | (2.1%) | 1.631 | 1.631 | (0.0%) |
| 294.1 | 1.135 | 1.113 | (2.0%) | 1.706 | 1.706 | (0.0%) |
| 323.5 | 1.207 | 1.185 | (1.8%) | 1.775 | 1.775 | (0.0%) |
| 352.9 | 1.275 | 1.254 | (1.7%) | 1.839 | 1.839 | (0.0%) |
| 441.2 | 1.458 | 1.439 | (1.4%) | 2.011 | 2.011 | (0.0%) |
| 588.2 | 1.714 | 1.696 | (1.0%) | 2.248 | 2.247 | (0.0%) |
| 735.3 | 1.927 | 1.912 | (0.8%) | 2.444 | 2.443 | (0.1%) |
| 882.4 | 2.112 | 2.098 | (0.7%) | 2.614 | 2.612 | (0.1%) |
| 1029.4 | 2.275 | 2.262 | (0.6%) | 2.764 | 2.761 | (0.1%) |
| 1176.5 | 2.423 | 2.411 | (0.5%) | 2.900 | 2.897 | (0.1%) |

Note: Figures in brackets denote the absolute percentage differences

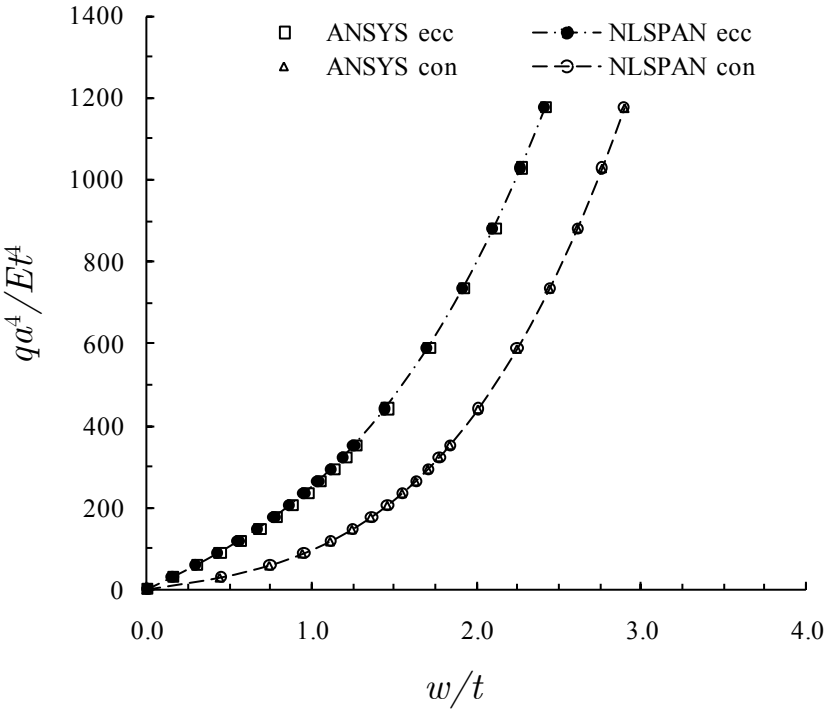


**Figure 5-13 Non-dimensional load-deflection result of the diagonally stiffened panel.**

**Table 5-14 Comparison of the out of the plane deflection results for the diagonally stiffened models at 200 times the initial load**

| $w/t$ | ANSYS | Samanta and Mukhopadhyay | | NLSPAN | |
|---|---|---|---|---|---|
| **Eccenctric** | 2.423 | 2.413 | (0.4%) | 2.411 | (0.5%) |
| **Concentric** | 2.900 | 2.929 | (1.0%) | 2.897 | (0.1%) |

Note: Figures in brackets denote the absolute percentage differences

### 5.3.4 **Square panel with arbitrary stiffeners**

In order to validate the applicability of the proposed formulation for the analysis of panels with arbitrary orientated stiffeners, a new problem is suggested. In previous examples, the performance of the current formulation was validated for panels where the stiffener was located within the shallow shell element. However, it can easily be observed that in those examples the stiffener trajectory intercepted either the mid-side or corner nodes of the shallow shell element.

To circumvent mesh limitations, a stiffened element should be able to produce accurate results when the trajectory of the stiffener is truly arbitrary, i.e. when it does not necessary intercept corner or mid-side nodes of the master element. Authors such as Ray and Satsangi (1998) claimed that their stiffened element formulation was capable of representing this structural response, though no validation work was presented to support their claim.

To validate the current formulation, and since such a validation example is not, to the author knowledge, currently available in the open literature, a new validation problem is proposed in this investigation. In this problem the orientation of the stiffener was selected in such way that the stiffener trajectory does not necessarily intercept the nodes of the master element. Again, both concentric and eccentric stiffener configurations were considered. All the relevant problem data is summarized in Figure 5-14.

The comparison data for this problem was obtained by modelling the complete stiffened panel in the general purpose finite element analysis package ANSYS. The model was generated using an irregular mesh composed of 272 SHELL93 shell and 16 BEAM189 beam elements. Both ANSYS models (concentric and eccentric) are presented in Figure 5-15.

The creation of each ANSYS model required performing a Boolean operation to account for the stiffener trajectory. This operation resulted in the creation of two separate areas with different topologies: the four-sided area on the left (upper) side of the stiffener and the three sided area on the right (lower) side of the stiffener.

| Material properties | | Dimensions | |
|---|---|---|---|
| E = 117.25 Gpa | a = | 25.400 mm |
| μ = 0.30 | t = | 0.254 mm |
| | $t_{st}$ = | 0.254 mm |
| | h = | 1.270 mm |

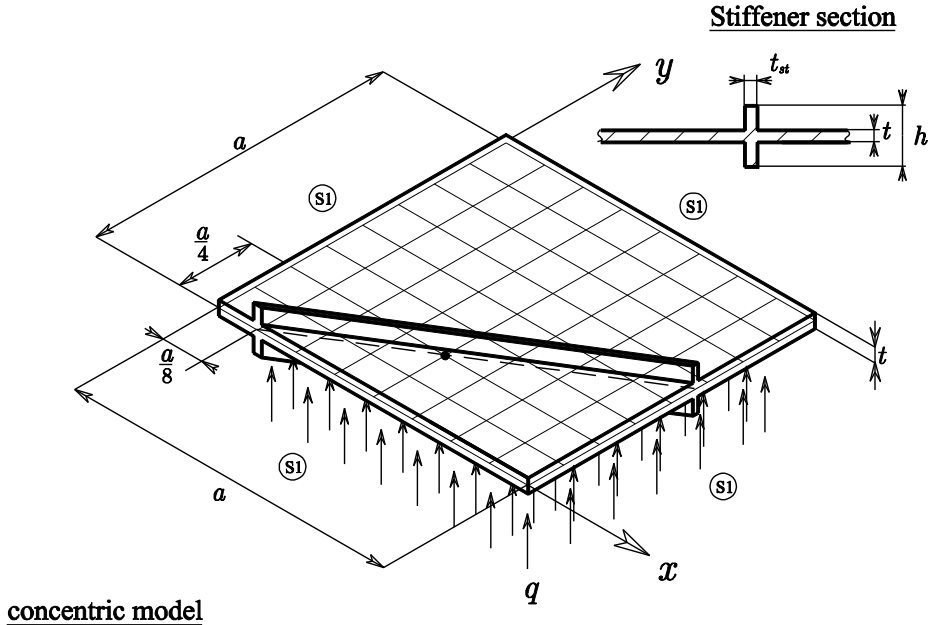


concentric model

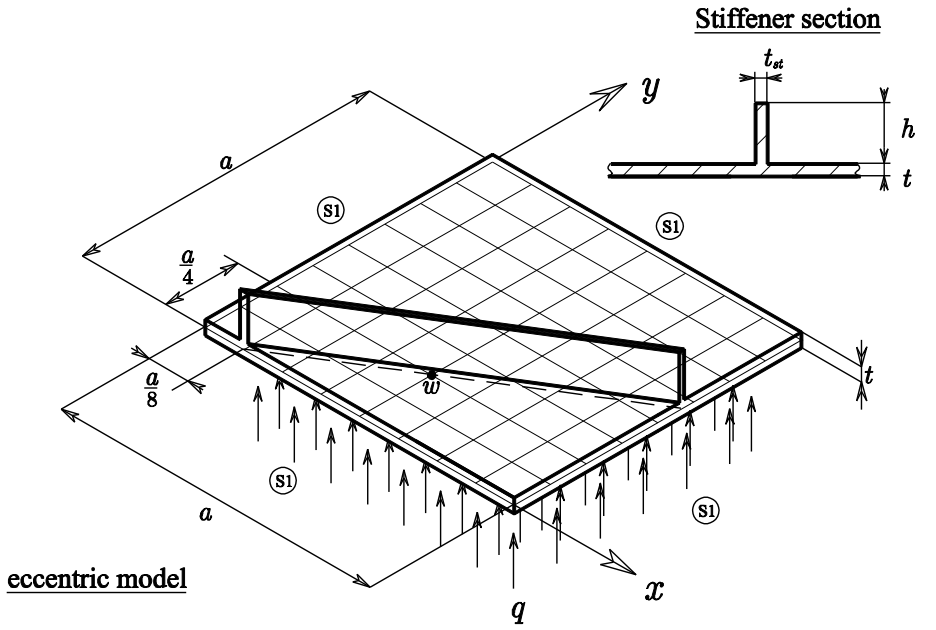


eccentric model

**Figure 5-14 Details of the square panel with an arbitrary orientated stiffener.**

In contrast, both NLSPAN models required only a single quadrilateral region to represent the same arbitrary stiffened panel, thus simplifying the modelling procedure by avoiding the use of Boolean operations.

Furthermore, although it was possible to discretize the ANSYS models by adopting an automatic meshing procedure, the topological constraints had a detrimental effect on the shape quality of the finite elements present in the model. This becomes evident when comparing ANSYS's conventional, finite element discretisation (Figure 5-15.) with NLSPAN's arbitrarily stiffened, finite element discretisation (Figure 5-14).

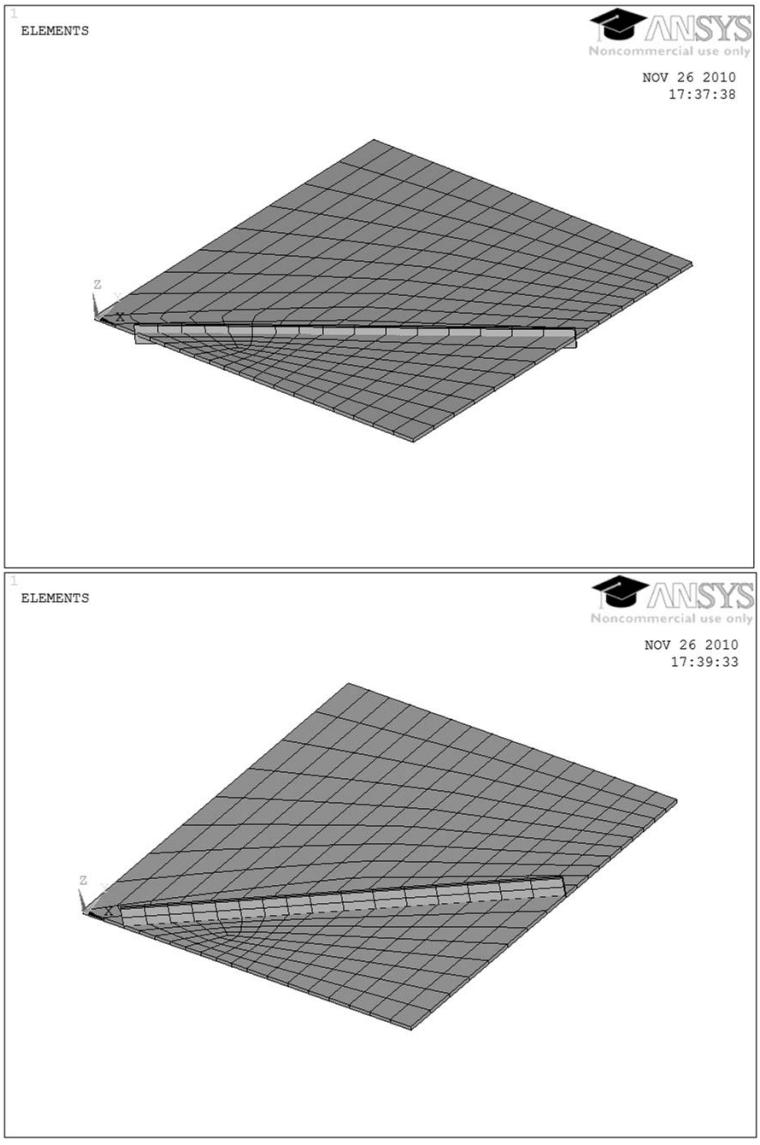


**Figure 5-15 ANSYS finite element models of the arbitrarily stiffened panel.**

The full non-linear response path was calculated in NLSPAN, using an 8x8 square mesh shown in Figure 5-14, and then compared with the one obtained using ANSYS. The comparison data for the out of the plane deflections of a point located at $x = a / 2$ and $y = a / 4$ is presented in Table 5-15 and illustrated in Figure 5-16.

It can be appreciated in Figure 5-16 that both panels exhibit a stiffening behaviour with the concentrically stiffened panel showing, as expected, the largest deformation. Furthermore, the low average absolute differences calculated for both the concentric (1.1%) and eccentric (1.4%) cases show that a close agreement was obtained between the present arbitrarily orientated stiffener formulation (NLSPAN) and ANSYS for both stiffener configurations (i.e. eccentrically and concentrically stiffened panels).

**Table 5-15 Comparison of the out of the plane deflection results for the arbitrary stiffened models.**

| $\frac{qa^4}{Et^4}$ | $w/t$ | | | |
|---|---|---|---|---|
| | Eccentric | | Concentric | |
| | ANSYS | NLSPAN | ANSYS | NLSPAN |
| 29.4 | 0.272 | 0.288 (6.0%) | 0.447 | 0.439 (1.8%) |
| 58.8 | 0.452 | 0.464 (2.7%) | 0.670 | 0.655 (2.3%) |
| 88.2 | 0.584 | 0.592 (1.4%) | 0.818 | 0.803 (1.8%) |
| 117.6 | 0.693 | 0.697 (0.5%) | 0.933 | 0.919 (1.6%) |
| 147.1 | 0.785 | 0.785 (0.1%) | 1.029 | 1.015 (1.4%) |
| 176.5 | 0.866 | 0.864 (0.3%) | 1.112 | 1.098 (1.3%) |
| 205.9 | 0.939 | 0.933 (0.6%) | 1.186 | 1.171 (1.3%) |
| 235.3 | 1.005 | 0.997 (0.8%) | 1.253 | 1.238 (1.2%) |
| 264.7 | 1.066 | 1.056 (1.0%) | 1.313 | 1.298 (1.1%) |
| 294.1 | 1.122 | 1.110 (1.1%) | 1.369 | 1.354 (1.0%) |
| 323.5 | 1.175 | 1.161 (1.2%) | 1.420 | 1.406 (1.0%) |
| 352.9 | 1.224 | 1.209 (1.2%) | 1.469 | 1.455 (0.9%) |
| 441.2 | 1.357 | 1.338 (1.4%) | 1.599 | 1.586 (0.8%) |
| 588.2 | 1.539 | 1.519 (1.3%) | 1.780 | 1.768 (0.7%) |
| 735.3 | 1.696 | 1.672 (1.4%) | 1.931 | 1.920 (0.6%) |
| 882.4 | 1.831 | 1.805 (1.4%) | 2.062 | 2.052 (0.5%) |
| 1029.4 | 1.951 | 1.923 (1.4%) | 2.178 | 2.169 (0.4%) |
| 1176.5 | 2.060 | 2.031 (1.4%) | 2.284 | 2.275 (0.4%) |

Note: Figures in brackets denote the absolute percentage differences

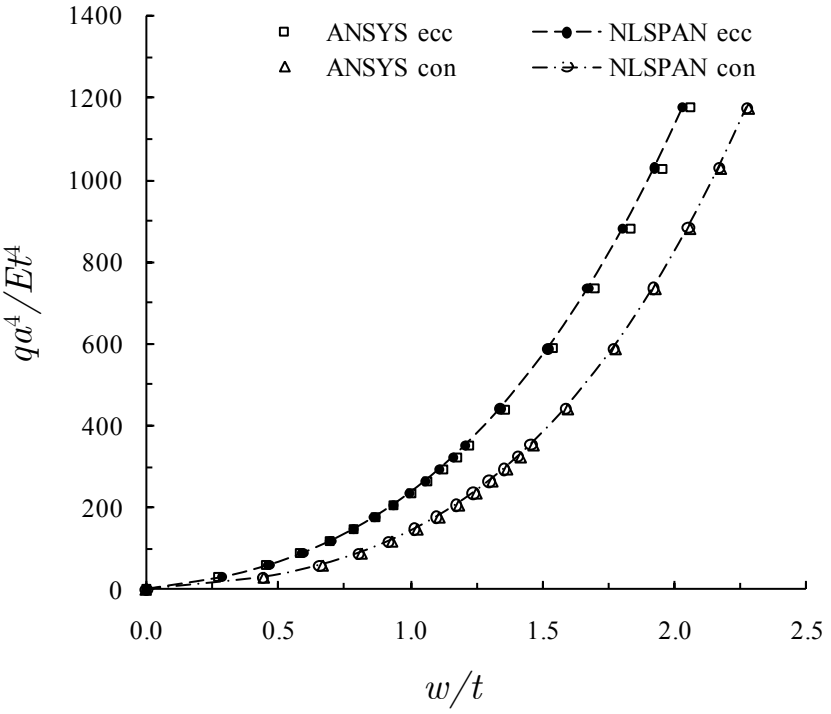


**Figure 5-16 Non-dimensional load-deflection result of the arbitrary stiffened plate.**

## 5.4 Summary

A validation has been conducted to evaluate the performance of the presented formulation in representing both unstiffened and stiffened panels under transverse loads.

The results obtained using the current formulation to represent unstiffened panels under transverse loads are in excellent agreement with analytical and numerical results presented by other authors. Good agreement was found with experimental results; however, due attention must be given to the correct representation of the boundary conditions of the panel.

A thorough validation of the present formulation capability of modelling stiffened panels was presented. Special attention was given to verify the claim that the slave element can be placed at an arbitrary orientation within the master element and not necessarily along the mesh lines. Excellent agreement was found in all investigated cases. In all cases the accuracy of the concentrically stiffened panel results normally outperforms the accuracy of eccentrically stiffened panels.

# Chapter 6. Post-buckling analysis validation

## 6.1 Introduction

In the previous Chapter, the performance, accuracy and applicability of NLSPAN in the analysis of stiffened and unstiffened panels under transverse loads was validated through a series of numerical examples. Similarly, in this Chapter the same qualities will be evaluated for the analysis of stiffened and unstiffened panels under in-plane loads.

Following the same approach used in Chapter 5, here the validation work was divided into two parts:

1. Analysis of unstiffened panels under in-plane load (Section 6.2)
2. Analysis of stiffened panels in-plane load (Section 6.3)

The validation of unstiffened panels not only ensures that the master element is capable of representing the behaviour of a unstiffened panel under in-plane loads but also gives guidance on the mesh density required in the subsequent validation of NLSPAN's stiffened panel analysis capability.

Section 6.3 includes a validation of the stiffener edge load modelling technique suggested in 4.4.2 of Chapter 4. The influence of the suggested method in the accuracy of the linear buckling calculations is demonstrated.

An illustration that summarizes important details of the investigated panel (panel dimensions, coordinate system, material properties and finite element mesh) has been provided in each validation problem. The boundary conditions are detailed in each illustration according to the notation defined in Table 4-1 and Table 4-2 of Section 4.4.2. The illustration also defines, using the letter $w$, the point where the out of the plane deflection is measured.

The non-dimensional results of each validation problem are presented in both graphical and tabular form in order to facilitate the study of the difference between the presented data sets. The non-dimensional quantities defined in order to present the validation results are listed in Table 6-1.

**Table 6-1 Non-dimensional quantities for panels under in-plane load.**

| | |
|---|---|
| $w/t$ | Non-dimensional out of the plane deflection |
| $\Delta = \frac{\overline{v}a}{t^2}$ | Non-dimensional edge shortening |
| $\overline{\sigma}_y a^2 / \pi^2 E t^2$ | Non-dimensional average edge stress |
| $q_{crit} b^2 / \pi^2 D$ | Non-dimensional linear buckling load |
| $A_{st}/at$ | Stiffener area ratio |
| $h / t$ | Stiffener height to plate thickness ratio |
| $EI_{st}/Db$ | Bending stiffness ratio |
| $\overline{\sigma}_y / E(\overline{v}a / t^2)$ | Effective width of the panel |

## 6.2 Unstiffened panels under in-plane load

The post-buckling behaviour of isotropic and laminated unstiffened panels under the action of in-plane loads is studied in this Section.

Three examples are analysed and discussed. The first two problems (Sections 6.2.1 and 6.2.2 respectively) investigate the performance of the current formulation in modelling the non-linear buckling response of isotropic panels under uniform edge shortening by comparing the results obtained using the proposed formulation with analytical and numerical results.

The third problem (Section 6.2.3) investigates NLSPAN's performance in representing the non-linear behaviour of laminated panels under uniform edge shortening by comparing the results obtained in this investigation with experimental and numerical results.

### 6.2.1 Post-buckling of rectangular simply supported isotropic unstiffened panels

The post-buckling behaviour of a simply supported square plate with small initial curvature loaded in edge compression was investigated first. The analytical solution of this problem was obtained by Yamaki (1959) using series solution. This problem was used by Pica and Wood (1980) to validate their nine node quadratic Lagrangian geometrically non-linear finite element formulation.

Here the post-buckling response was found using a quarter symmetry model with a 4x4 mesh density. An initial deformation factor, equal to 0.1 times the plate thickness, was applied to the linear buckling mode shape (half wave in the x and y directions) to obtain the initially deflected shape. Due to symmetry only half of the uniform end-shortening, $\overline{v}\,/\,2$, was applied on the edge located at $y = a\,/\,2$ in the negative y direction. The non-linear solution was obtained using force and displacement convergence tolerances of 1%. A summary of the plate dimension, mesh density and material properties is presented in Figure 6-1.

The analytical non-dimensional deflection results obtained by Yamaki, the finite element results of Pica and those obtained using the proposed formulation are presented in Table 6-2. The results obtained using NLSPAN were found to be in excellent agreement with those of Yamaki with an average error of only 0.9%. Pica's results were found to contain a much higher average error (4.8%), however this discrepancy is mainly due to a single large error on the first load step (54.3%).

The analytical non-dimensional average edge stress results obtained by Yamaki, the finite element results of Pica and those obtained using NLSPAN are presented in Table 6-3. As expected for a nine node Lagrangian element, the average edge stress results of Pica *et al.* show a better correlation (0.9%) with the analytical results of Yamaki than the current formulation (3.1%).

| Material properties | Dimensions |
|---|---|
| $E =$ 30.0 $(10^6)$ psi [207 Gpa] | $a =$ 400.0 in [10.16 m] |
| $\mu =$ 0.333 | $t =$ 1.5 in [38.10 mm] |

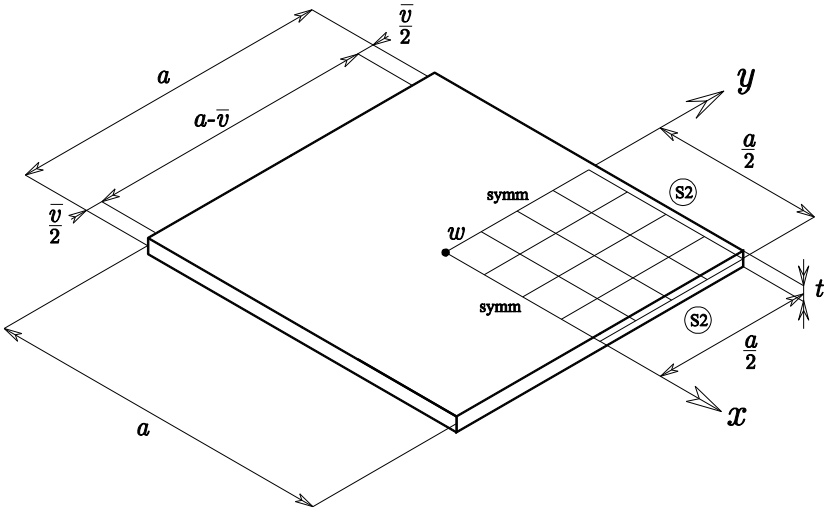


**Figure 6-1 Details of the simply supported panel under uniform edge compression.**

**Table 6-2 Non-dimensional out of the plane deflection of a simply supported square panel under uniform edge shortening.**

| $\Delta = \frac{\overline{v}a}{t^2}$ | $w/t$ | | | | |
|---|---|---|---|---|---|
| | Yamaki (analytical) | Pica | | NLSPAN | |
| 2.133 | 0.125 | 0.057 | (54.3%) | 0.120 | (4.0%) |
| 2.880 | 0.249 | 0.251 | (0.6%) | 0.242 | (2.8%) |
| 3.805 | 0.496 | 0.494 | (0.4%) | 0.495 | (0.1%) |
| 4.729 | 0.739 | 0.740 | (0.2%) | 0.731 | (1.1%) |
| 5.796 | 0.976 | 0.976 | (0.0%) | 0.975 | (0.1%) |
| 8.533 | 1.435 | 1.447 | (0.8%) | 1.428 | (0.5%) |
| 12.124 | 1.871 | 1.879 | (0.4%) | 1.869 | (0.1%) |
| 16.498 | 2.288 | 2.294 | (0.2%) | 2.288 | (0.0%) |
| 21.760 | 2.693 | 2.700 | (0.3%) | 2.693 | (0.0%) |
| 27.875 | 3.091 | 3.097 | (0.2%) | 3.084 | (0.2%) |
| 34.844 | 3.487 | 3.487 | (0.0%) | 3.471 | (0.5%) |
| 42.737 | 3.885 | 3.877 | (0.2%) | 3.857 | (0.7%) |

Note: Figures in brackets denote the absolute percentage error

**Table 6-3 Non-dimensional average edge stress of a simply supported square panel under uniform edge shortening.**

| $\Delta = \frac{\overline{v}a}{t^2}$ | $\overline{\sigma}_y a^2 / \pi^2 E t^2$ | | | | |
|---|---|---|---|---|---|
| | Yamaki (analytical) | Pica | | NLSPAN | |
| 2.133 | 0.212 | 0.215 | (1.3%) | 0.205 | (3.3%) |
| 2.880 | 0.278 | 0.278 | (0.0%) | 0.269 | (3.2%) |
| 3.805 | 0.342 | 0.342 | (0.1%) | 0.331 | (3.3%) |
| 4.729 | 0.390 | 0.390 | (0.1%) | 0.372 | (4.5%) |
| 5.796 | 0.438 | 0.437 | (0.2%) | 0.417 | (4.9%) |
| 8.533 | 0.546 | 0.540 | (1.1%) | 0.518 | (5.2%) |
| 12.124 | 0.672 | 0.669 | (0.4%) | 0.637 | (5.3%) |
| 16.498 | 0.810 | 0.808 | (0.2%) | 0.779 | (3.8%) |
| 21.760 | 0.963 | 0.959 | (0.4%) | 0.937 | (2.7%) |
| 27.875 | 1.126 | 1.117 | (0.8%) | 1.107 | (1.7%) |
| 34.844 | 1.300 | 1.281 | (1.5%) | 1.290 | (0.8%) |
| 42.737 | 1.486 | 1.451 | (2.4%) | 1.486 | (0.0%) |

Note: Figures in brackets denote the absolute percentage error

### 6.2.2 Post-buckling of rectangular simply supported/clamped isotropic unstiffened panels

In this Section, the post-buckling behaviour of a simply supported/clamped square plate with small initial curvature loaded in edge compression has been investigated using the current formulation. The analytical solution of this problem was also obtained by Yamaki (1959) using series solution.

Here, the post-buckling response was obtained using a full model with an 8x8 mesh. The initial deformation factor used by Yamaki, i.e. 0.1 times the plate thickness, was applied to the linear buckling mode shape to obtain the initially deflected shape. In this case the clamped boundary conditions, along the edges located at $x = 0$ and $x = a$, force the buckling mode shape to adopt a full sine wave in the $y$ direction whilst maintaining a half sine wave in the $x$ direction.

Uniform end-shortening $\overline{v}$ was applied along the edge located at $y = a$ in the negative y direction. The non-linear solution was obtained using force and displacement convergence tolerances of 1%. A summary of the plate dimension, mesh density and material properties is presented in Figure 6-2.

The non-dimensional maximum displacement results and the non-dimensional average edge stress results obtained by Yamaki, Pica *et al.* and in the present investigation at different non-dimensional edge shortenings levels are presented in Table 6-4 and Table 6-5, respectively.

The non-dimensional deflection results obtained using NLSPAN did not perform as well as those of Pica. However, the average edge stress results show a similar accuracy.

| Material properties | Dimensions |
|---|---|
| $E =$ 30.0 ($10^6$) psi [207 Gpa] | $a =$ 400.0 in [10.16 m] |
| $\mu =$ 0.333 | $t =$ 1.5 in [38.10 mm] |

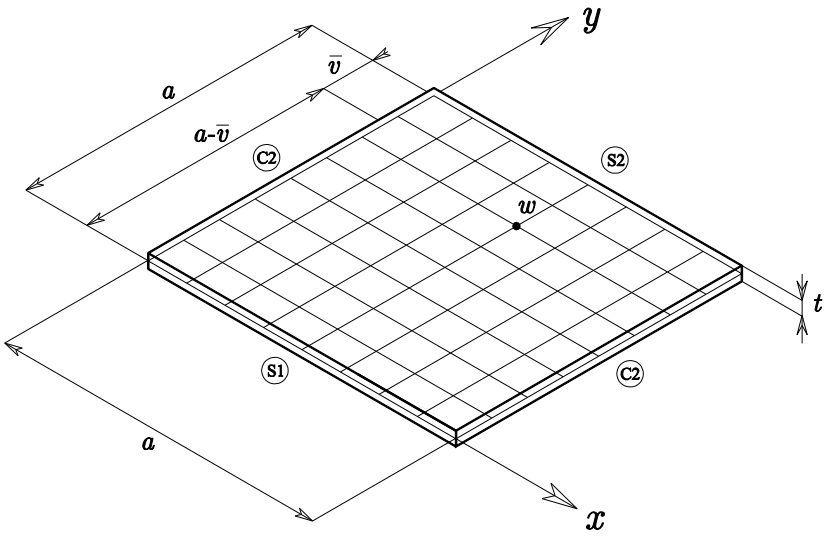


**Figure 6-2 Details of the simply supported /clamped panel under uniform edge compression.**

**Table 6-4 Non-dimensional out of the plane deflection of a simply supported/clamped square panel under uniform edge shortening.**

| $\Delta = \frac{\bar{v}a}{t^2}$ | $w/t$ | | | | |
|---|---|---|---|---|---|
| | Yamaki (analytical) | Pica | | NLSPAN | |
| 3.9314 | 0.1020 | 0.1022 | (0.2%) | 0.0987 | (3.2%) |
| 5.5035 | 0.2042 | 0.2061 | (0.9%) | 0.1946 | (4.7%) |
| 7.6926 | 0.4091 | 0.4107 | (0.4%) | 0.3932 | (3.9%) |
| 10.0244 | 0.6152 | 0.6156 | (0.1%) | 0.5995 | (2.5%) |
| 12.9370 | 0.8324 | 0.8230 | (1.1%) | 0.8103 | (2.7%) |
| 21.2461 | 1.2515 | 1.2586 | (0.6%) | 1.2443 | (0.6%) |
| 34.0752 | 1.7060 | 1.7013 | (0.3%) | 1.7019 | (0.2%) |
| 52.8774 | 2.1964 | 2.1813 | (0.7%) | 2.1885 | (0.4%) |

Note: Figures in brackets denote the absolute percentage error

**Table 6-5 Non-dimensional average edge stress of a simply supported/clamped square panel under uniform edge shortening.**

| $\Delta = \frac{\overline{v}a}{t^2}$ | $\overline{\sigma}_y a^2 \Big/ \pi^2 E t^2$ | | | | |
|---|---|---|---|---|---|
| | Yamaki (analytical) | Pica | | NLSPAN | |
| 3.9314 | 0.3860 | 0.3859 | (0.0%) | 0.3810 | (1.3%) |
| 5.5035 | 0.5240 | 0.5189 | (1.0%) | 0.5165 | (1.4%) |
| 7.6926 | 0.6750 | 0.6739 | (0.2%) | 0.6655 | (1.4%) |
| 10.0244 | 0.7990 | 0.7969 | (0.3%) | 0.7893 | (1.2%) |
| 12.9370 | 0.9340 | 0.9307 | (0.4%) | 0.9264 | (0.8%) |
| 21.2461 | 1.2690 | 1.2503 | (1.5%) | 1.2774 | (0.7%) |
| 34.0752 | 1.7210 | 1.6964 | (1.4%) | 1.7525 | (1.8%) |
| 52.8774 | 2.3200 | 2.2647 | (2.4%) | 2.3543 | (1.5%) |

Note: Figures in brackets denote the absolute percentage differences

### 6.2.3 **Post-buckling of rectangular laminated unstiffened panels**

The behaviour of composite panels under uniform edge compression was investigated experimentally and analytically by Starnes and Rouse (1981). In this investigation various laminated specimens were fabricated from commercially available unidirectional Thornel 300 graphite fibre tapes pre-impregnated with 450K cure Narmco 5208 thermosetting epoxy resin. The tapes were laid up to a 24-ply orthotropic laminate. It must be noted that the 0° ply orientation angle was parallel to the $y$ axis.

The specimen considered here was 508 mm long and 177.8 mm wide (panel C4). The loading condition assumed for these calculations was uniform edge shortening $\overline{v}$ along on the edge located at $y = b$ in the negative $y$ direction, and the boundary conditions were assumed to be clamped along the loaded edges (C1-C2) and simply supported (S4) along the unloaded edges.

An initial deformation factor of 5% of the specimen's thickness was applied to the linear buckling mode shape to obtain the initially deflected shape. The geometrically non-linear response of the model was obtained at using a force and displacement convergence tolerance of 1%. A summary of the model dimension, mesh density, lamination details and material properties is presented in Figure 6-3.

The non-dimensional deflection behaviour along the longitudinal ( $x = b/2$ ) and transverse ( $y = a/4$ ) directions of the plate at different non-dimensional end shortening levels are presented in Figure 6-4 and Figure 6-5 respectively. A cubic spline was fitted to the nodal results to appreciate the buckled shape of the panel.

It can be seen that the plate adopts a full sine wave in the longitudinal direction and a half sine wave in the transverse direction. In these plots the edge shortening levels were normalized using the end shortening at buckling calculated by Starnes and Rouse using STAGS general shell analysis computer code ( $\overline{v}_{crit} = 0.5mm$ ) whilst the maximum out of plane deflection was normalized with the total panel thickness.

A comparison between the results obtained in this investigation using NLSPAN, the experimental results of Starnes and Rouse, as well as the analytical results obtained by Starnes and Rouse using the STAGS are presented in Figure 6-6 and Figure 6-7. It must be noted that the comparison results were obtained by digitizing the data presented by Starnes and Rouse's in graphical form (Starnes and Rouse, 1981).

In Figure 6-7 the maximum out of plane deflections are plotted against the average longitudinal edge stress in the $y$ direction. In this plot the average longitudinal edge stress was normalized using the critical edge stress calculated by Starnes and Rouse using STAGS ( $\sigma_{crit} = 70MPa$ ).

NLSPAN results are in excellent agreement with the experimental results that Starnes and Rouse over the whole response history. The analytical results obtained by Starnes and Rouse using STAGS show stiffer pre-buckling behaviour, however they also are in close agreement in the post-buckling zone.

The edge shortening results are shown as function of the average edge stress in Figure 6-7. In this plot edge shortening was normalized using the end shortening at buckling calculated by Starnes and Rouse using STAGS ( $\overline{v}_{crit} = 0.5mm$ ). Good agreement was found with both the experimental and numerical results.

**Material properties**

$E_{11}$ = 131.00 GPa
$E_{22}$ = 13.03 GPa
$G_{12}$ = 6.41 Gpa
$G_{23}$ = 2.61 Gpa
$\mu_{12}$ = 0.38

**Dimensions**

$b$ = 177.80 mm
$a$ = 508.00 mm
$t$ = 3.23 mm
$t_{ply}$ = 0.14 mm

**Lamination**

$[\pm 45/0_2/\pm 45/0_2/0/90]_S$

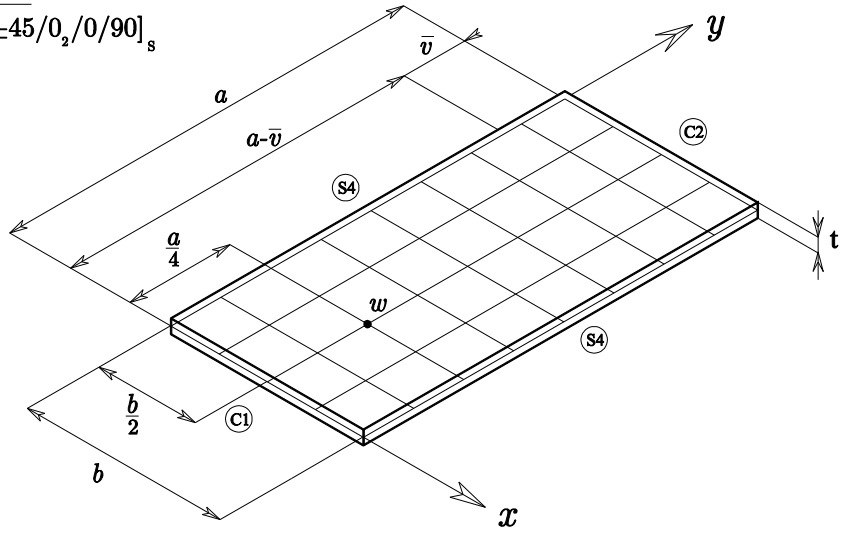


**Figure 6-3 Details of the rectangular laminated panel.**

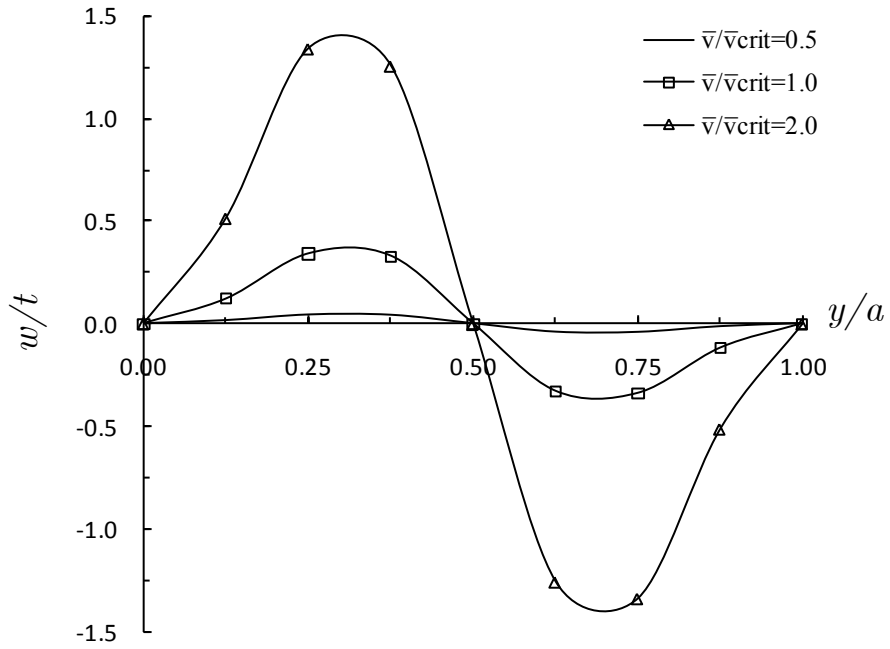


**Figure 6-4 Non-dimensional out of the plane deflection along the longitudinal direction of the panel at different non-dimensional end shortening levels.**

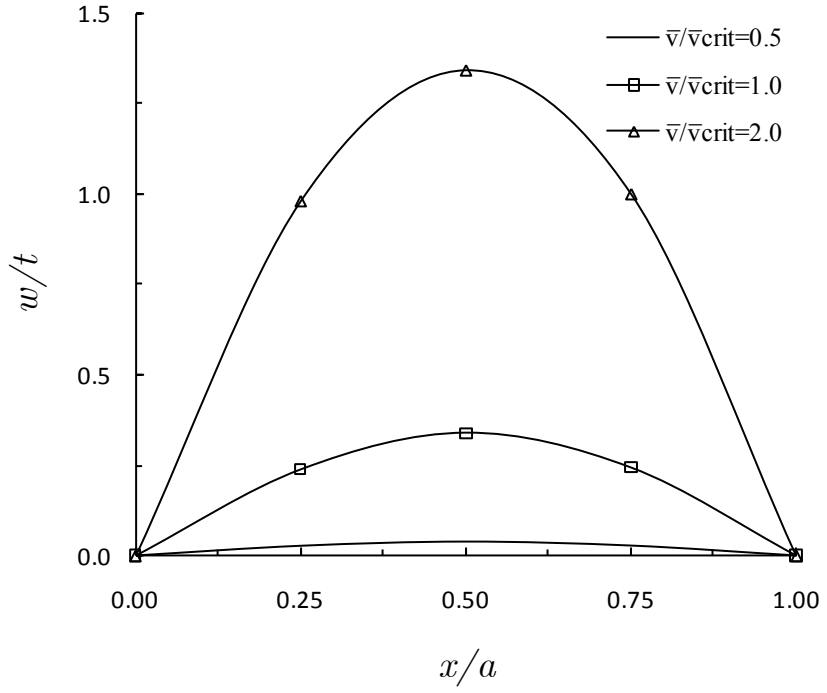


**Figure 6-5 Non-dimensional out of the plane deflection along the transverse direction of the panel at different non-dimensional end shortening levels.**

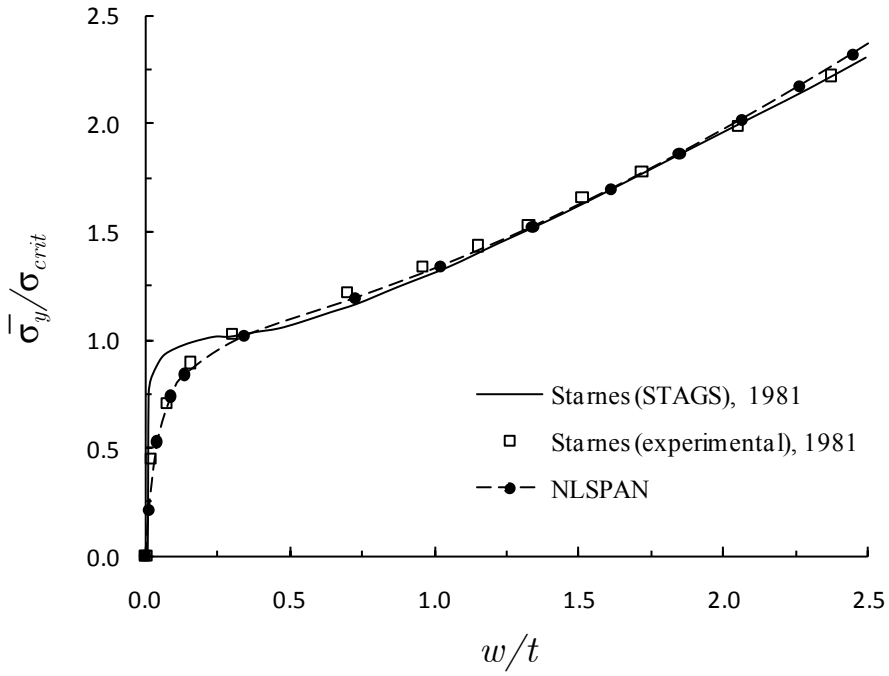


**Figure 6-6 Non-dimensional average edge stress-deflection behaviour of the rectangular laminated panel.**

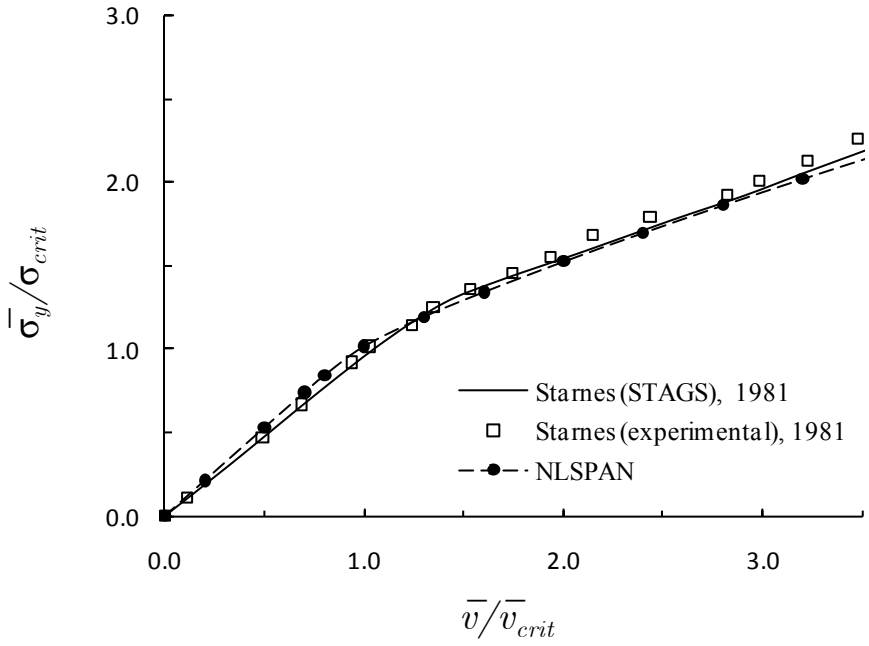


**Figure 6-7 Non-dimensional average edge stress-end shortening behaviour of the rectangular laminated panel.**

## 6.3 Linear buckling of stiffened panels

The linear buckling behaviour of concentrically and eccentrically stiffened panels under in-plane compression is investigated in this Section.

First, in Section 6.3.1, the compressive edge load modelling method for arbitrarily stiffened elements suggested in Section 4.4.2 is discussed and validated.

After that, the effect of the load modelling method in the linear buckling calculations of stiffened panels under the action of edge compression is investigated for stiffened panels with different $h / t$ and $a / b$ ratios in Sections 6.3.2 and 6.3.3 respectively.

### 6.3.1 In-plane stress in stiffened panels under uniform edge compression

In this Section the influence of the in-plane load application method, suggested in Section 4.4.2, in the in-plane stress calculations of stiffened panels under in plane compressive loads, is discussed and validated for both the concentrically and eccentrically stiffened panels.

First the concentric configuration is investigated by analysing the in-plane behaviour of the isotropic stiffened panel shown in Figure 6-8. In this problem the panel resists the action of uniform edge compression, of unitary magnitude, applied to both the plate and the stiffener cross sectional areas. In such a panel the in-plane displacement field and the in-plane stress field should have a unitary value.

It must be noted that the stiffener was not placed along the edges of the shallow shell elements. In addition, the dimensions and mesh density used in this problem were selected in such a way that the ends of the stiffener do not coincide with the edge nodes of the shallow shell elements.

First, and in order to highlight the magnitude of the error in the in-plane results generated if stiffener load is not accurately modelled, the panel is loaded by only applying a uniform in-plane compressive load along the edge of the finite element model.

The magnitude of the error in the in-plane compressive stress calculated at each corner node of the concentrically stiffened panel model, in absence of the stiffener load, is

presented in Figure 6-9. It can be appreciated that very high levels of error are present across the entire model.

Most significant is the magnitude of error on the section of the loaded edge close to which the end point of the stiffener is located ($x / a = 2 / 5$ and $y / a = 1$). At this location the magnitude of error in the calculated in-plane stress values reaches a maximum of more than 80%.

In comparison, if the stiffener load is modelled using the method suggested in Section 4.4.2.1, no appreciable error in the in-plane compressive stress results, shown in Figure 6-10, can be observed across the entire model.

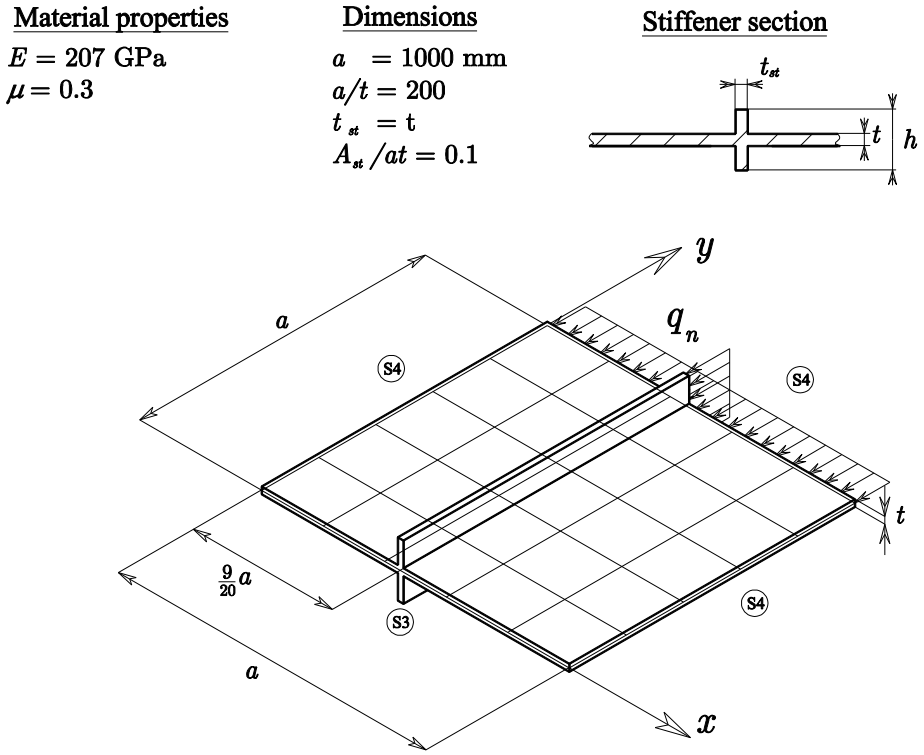


**Figure 6-8 Details of the concentrically stiffened panel under uniform edge compression.**

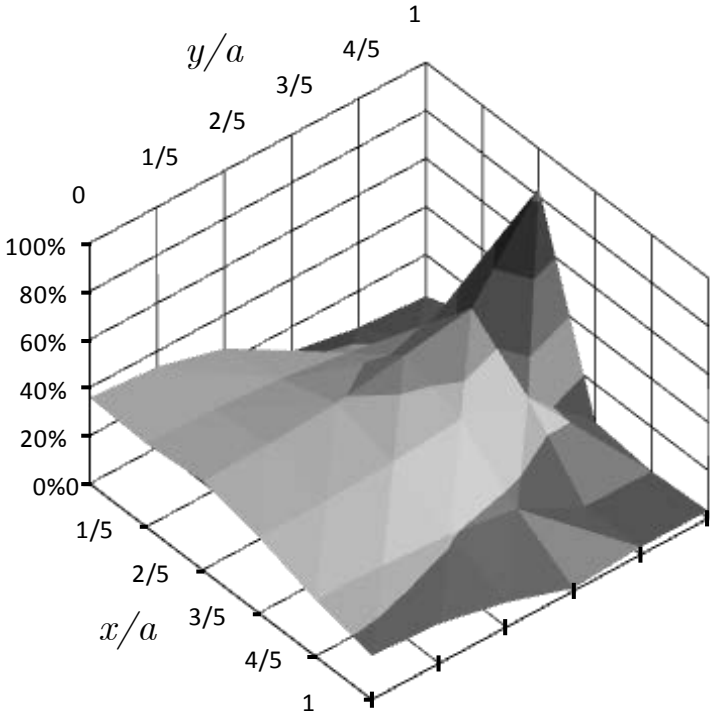


**Figure 6-9 Magnitude of the error of the in-plane compressive stress of the concentrically stiffened panel in absence of the stiffener load.**

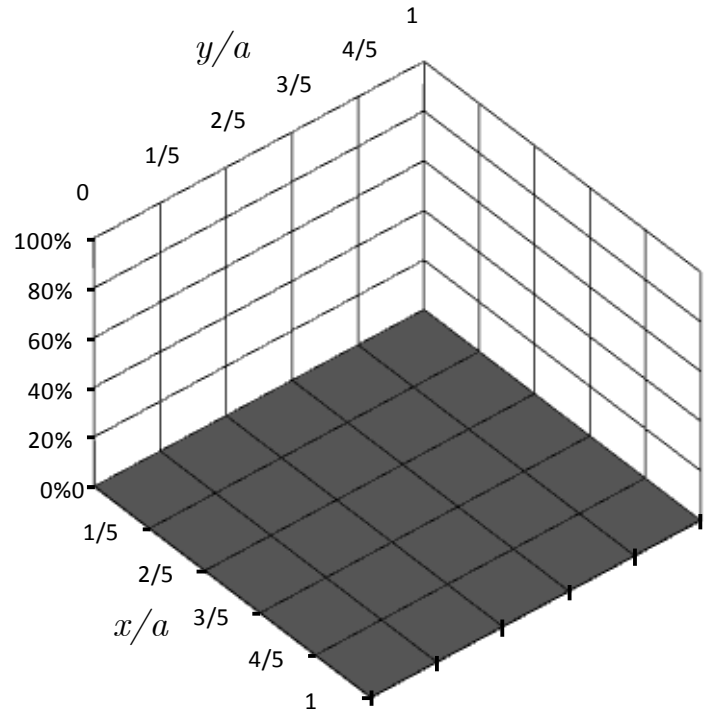


**Figure 6-10 Magnitude of the error of the in-plane compressive stress of the concentrically stiffened panel when the stiffener load is included.**

Next, the eccentric configuration is investigated by analysing the in-plane behaviour of the stiffened panel shown in Figure 6-11. As in the previous example, here the panel resists the action of uniform edge compression applied to both the plate and the stiffener cross sectional areas. Again, the stiffener location was selected so it is not aligned with the shallow shell element nodes.

In order to demonstrate the magnitude of the error in the in-plane results, generated if both stiffener loads (force and couple) are not accurately modelled, the panel is loaded first by only applying uniform in-plane compressive loading along the edge of the finite element model.

The magnitude of the error in the in-plane compressive stress calculated at each corner node of the concentrically stiffened panel model, in absence of the stiffener loads, is presented in Figure 6-12.

It can be appreciated that high levels of error are present across the entire model. Most significant is the magnitude of error on the section of the loaded edge close to which the end point of the stiffener is located ($x / a = 2 / 5$ and $y / a = 1$). At this location the magnitude of error in the calculated in-plane stress values reaches a maximum close to 40%.

In addition, the absence of the stiffener couple generates noticeable out of plane deflections (Figure 6-13) along the entire panel.

Nevertheless, Figure 6-14 and Figure 6-15 demonstrate that, if the in-plane load modelling method suggested in Section 4.4.2.2 is utilized, i.e. an extra stiffener force and couple are applied to the model, both the in-plane compressive stress error and the fictitious out of plane deflections completely vanish from the panel.

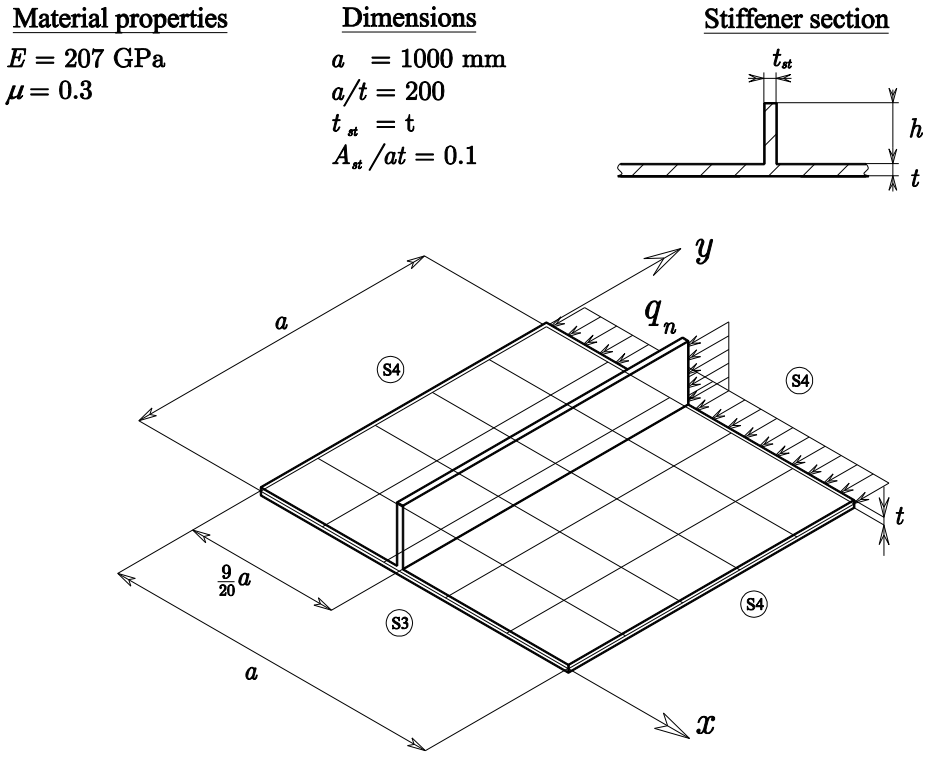


**Figure 6-11 Details of the eccentrically stiffened panel under uniform edge compression.**

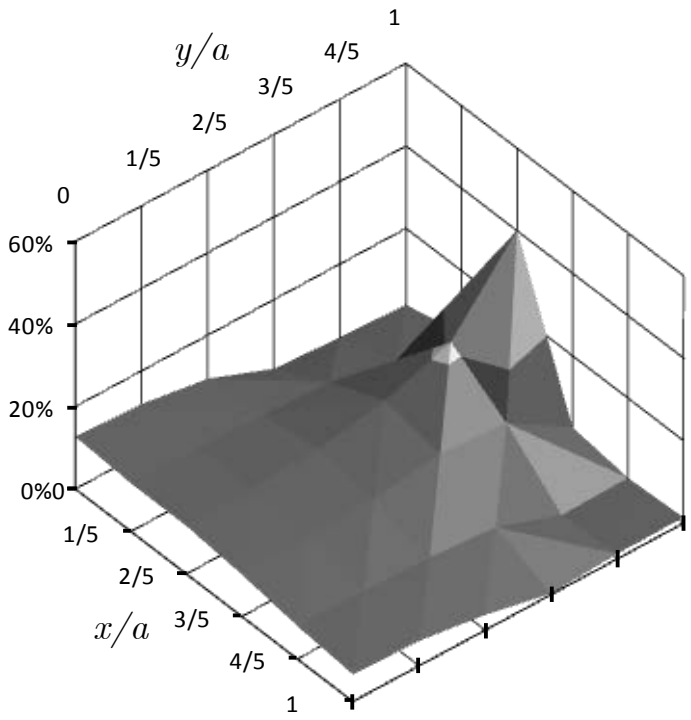


**Figure 6-12 Magnitude of the error of the in-plane compressive stress of the eccentrically stiffened panel in absence of the stiffener load.**

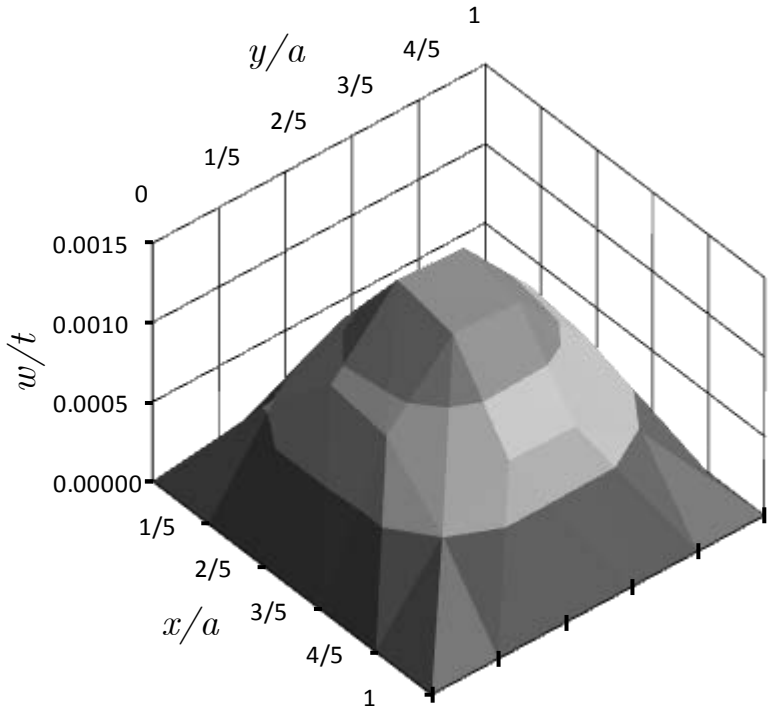


**Figure 6-13 Non-dimensional out of plane deflections due to stiffener eccentricity in absence of the stiffener couple.**

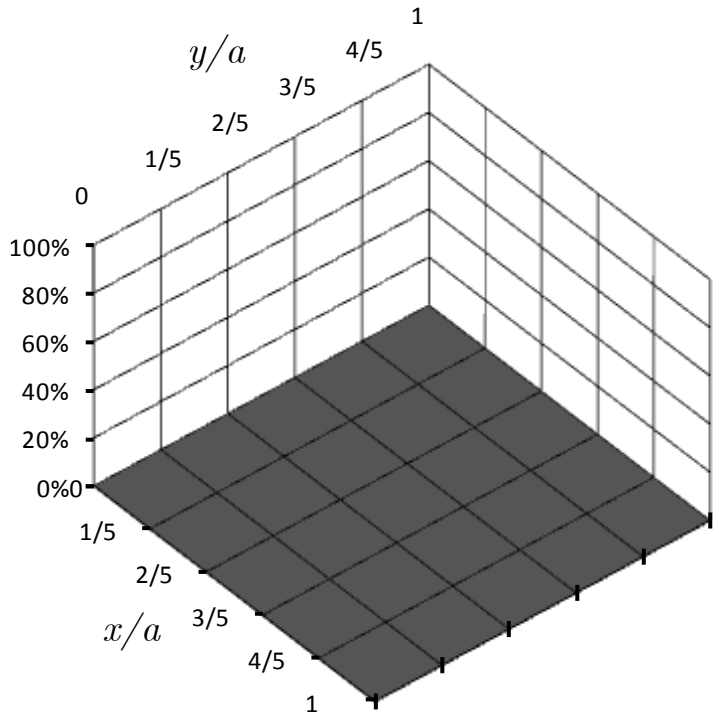


**Figure 6-14 Magnitude of the error of the in-plane compressive stress of the eccentrically stiffened panel when the stiffener load is included.**

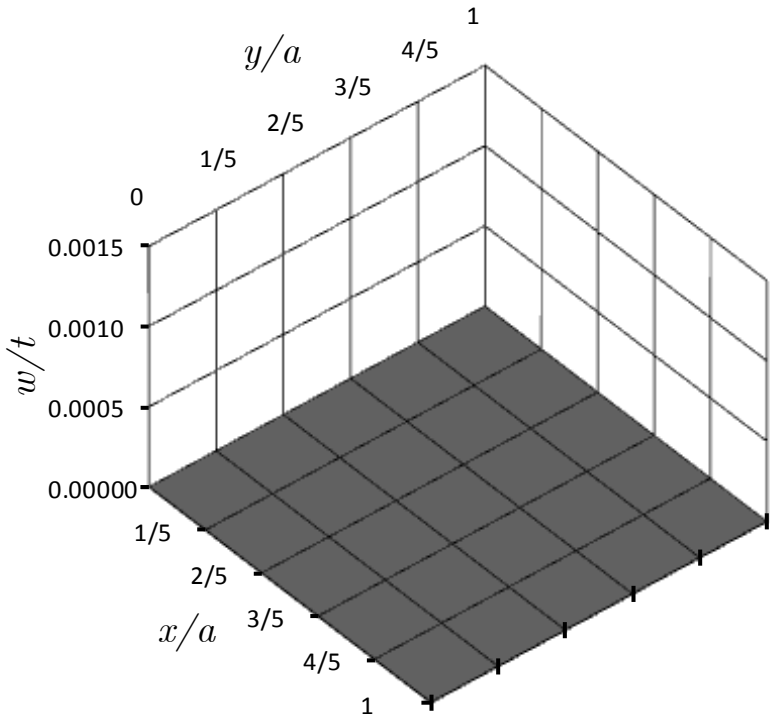


**Figure 6-15 Non-dimensional out of plane deflections due to stiffener eccentricity when the stiffener couple is included.**

### 6.3.2 Linear buckling of stiffened panels with different h/t ratios

The effect of a correct stiffener load modelling method in the accuracy of the linear buckling calculations is investigated next for stiffened panels with different $h/t$ ratios. The linear buckling calculations are of critical importance for the non-linear buckling calculation as they provide the buckling mode shape used to define the initial deformations in the panel.

In this Section, the relationship between the non-dimensional linear buckling load and the height of the stiffener ($h$) to plate thickness ($t$) ratio for a two simply supported stiffened panels with a single stiffener running in the direction of the applied load is presented and compared with the semi-analytical results obtained by Bedair (1998).

Both eccentrically and concentrically stiffened panels are considered. All panels were analysed using a full model with a 11x11 mesh in order to capture different buckling mode shapes caused by the variation in the $h/t$ ratio. A summary of the panel dimensions, material properties and mesh density is presented in Figure 6-16.

The non-dimensional linear buckling load results for concentrically and eccentrically stiffened panels with different $h/t$ ratios, and no torsional stiffness, calculated by Bedair are presented in Figure 6-17 and Figure 6-18 respectively. It must be noted that these results were obtained in this investigation by digitizing the data presented by Bedair (1998) in graphical form.

Each of Bedair's results sets, i.e. concentric and eccentric results, was compared with two different sets of results obtained in the present investigation using NLSPAN. In the first set of results the geometric stiffness matrix was calculated using the in-plane stresses obtained for the traditional load case that omits the stiffener load, whilst in the second set the geometric stiffness matrix was calculated using in-plane stress results obtained following the load calculation method described in sections 4.4.2.1 and 4.4.2.2 respectively.

Figure 6-17 and Figure 6-18 show that the absence of the stiffener load in the in-plane stress calculation caused an overestimation of the critical buckling load in both the eccentric and concentric models. Furthermore, In both the concentric and eccentric case, excellent agreement was found for all $h/t$ ratios when the suggested method was followed.

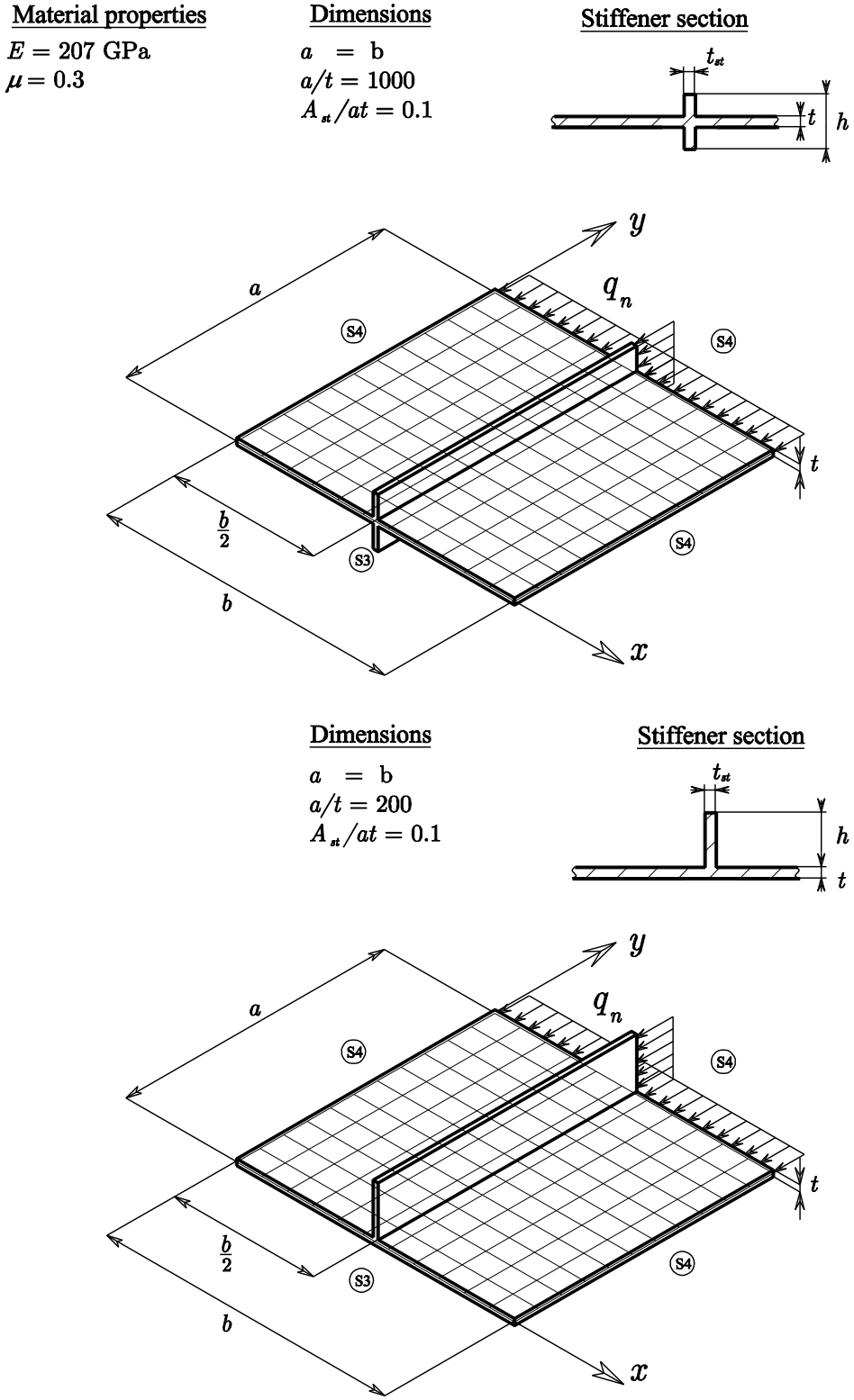


**Figure 6-16 Details of the stiffened panels with different h/t ratios.**

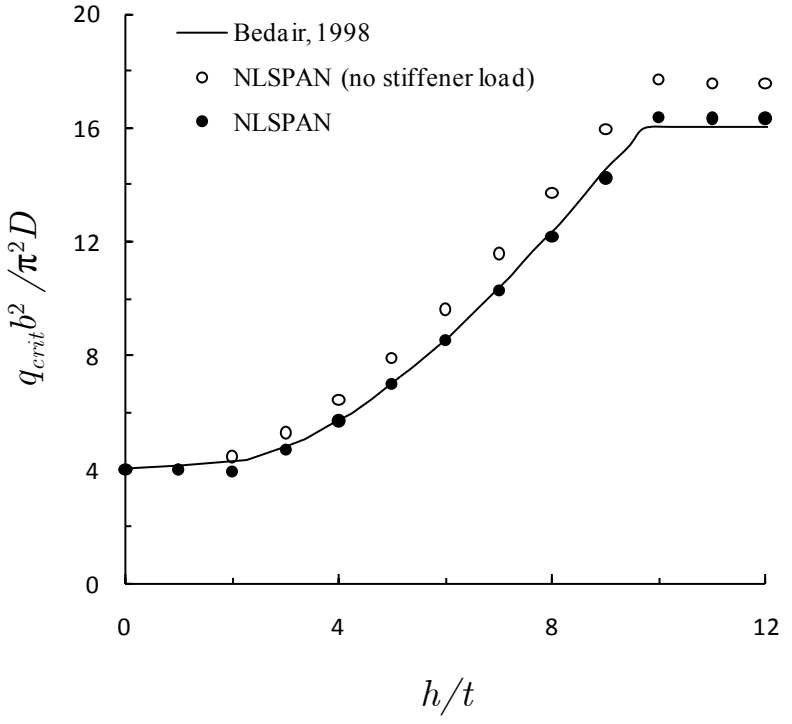


**Figure 6-17 Non-dimensional linear buckling load for concentrically stiffened panels with different h/t ratios.**

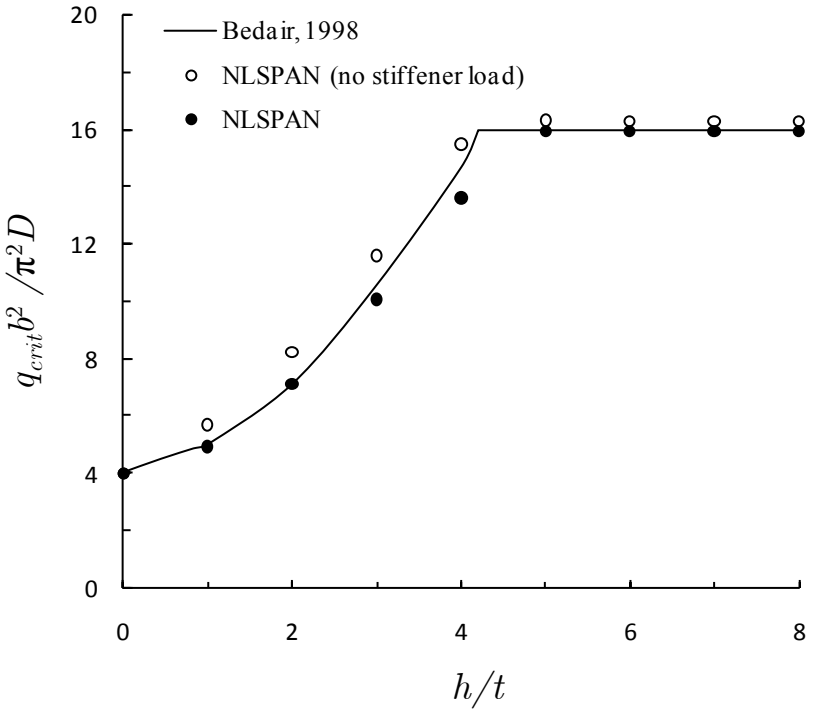


**Figure 6-18 Non-dimensional linear buckling load for eccentrically stiffened panels with different h/t ratios.**

### 6.3.3 Linear buckling of two-bay stiffened panels with different aspect ratios

The effects of the stiffener load modelling method in the accuracy of the linear stability calculations is investigated next for two-bay stiffened panels with different aspect ratios.

Here the relationship between the non-dimensional linear buckling load and the height of aspect ratio for a simply supported stiffened panel with two stiffeners running in the direction of the applied load is presented and compared with the analytical results presented by Barbre (1939).

All panels were analysed using a full model with a 18x18 mesh in order to capture different buckling mode shapes caused by the variation in the $a / b$ ratio. A summary of the panel dimensions, material properties and mesh density is presented in Figure 6-19.

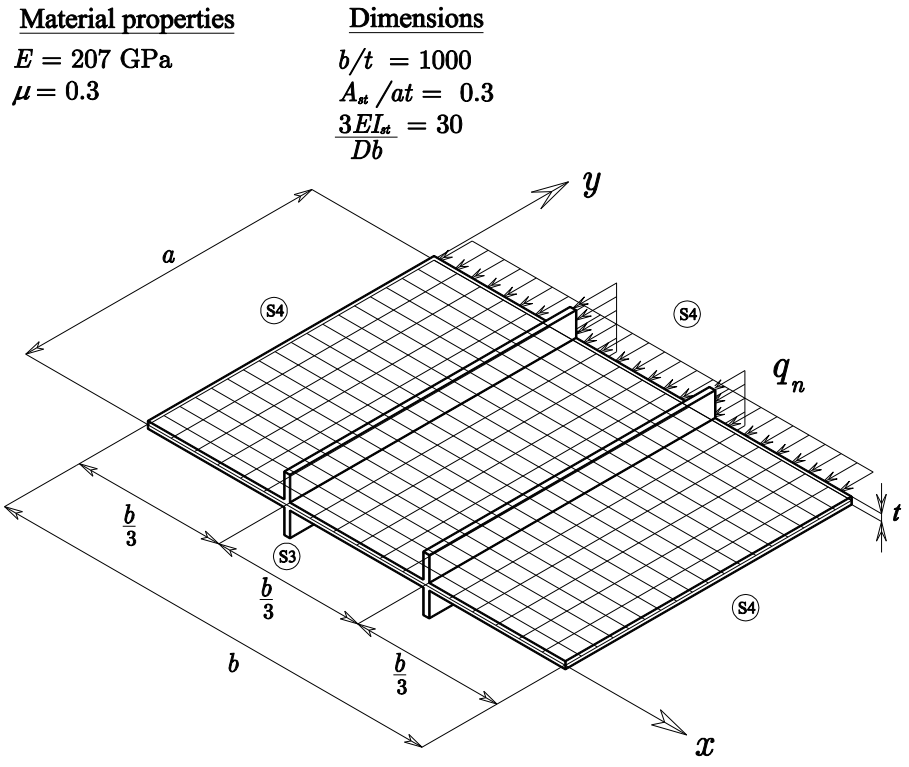


**Figure 6-19 Details of the two-bay stiffened panels with different aspect ratios.**

Babre's results were compared with two different sets of results obtained in the present investigation using NLSPAN. In the first set of results the geometric stiffness matrix was calculated using the in-plane stresses obtained for a load case that omits the stiffener load, whilst in the second set it was calculated using in-plane stress results obtained following the load calculation method described in sections 4.4.2.1 and 4.4.2.2 respectively.

In Figure 6-20, Babre's results are compared with two different sets of results obtained in the present investigation using NLSPAN. In the first set of results the geometric stiffness matrix was calculated using the in-plane stresses obtained for a load cases that omits the stiffener load, whilst in the second set the geometric stiffness matrix was calculated using in-plane stress results obtained following the load calculation method described in sections 4.4.2.1 and 4.4.2.2 respectively. The results obtained by adopting suggested load modelling method are in excellent agreement with the analytical results of Barbre, whilst the results that omit the stiffener load overestimate the buckling load for aspect ratios smaller than 1.0.

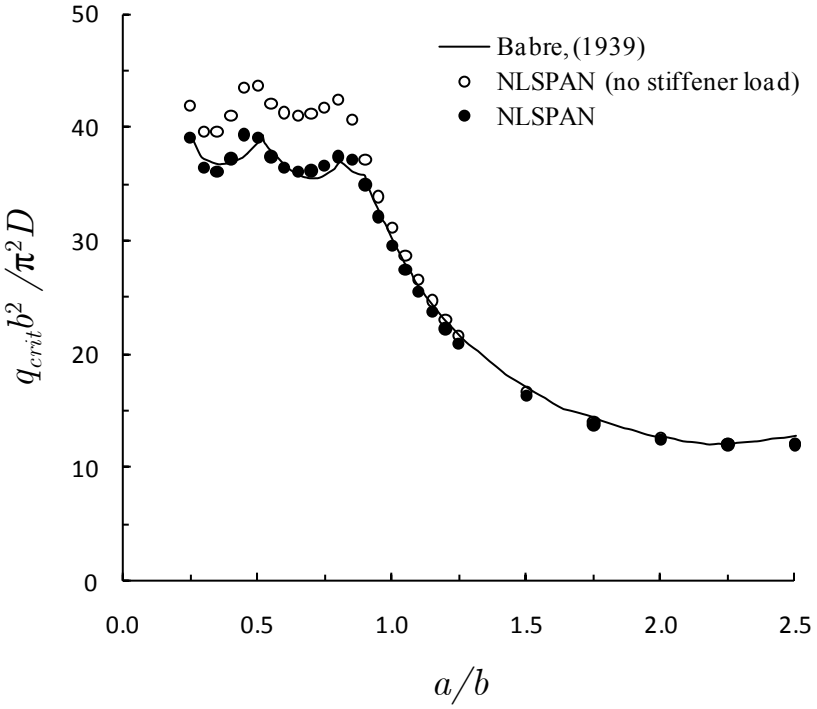


**Figure 6-20 Non-dimensional linear buckling load for two-bay stiffened panels with different aspect ratios.**

## 6.4 Non-linear buckling of stiffened panels

The non-linear buckling of squared stiffened panels is investigated in this Section using the proposed formulation. A total of ten models were considered in this analysis. Analysed models include both unstiffened and stiffened panels with different levels of initial deformations. Stiffened panels models included concentric and eccentric stiffeners with different bending stiffness ratios.

A summary of the main parameters of each panel is presented in Table 6-6. The geometric parameters proposed by Bedair (1998), described in Section 6.3.2, were used to define the dimensions of the panel.

It was shown in Section 6.2.1 that an 8x8 mesh density was sufficient to accurately model the non-linear buckling of an unstiffened simply supported panel. Consequently, in this study, a 16x16 mesh was selected to model the entire panel, as it was expected that the models with strong stiffeners will force the panel to buckle into four square sub-regions (i.e. full sine wave in the $x$ and $y$ direction). All panels were loaded by applying uniform edge shortening to the edge located at $y = a$. Boundary conditions were simple supports on all edges.

Changes in the bending stiffness ratio of the panel were obtained by varying the ratio of the height of the stiffener to thickness of the plate ($h / t$), whilst keeping the ratio of the area of the stiffener to cross sectional area of the plate to ($A_{st} / at$) constant at 0.1.

Models M1/M2 are unstiffened panels ($h / t$ =0) and are used only to provide a comparison of the overall panel behaviour.

The height of the stiffener to thickness of the plate ratios for models M3/M4 and M5/M6 were selected using Figure 6-17. Models M3/M4 were selected to have a $h / t = 6$ in order to induce overall panel buckling whilst panels M5/M6 were selected to have a $h / t = 12$ to induce local buckling of the panel skin. The $h / t$ ratios for models M7/M8 and M9/M10 were selected using Figure 6-18 in a similar way. Models M3/M4 and M9/M10 were chosen to share the same $h / t$ ratio in order to compare concentrically and eccentrically stiffened panel results.

The effect of the magnitude of the initial deformations in the non-linear buckling response of the both unstiffened and stiffened panels was studied at two different initial deformation values. Nearly perfect and imperfect panels were created by applying an initial deformation magnitude equal to 1% and 10 % of the plate thickness to the linear buckling mode shape respectively. The linear buckling mode shape of all stiffened panels was obtained using the edge load modelling method suggested in Section 4.4.2.

**Table 6-6 Details of the panels used for non-linear buckling analysis.**

| Designation | $A_{st}/at$ | $h/t$ | $EI_{st}/Db$ | % Deformation | Description |
|---|---|---|---|---|---|
| M1 | 0.1 | 0.0 | 0.0 | 1% | unstiffened panel |
| M2 | 0.1 | 0.0 | 0.0 | 10% | unstiffened panel |
| M3 | 0.1 | 6.0 | 3.3 | 1% | weak concentrically stiffened panel |
| M4 | 0.1 | 6.0 | 3.3 | 10% | weak concentrically stiffened panel |
| M5 | 0.1 | 12.0 | 13.1 | 1% | strong concentrically stiffened panel |
| M6 | 0.1 | 12.0 | 13.1 | 10% | strong concentrically stiffened panel |
| M7 | 0.1 | 3.0 | 5.2 | 1% | weak eccentrically stiffened panel |
| M8 | 0.1 | 3.0 | 5.2 | 10% | weak eccentrically stiffened panel |
| M9 | 0.1 | 6.0 | 16.7 | 1% | strong eccentrically stiffened panel |
| M10 | 0.1 | 6.0 | 16.7 | 10% | strong eccentrically stiffened panel |

In order to obtain the comparison data necessary to gauge the accuracy of the proposed finite element formulation, validation models were created and solved using the general purpose finite element code ANSYS. All comparison models were generated using a combination of SHELL93 and BEAM189 elements.

### 6.4.1 **Non-linear buckling of concentrically stiffened panels**

The non-linear buckling of concentrically stiffened panels was analysed first. A comparison of the results obtained using the current formulation and ANSYS for model M3/M4 and M5/M6 are presented in Table 6-7 and Table 6-8 respectively. Excellent agreement was found for both stiffener bending stiffness ratios.

The results of the nearly perfect and weakly stiffened panel (M3) show very good agreement with the ANSYS results with an average absolute difference of 0.15%, whilst the nearly perfect and strongly stiffened panel (M5) was found to have an absolute average difference of 0.99%.

The same conclusion can be drawn in regards to the effects of an increment in the magnitude of the initial deformations in the accuracy of the models. The weakly stiffened models (M4) and strongly stiffened models (M6) were found to have an absolute average difference of 0.09% and 0.21% respectively when the initial deformation were increased from 1% to 10%.

A graphical comparison of the non-linear response of the concentrically stiffened panels and the two unstiffened models is presented in Figure 6-21. In general, nearly perfect and imperfect models of same bending stiffness ratios show a similar trend in their non-linear response path. Furthermore, the nearly perfect panels show a much stiffer pre-buckling behaviour with a clear pre and post buckling zones. The figure also shows that the post-buckling stiffness of the panels increases as the bending stiffness ratio of the panel is increased.

A graphical comparison of the effective width of the unstiffened and concentrically stiffened panels, as function of the non-dimensional edge shortening, is presented in Figure 6-22.

As in the case of the deflections, here the effective width of nearly perfect and imperfect panels follow a similar trend, with the perfect panels showing consistently higher values across all load levels.

It can also be seen that the increment in the bending stiffness ratio in models M5 and M6 helps the panel to maintain an effective width close to unity to higher end-shortening values. This behaviour can be explained by observing distribution of stresses along the loaded edge of the panels at different edge shortening levels of strongly and weakly stiffened panels shown in Figure 6-23 and Figure 6-24 respectively. In effect, whilst the weakly stiffened panels (M3/M4) behave similar to an unstiffened panel (i.e. they show an overall panel buckling mode) the increment in the bending stiffness ratio in models M5 and M6 generates an extra support in the middle of the panel that divides the panel longitudinally into two sub panels.

In addition, Figure 6-23 and Figure 6-24 explain the softer pre-buckling behaviour of the imperfect panel (M4/M6) over the nearly perfect panel (M3/M5), as it becomes evident that the presence of larger initial deformations diminishes the panel's ability to support compressive stresses.

**Table 6-7 Comparison of the non-dimensional out of the plane deflection for the weak concentrically stiffened panels.**

| $\Delta = \frac{\bar{v}a}{t^2}$ | $w/t$ | | | |
|---|---|---|---|---|
| | M3 | | M4 | |
| | ANSYS | NLSPAN | ANSYS | NLSPAN |
| 2.95 | 0.006 | 0.006 (0.1%) | 0.060 | 0.061 (0.1%) |
| 4.00 | 0.011 | 0.011 (0.1%) | 0.103 | 0.103 (0.1%) |
| 5.35 | 0.022 | 0.022 (0.2%) | 0.201 | 0.202 (0.2%) |
| 5.88 | 0.032 | 0.032 (0.3%) | 0.263 | 0.263 (0.2%) |
| 6.60 | 0.058 | 0.058 (0.5%) | 0.377 | 0.378 (0.2%) |
| 8.15 | 0.495 | 0.497 (0.5%) | 0.694 | 0.695 (0.2%) |
| 11.95 | 1.369 | 1.369 (0.1%) | 1.355 | 1.355 (0.0%) |
| 17.00 | 2.013 | 2.014 (0.0%) | 1.960 | 1.960 (0.0%) |
| 23.20 | 2.583 | 2.583 (0.0%) | 2.515 | 2.516 (0.0%) |
| 30.60 | 3.117 | 3.117 (0.0%) | 3.042 | 3.043 (0.0%) |
| 39.15 | 3.627 | 3.626 (0.0%) | 3.548 | 3.548 (0.0%) |
| 48.95 | 4.127 | 4.126 (0.0%) | 4.046 | 4.046 (0.0%) |
| 60.05 | 4.624 | 4.623 (0.0%) | 4.541 | 4.541 (0.0%) |

Note: Figures in brackets denote the absolute percentage differences

**Table 6-8 Comparison of the non-dimensional out of the plane deflection for the strong concentrically stiffened panels.**

| $\Delta = \frac{\bar{v}a}{t^2}$ | $w/t$ | | | |
|---|---|---|---|---|
| | M4 | | M5 | |
| | ANSYS | NLSPAN | ANSYS | NLSPAN |
| 2.95 | 0.003 | 0.003 (0.2%) | 0.025 | 0.025 (0.2%) |
| 4.00 | 0.004 | 0.004 (0.2%) | 0.037 | 0.037 (0.2%) |
| 5.35 | 0.006 | 0.006 (0.2%) | 0.056 | 0.056 (0.2%) |
| 5.88 | 0.007 | 0.007 (0.2%) | 0.065 | 0.065 (0.2%) |
| 6.60 | 0.008 | 0.008 (0.3%) | 0.079 | 0.079 (0.3%) |
| 8.15 | 0.013 | 0.013 (0.4%) | 0.117 | 0.117 (0.3%) |
| 11.95 | 0.047 | 0.047 (0.9%) | 0.284 | 0.283 (0.4%) |
| 17.00 | 0.544 | 0.504 (7.3%) | 0.612 | 0.611 (0.2%) |
| 23.20 | 0.971 | 0.974 (0.3%) | 0.950 | 0.948 (0.1%) |
| 30.60 | 1.308 | 1.318 (0.8%) | 1.259 | 1.257 (0.1%) |
| 39.15 | 1.605 | 1.618 (0.8%) | 1.542 | 1.541 (0.1%) |
| 48.95 | 1.882 | 1.895 (0.7%) | 1.812 | 1.809 (0.1%) |
| 60.05 | 2.143 | 2.156 (0.6%) | 2.069 | 2.065 (0.2%) |

Note: Figures in brackets denote the absolute percentage differences

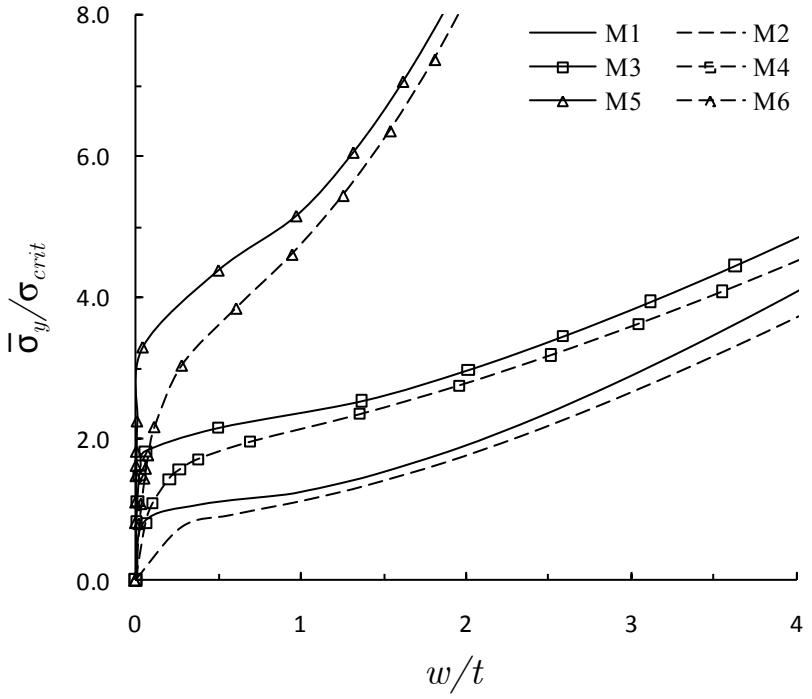


**Figure 6-21 Comparison of the non-dimensional average edge stress-deflection behaviour of the unstiffened and concentrically stiffened panels.**

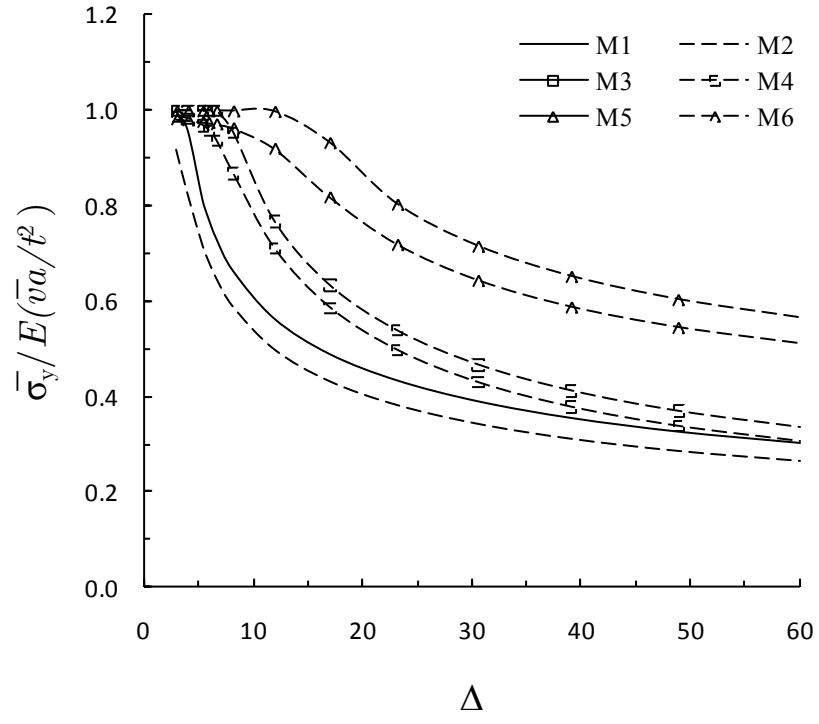


**Figure 6-22 Comparison of the effective width of unstiffened and concentrically stiffened panels at different end-shortening levels.**

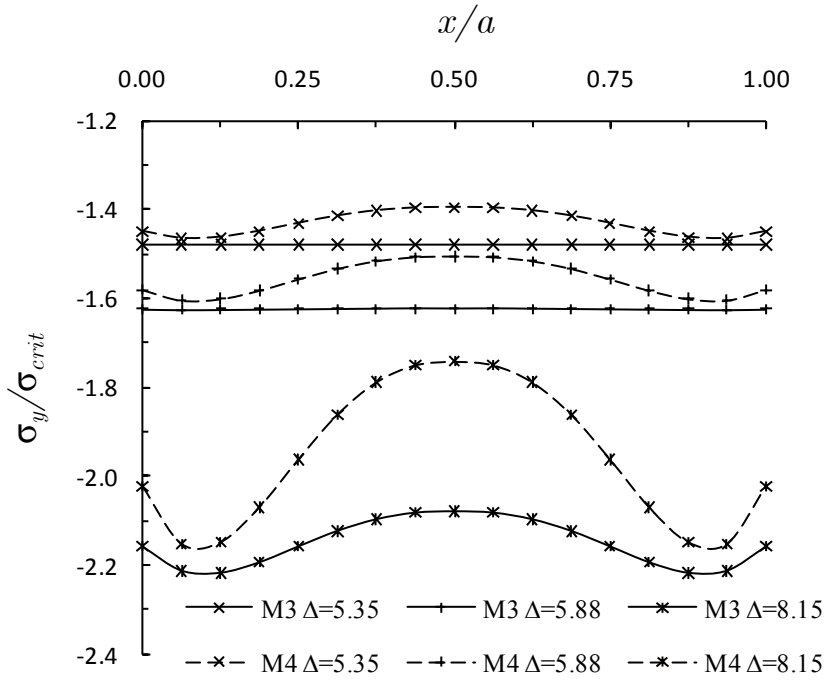


**Figure 6-23 Non-dimensional edge stress distribution along the loaded edge of weak concentrically stiffened panels at different end-shortening levels.**

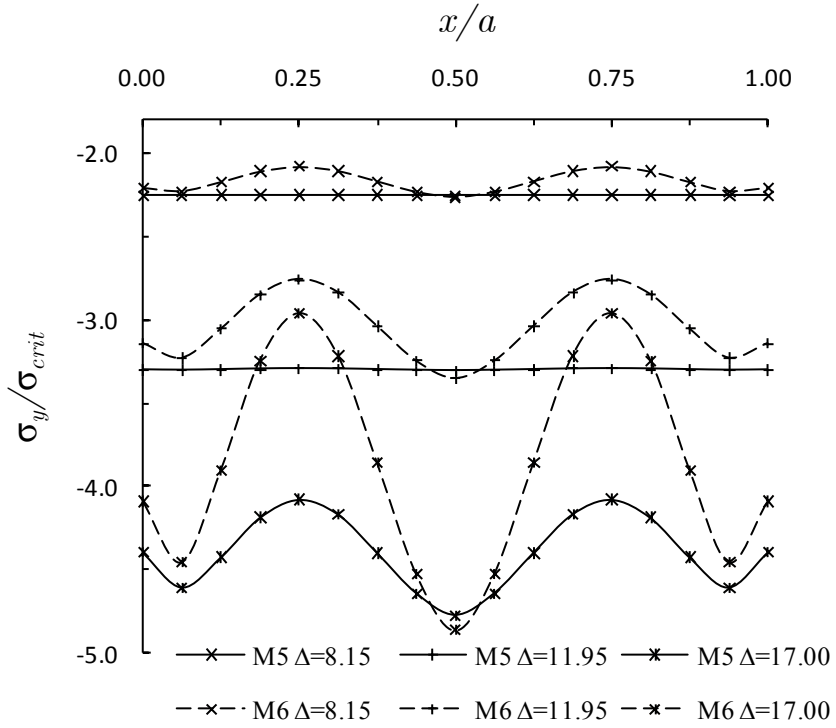


**Figure 6-24 Non-dimensional edge stress distribution along the loaded edge of strong concentrically stiffened panels at different end-shortening levels.**

### 6.4.2 **Non-linear buckling of eccentrically stiffened panels**

The non-linear buckling of eccentrically stiffened panels was analysed next. A comparison of the results obtained using the current formulation and ANSYS for model M7/M8 and M9/M10 are presented in Table 6-9 and Table 6-10 respectively.

Good agreement was found for both stiffener bending stiffness ratios. The nearly perfect, weakly stiffened model (M7) results were found to have an absolute average difference of 5.1%, whilst the nearly perfect, strongly stiffened model (M9) was found to have an absolute average difference of 0.3%. The larger differences found in the M7 model was located at the point of the non-linear response path with a nearly horizontal slope where small increments in end-shortening have large effects in the deflection of the panel and hence are deemed of low importance.

The imperfect models (M8/M10) were found to correlate much closer with the ANSYS results. The weakly stiffened imperfect model (M8) and strongly stiffened imperfect model (M10) were found to have absolute average errors of 1.8% and 0.2% respectively.

A graphical comparison of the non-linear response of the eccentrically stiffened panels and the two unstiffened models is presented in Figure 6-25. In general, nearly perfect and imperfect models of same bending stiffness ratio show a similar trend in their non-linear response path with the nearly perfect panels showing a much stiffer pre-buckling behaviour.

A graphical comparison of the effective width of the unstiffened and eccentrically stiffened panels, as function of the non-dimensional edge shortening, is presented in Figure 6-26. Both the strongly stiffened models (M9/M10) and the nearly perfect weakly stiffened model (M7) maintain an effective width close to unity to higher end-shortening values.

The distribution of stresses along the loaded edge of the strongly and weakly stiffened panels at different edge shortening levels can be observed in Figure 6-27 and Figure 6-28 respectively.

It can be appreciated from Figure 6-28 that the strongly and eccentrically stiffened panels show a similar behaviour to that of the strongly and concentrically stiffened panel shown in Figure 6-24 in which the stiffener acts as extra support that divides the panel into two longitudinal sub-panels.

The behaviour of the weakly stiffened panels is less straightforward. The edge-stress distribution of these panels shows a more complex pattern that combines an overall buckling behaviour with a limited local longitudinal support from the stiffener.

**Table 6-9 Comparison of the non-dimensional out of the plane deflection for the weak eccentrically stiffened panels.**

| $\Delta = \frac{\overline{v}a}{t^2}$ | $w/t$ | | | |
|---|---|---|---|---|
| | M7 | | M8 | |
| | ANSYS | NLSPAN | ANSYS | NLSPAN |
| 2.50 | 0.001 | 0.001 (1.0%) | 0.010 | 0.010 (1.0%) |
| 8.00 | 0.004 | 0.004 (1.1%) | 0.044 | 0.043 (1.1%) |
| 12.00 | 0.009 | 0.009 (1.3%) | 0.093 | 0.092 (1.4%) |
| 15.00 | 0.018 | 0.017 (2.2%) | 0.175 | 0.171 (2.1%) |
| 17.00 | 0.036 | 0.034 (7.7%) | 0.302 | 0.292 (3.4%) |
| 18.00 | 0.094 | 0.067 (28.4%) | 0.399 | 0.387 (3.0%) |
| 19.00 | 0.280 | 0.242 (13.6%) | 0.503 | 0.494 (1.8%) |
| 19.50 | 0.351 | 0.328 (6.5%) | 0.553 | 0.547 (1.1%) |
| 20.00 | 0.413 | 0.401 (3.0%) | 0.601 | 0.598 (0.5%) |
| 20.50 | 0.469 | 0.464 (1.0%) | 0.647 | 0.647 (0.0%) |
| 21.00 | 0.520 | 0.522 (0.3%) | 0.691 | 0.695 (0.5%) |
| 24.00 | 0.780 | 0.805 (3.2%) | 0.927 | 0.948 (2.3%) |
| 30.00 | 1.198 | 1.244 (3.8%) | 1.311 | 1.354 (3.3%) |
| 40.00 | 1.784 | 1.843 (3.3%) | 1.856 | 1.911 (3.0%) |
| 50.00 | 2.298 | 2.358 (2.6%) | 2.344 | 2.400 (2.4%) |
| 60.00 | 2.768 | 2.824 (2.0%) | 2.812 | 2.851 (1.4%) |

Note: Figures in brackets denote the absolute percentage differences

**Table 6-10 Comparison of the non-dimensional out of the plane deflection for the strong eccentrically stiffened panels.**

| $\Delta = \frac{\overline{v}a}{t^2}$ | $w/t$ | | | |
|---|---|---|---|---|
| | **M9** | | **M10** | |
| | **ANSYS** | **NLSPAN** | **ANSYS** | **NLSPAN** |
| 2.50 | 0.002 | 0.002 (0.2%) | 0.020 | 0.020 (0.2%) |
| 8.00 | 0.012 | 0.012 (0.3%) | 0.113 | 0.113 (0.3%) |
| 12.00 | 0.048 | 0.048 (1.0%) | 0.287 | 0.286 (0.4%) |
| 15.00 | 0.319 | 0.315 (1.1%) | 0.482 | 0.481 (0.3%) |
| 17.00 | 0.544 | 0.541 (0.4%) | 0.612 | 0.610 (0.2%) |
| 18.00 | 0.631 | 0.629 (0.3%) | 0.672 | 0.671 (0.2%) |
| 19.00 | 0.709 | 0.707 (0.3%) | 0.731 | 0.729 (0.2%) |
| 19.50 | 0.745 | 0.743 (0.2%) | 0.759 | 0.758 (0.2%) |
| 20.00 | 0.779 | 0.777 (0.2%) | 0.786 | 0.785 (0.2%) |
| 20.50 | 0.812 | 0.810 (0.2%) | 0.813 | 0.812 (0.1%) |
| 21.00 | 0.843 | 0.842 (0.2%) | 0.839 | 0.838 (0.1%) |
| 24.00 | 1.012 | 1.011 (0.1%) | 0.986 | 0.984 (0.1%) |
| 30.00 | 1.283 | 1.281 (0.1%) | 1.234 | 1.233 (0.1%) |
| 40.00 | 1.630 | 1.628 (0.1%) | 1.566 | 1.564 (0.1%) |
| 50.00 | 1.907 | 1.904 (0.1%) | 1.836 | 1.833 (0.2%) |
| 60.00 | 2.141 | 2.137 (0.2%) | 2.067 | 2.063 (0.2%) |

Note: Figures in brackets denote the absolute percentage differences

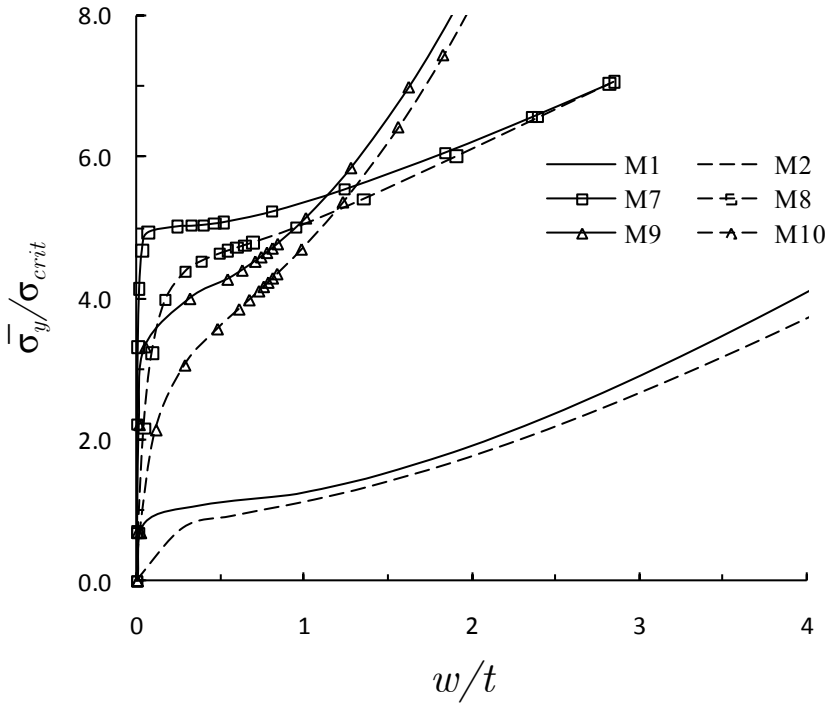


**Figure 6-25 Comparison of the non-dimensional average edge stress-deflection behaviour of the unstiffened and eccentrically stiffened panels.**

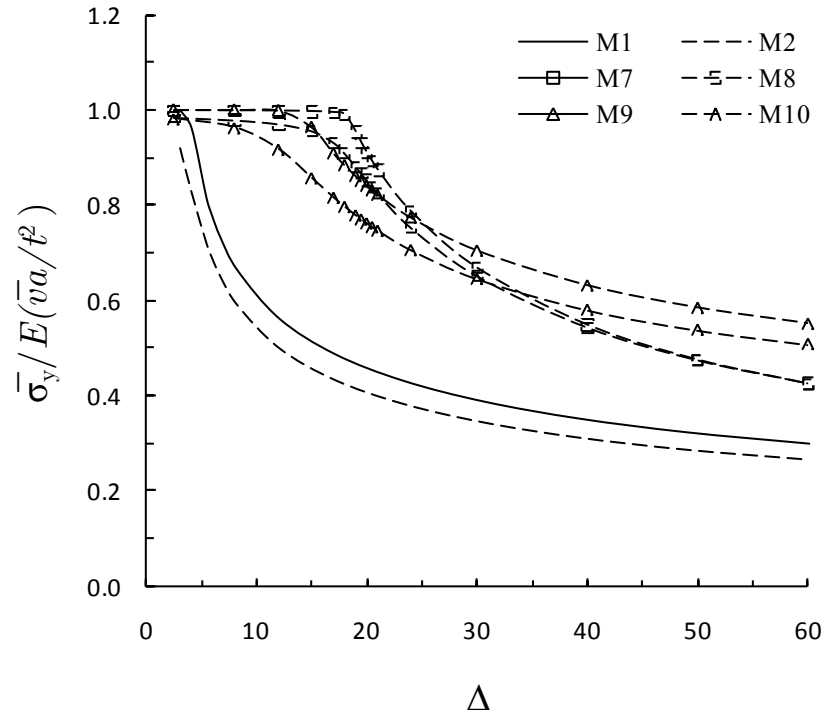


**Figure 6-26 Comparison of the effective width of unstiffened and eccentrically stiffened panels at different end-shortening levels.**

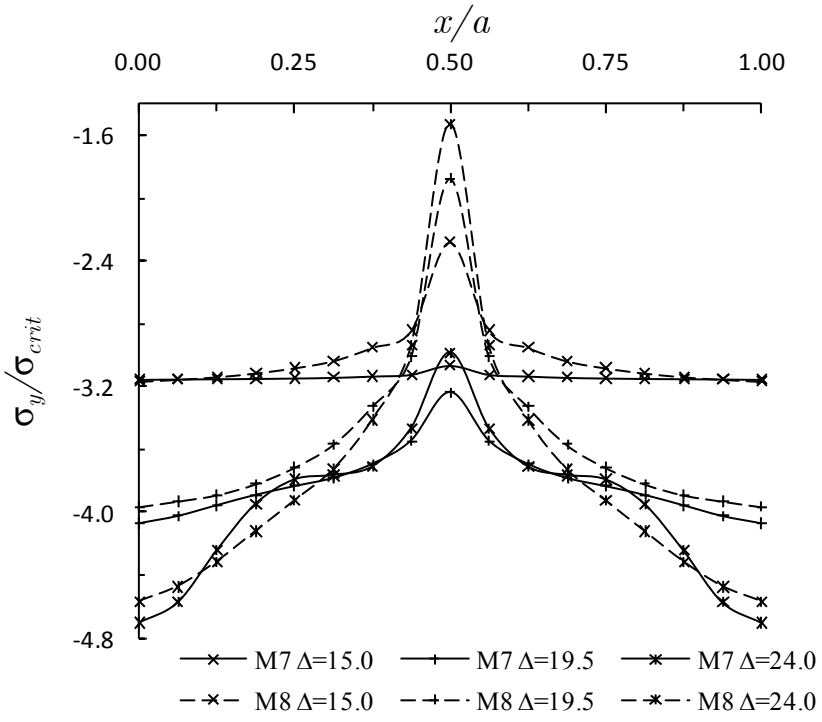


**Figure 6-27 Non-dimensional edge stress distribution along the loaded edge of weak eccentrically stiffened panels at different end-shortening levels.**

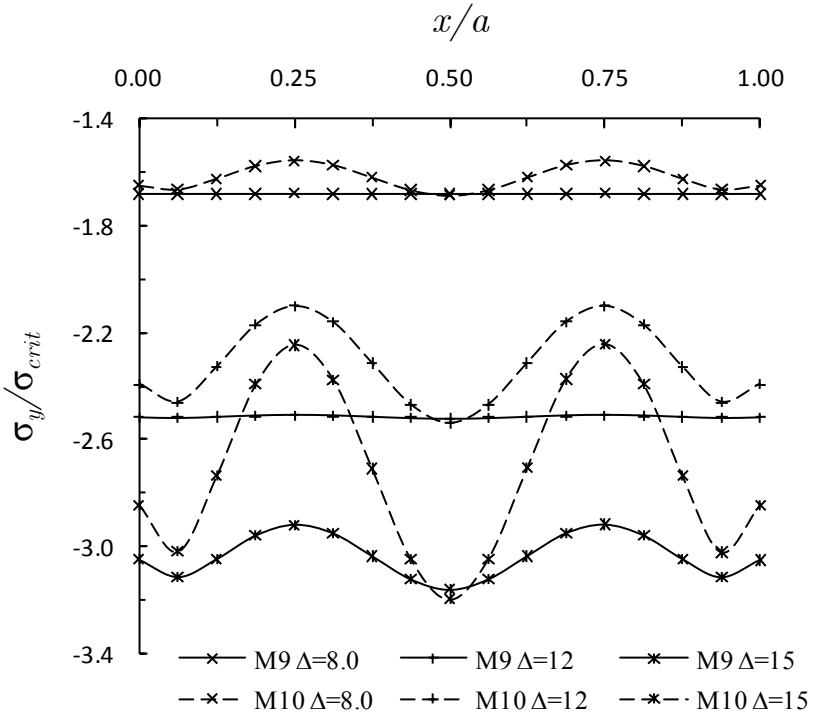


**Figure 6-28 Non-dimensional edge stress distribution along the loaded edge of strong eccentrically stiffened panels at different end-shortening levels.**

### 6.4.3 Comparison of the non-linear buckling response of eccentrically and concentrically stiffened panels

Finally the non-linear buckling of eccentrically and concentrically stiffened panels with the same $h / t$ ratio is presented. Here, the weak and concentrically stiffened models M3/M4 are compared with the strong and eccentrically stiffened models M9/M10.

Figure 6-29 presents a graphical comparison of the non-linear load-deflection response of all four models, whilst a graphical comparison of the effective width of the unstiffened and concentrically stiffened panels, as function of the non-dimensional edge shortening, can be found in Figure 6-30.

Figure 6-29 suggests that both the nearly perfect and the imperfect eccentric models experience a much stiffer pre and post buckling behaviour than the concentrically stiffened models. Indeed both eccentrically stiffened models are able to carry almost twice as much load as the concentrically stiffened models.

This can be explained by analysing Figure 6-30, where the effective width behaviour of the eccentrically stiffened panels remain closer to unit for a much larger interval than in the concentrically stiffened panels.

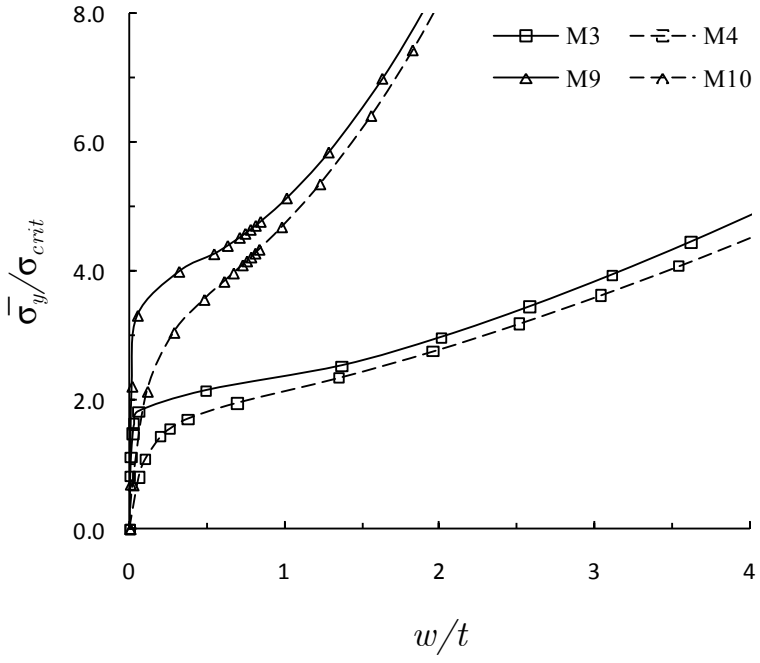


**Figure 6-29 Comparison of the non-dimensional average edge stress-deflection behaviour of the concentrically and eccentrically stiffened panels.**

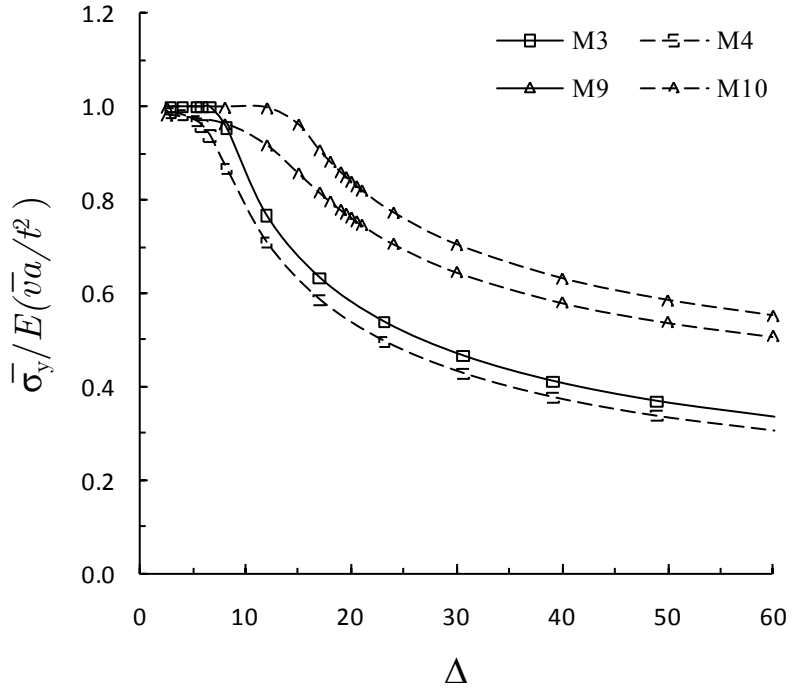


**Figure 6-30 Comparison of the effective width of concentrically and eccentrically stiffened panels at different end-shortening levels.**

## 6.5 Summary

A validation has been conducted to evaluate the performance of the presented formulation in representing both unstiffened and stiffened panels under in-plane loads.

The results obtained using the current formulation in representing unstiffened panels under the action of compressive loads were found to be in excellent agreement with analytical and numerical, and experimental results presented by other authors.

The new method proposed to model the uniform in-plane compressive load acting on the cross sectional area of stiffeners located at the edges of the master element was discussed and validated. The importance of this new method in the linear buckling calculations was demonstrated.

A thorough investigation on the non-linear buckling of concentrically and eccentrically stiffened panels with different geometric parameters and levels of initial deformation was conducted.

The investigation demonstrates that the panel load carrying capacity is improved by increasing the bending stiffness ratio of the panel. This can be achieved by increasing the dimensions of the stiffener or by placing it eccentrically with respect to the panel mid-surface.

# Chapter 7. Summary and conclusions

The present chapter summaries the main work and findings of the current investigation, highlights the implications of the research and identifies possible future work in this area.

## 7.1 Summary

The key subjects investigated and developed in this thesis can be summarised as follows:

1. A geometrically non-linear finite element was formulated by combining a shallow shell (master) element and beam (slave) element. The displacement field at any point within the slave element is defined in terms of the field variables of the master element. Therefore, only the master element's degrees of freedom are needed to discretise the entire stiffened panel. Furthermore, the stiffener location across the panel has no influence on the topology of area of the panel.

2. An eight node, quadratic, isoparametric, shallow shell element with five degrees of freedom at each node was formulated to act as the master element. Marguerre's shallow shell theory was adopted in the formulation to include the effects of initial deformations, whilst Mindlin-Reissener hypothesis was considered to take into account transverse shear deformations.

3. A three node, isoparametric beam element having four degrees of freedom at each node was formulated according to Timoshenko's shear deformable beam theory to act as the slave element. The stiffener rigidity is initially concentrated along the centroidal axis of the beam element, and is later transformed into the master element by considering the stiffener location, orientation and eccentricity with respect to the mid-surface of the master element.

4. A new method to account for uniform in-plane compressive load acting on the cross sectional area of stiffeners at the edges of the master element was formulated for both concentrically and eccentrically stiffened elements.

5. Initial deformations of the unstiffened and stiffened panels were calculated by performing an Eigen-value buckling analysis followed by a normalization buckling mode shape. A new technique to calculate the initial deformation in the slave elements from the initial deformations of the master element was developed.

6. The formulation was coded into a FORTRAN 90 computer program named NLSPAN (Non-Linear Stiffened Panel ANalysis) using the Intel Visual Fortran compiler. Both conventional Newton-Raphson and modified Newton-Raphson incremental iterative solution algorithm were implemented to obtain the non-linear response path.

7. A wide range of stiffened panel examples were solved using this program and the results compared both with those available in the open literature and those obtained using ANSYS commercial finite element package. The range of examples covers a variety of panel aspect ratios, load cases, arrangements of stiffeners, stiffener geometries, initial deformations and boundary conditions. New validation problems were presented for arbitrarily orientated stiffened panels.

## 7.2 Conclusions

The following conclusions are drawn based on the outcomes of the present investigation:

1. The proposed arbitrarily stiffened element finite element formulation was found capable of representing the geometrically non-linear behaviour of unstiffened isotropic and laminated composite panels under in-plane and transverse loads with an excellent level of accuracy. Moreover, since only the degrees of freedom of the master element were included in the finite element models the present approach has a greater numerical efficiency than conventional finite element models.

2. The numerical validation results also demonstrate that the present formulation is capable of modelling the geometrically non-linear response of stiffened panels in which the slave elements (stiffeners) were placed at arbitrary orientation within the master element. This was demonstrated for both concentrically and eccentrically stiffened panels. Since this feature lifts the restriction of having to place the stiffeners along the mesh lines of the shell elements, the present formulation has another significant advantage over conventional discretely stiffened finite element models, as it greatly reduces the complexities of the solid model topology. This greater topological flexibility makes the current formulation an excellent candidate for the generation of finite element models for structural optimization.

3. The effects of the edge load modelling method in the in-plane behaviour of arbitrarily stiffened elements was discussed and analysed for the first time. Large errors in the in-plane stresses as well as fictitious out-of-plane displacements were found to occur if the load is not appropriately modelled. A new modelling method was suggested to account for this inaccurate behaviour and it was found to succeed in overcoming these issues. Furthermore, the suggested method is not only applicable for an arbitrarily stiffened finite element model but it can also be applied to discretely stiffened models generated using general purpose finite element packages.

4. The present formulation was found capable of performing the non-linear buckling analysis of stiffened panels. The formulation succeeded in representing different initial deformation levels generated using the linear buckling mode shape. It was found that the non-linear buckling behaviour of eccentrically stiffened panels was superior to that of concentrically stiffened panels with the same stiffener dimensions.

5. The structural optimization of stiffened panels requires efficient automated changes to the panel configuration to allow for a thorough exploration of the design space. The present formulation describes the stiffeners parametrically, i.e. the stiffeners are not physically modelled but described using numerical parameters that define the stiffener(s) position, cross sectional properties and eccentricity. Therefore, the panel configuration can be modified without the need of manual topological alterations to the finite element model. Also, the finite element discretization was proven to be independent of the stiffener orientation and hence changes in the stiffener(s) position within the panel do not require manual changes to the model mesh. Consequently the present formulation becomes an excellent potential candidate for the automated model generation required in the structural optimization process of stiffened panels.

## 7.3 Further work

Should the research into this area be continued, the following subjects would be obvious candidates for further investigation:

1. The main emphasis of this investigation was on the analysis of an isolated stiffened panel. However, the author believes that the presented formulation can be useful for the future development of an integrated hull girder preliminary design model. In such a model, drilling rotational degrees of freedom (those whose vector is normal to the analysis plane) should be added to the current formulation to allow the representation of hull girder stiffened panels jointed at square angles.

2. The application of the present formulation to the ultimate failure analysis of stiffened panels could be investigated. This would involve an investigation into the material non-linearity, i.e. plasticity/composite failure, to evaluate the progression of failure in stiffened panels. In addition, the effect of in-plane shear load and combined in-plane and out of plane loads should be included in the present formulation to investigate the failure of panels of the hull girder located in the side plating and/or under the water plane.

3. Finally, experimental investigations on the geometrically non-linear response of isotropic and laminated panels, stiffened at arbitrary orientations should be carried out to provide much needed physical validation data for this specific structural configuration.

# References


AKIN, J. E. 1994. *Finite Elements for Analysis and Design*, Academic Press.

ALMROTH, B. O. 1966. Influence of edge conditions on the stability of axially compressed cylindrical shells. *AIAA Journal,* 4**,** 134-140.

ANSYS INC. 2004. ANSYS University Advance. 9.0 ed. Berkeley, CA: ANSYS Inc.

ARGYRIS, J. & TENEK, L. 1994. Linear and geometrically nonlinear bending of isotropic and multilayered composite plates by natural mode method. *Computer Methods in Applied Mechanics and Engineering,* 113**,** 207-251.

BARBRE, R. 1939. Stability of rectangular plates with longitudinal or transverse stiffeners under uniform compression *In:* NACA (ed.) *NACA Technical Memorandum.* NACA.

BARIK, M. & MUKHOPADHYAY, M. 2002. A New Stiffened Plate Element for the Analysis of Arbitrary Plates. *Thin-Walled Structures,* 40**,** 625-639.

BARUT, A., MADENCI, E., TESSLER, A. & STARNES, J. H. J. 2000. A New Stiffened Shell Element for Geometrically Nonlinear Analysis of Composite Laminates. *Computers & Structures,* 77**,** 11-40.

BATHE, K.-J. & BOLOURCHI, S. 1980. A Geometric and Material Nonlinear Plate and Shell Element. *Computers & Structures,* 11**,** 23-48.

BATHE, K.-J. & CIMENTO, A. P. 1980. Some Practical Procedures for the Solution of Nonlinear Finite Element Equations. *Computer Methods in Applied Mechanics and Engineering,* 22**,** 59-85.

BATHE, K.-J. & GRACEWSKI, S. 1981. On Nonlinear Dynamic Analysis using Substructuring and Mode Superposition. *Computers & Structures,* 13**,** 699-707.

BAU-MADSEN, N. K., SVENDSEN, K.-H. & KILDEGAARD, A. 1993. Large Deflections of Sandwich Plates - An Experimental Investigation. *Composite Structures,* 23**,** 47-56.

BEDAIR, O. K. 1998. A contribution to the stability of stiffened plates under uniform compression. *Computers & Structures,* 66**,** 535-570.

BERGAN, P. G. 1972. Convergence Criteria for Iterative Processes. *AIAA Journal,* 10**,** 1107-1108.

BOFFOLI , C. 2007. 787 fuselage. wikimedia fundation.

BRUBAK, L., HELLESLAND, J. & STEEN, E. 2007. Semi-analytical buckling strength analysis of plates with arbitrary stiffener arrangements. *Journal of Constructional Steel Research,* 63**,** 532-543.

BYKLUM, E. & AMDAHL, J. 2002. A simplified method for elastic large deflection analysis of plates and stiffened panels due to local buckling. *Thin-Walled Structures,* 40**,** 925-953.

CAMILLERI, D., COMLEKCI, T. & GRAY, T. G. F. 2005. Design Support Tool for Prediction of Welding Distortion in Multiply Stiffened Plate Structures: Experimental and Computational Investigation. *Journal of Ship Production,* 21**,** 219-234.

CHATTOPADHYAY, B., SINHA, P. K. & MUKHOPADHYAY, M. 1992. Finite Element Free Vibration Analysis of Eccentrically Stiffened Composite Plates. *Journal of Reinforced Plastics and Composites,* 11**,** 1003-1034.

CHATTOPADHYAY, B., SINHA, P. K. & MUKHOPADHYAY, M. 1993. Finite Element Analysis of Blade-Stiffened Composite Plates under Transverse Loads. *Journal of Reinforced Plastics and Composites,* 12**,** 76-100.

CHATTOPADHYAY, B., SINHA, P. K. & MUKHOPADHYAY, M. 1995. Geometrically Nonlinear Analysis of Composite Stiffened Plates using Finite Elements. *Composite Structures,* 31**,** 107-118.

CHEN, N.-Z. & GUEDES SOARES, C. 2007. Longitudinal Strength Analysis of Ship Hulls of Composite Materials under Sagging Moments. *Composite Structures,* 77**,** 36-44.

CHEN, N.-Z. & GUEDES SOARES, C. 2008. Ultimate longitudinal strength of ship hulls of composite materials. *Journal of Ship Research,* 52**,** 184-193.

CHEN, N.-Z., SUN, H.-H. & GUEDES SOARES, C. 2003. Reliability analysis of a ship hull in composite material. *Composite Structures,* 62**,** 59-66.

CHEUNG, Y. K. & THAM, L. G. 1998. *Finite strip method (New Directions in Civil Engineering)*, CRC Press.

COOK, R. D. 1995. *Finite element modelling for stress analysis*.

COOK, R. D., MALKUS, D. S. & PLESHA, M. E. 1989. *Concepts and applications of finite element analysis,* New York, Wiley.

CORR, R. B. & JENNINGS, A. 1976. A simultaneous Iteration Algorithm for Symmetric Eigenvalue Problems. *International Journal for Numerical Methods in Engineering,* 10**,** 647-663.

CRISFIELD, M. A. 1979. A Faster Modified Newton-Raphson Iteration. *Computer Methods in Applied Mechanics and Engineering,* 20**,** 267-278.

CRISFIELD, M. A. 1981. A Fast Incremental/Iterative Solution Procedure That Handles "Snap-Through". *Computers & Structures,* 13**,** 55-62.

DAWE, D. J. 2002. Use of the finite strip method in predicting the behaviour of composite laminated structures. *Composite Structures,* 57**,** 11-36.

GERADIN, M., IDELSOHN, S. & HOGGE, M. 1981. Computational Strategies for the Solution of Large Nonlinear Problems via Quasi-Newton Methods. *Computers & Structures,* 13**,** 73-81.

GORDO, J. M., GUEDES SOARES, C. & FAULKNER, D. 1996. Approximate assessment of the ultimate longitudinal strength of the hull girder. *Journal of Ship Research,* 40**,** 60-69.

GORGI, M. 1986. On large deflection of symmetric composite plates under static loading. *Proceedings of the Institution of Mechanical Engineers. Part C, Journal of mechanical engineering science,* 200**,** 9.

GOSWAMI, S. & MUKHOPADHYAY, M. 1995. Geometrically Non-Linear Transient Dynamic Response of Laminated Composite Stiffened Shells. *Journal of Reinforced Plastics and Composites,* 14**,** 618-640.

GÜNAY, E. 1999. Finite-Element Analysis of Laminated Stiffened Cylindrical Shallow Shell. *Applied Composite Materials,* 6**,** 381-395.

HUGHES, O. F. 1988. *Ship structural design: A rationally-based, computer-aided optimization approach*, Society of Naval Architects and Offshore Engineers.

HUGHES, O. F. & DAVIES, J. 1975. An analytical orthotropic plane stress element for automated structural design. The Univeristy of New South Wales.

HUGHES, O. F., DAVIES, J. & MISTREE, F. 1976. Finite elements in the design of optimum ship structures.: The University of New South Wales.

JIANG, J. & OLSON, M. D. 1994. Nonlinear Analysis of Orthogonally Stiffened Cylindrical Shells by a Super Element Approach. *Finite Elements in Analysis and Design,* 18**,** 99-110.

KANT, T. & KOMMINENI, J. R. 1992. $C^0$ Finite Element Geometrically Non-Linear Analysis of Fibre Reinforced Composite and Sandwich Laminates Based on a Higher-Order Theory. *Computers & Structures,* 45**,** 511-520.

KAO, R. 1974. A Comparison of Newton-Raphson Methods and Incremental Procedures for Geometrically Nonlinear Analysis. *Computers & Structures,* 4**,** 1091-1097.

KASSEGNE, S. K. & REDDY, J. N. 1998. Local Behaviour of Discretely Stiffened Composite Plates and Cylindrical Shells. *Composite Structures,* 41**,** 13-26.

KEY, C. T., GARNICH, M. R. & HANSEN, A. C. 2004. Progressive failure predictions for rib-stiffened panels based on multicontinuum technology. *Composite Structures,* 64**,** 357-366.

KHEDMATI, M. R., BAYATFAR, A. & RIGO, P. 2010. Post-buckling behaviour and strength of multi-stiffened aluminium panels under combined axial compression and lateral pressure. *Marine Structures,* 23**,** 39-66.

KOKO, T. S. & OLSON, M. D. 1991a. Non-Linear Analysis of Stiffened Plates using Super Elements. *International Journal for Numerical Methods in Engineering,* 31**,** 319-343.

KOKO, T. S. & OLSON, M. D. 1991b. Nonlinear Transient Response of Stiffened Plates to Air Blast loading by a Superelement Approach. *Computer Methods in Applied Mechanics and Engineering,* 90**,** 737-760.

KOKO, T. S. & OLSON, M. D. 1992. Vibration analysis of stiffened plates by super elements. *Journal of Sound and Vibration,* 158**,** 149-167.

KUMAR, Y. V. S. & MUKHOPADHYAY, M. 1999. A new finite element for buckling analysis of laminated stiffened plates. *Composite Structures,* 46**,** 321-331.

KUMAR, Y. V. S. & MUKHOPADHYAY, M. 2000a. Finite element analysis of ship structures using a new stiffened plate element. *Applied Ocean Research,* 22**,** 361-374.

KUMAR, Y. V. S. & MUKHOPADHYAY, M. 2000b. A new triangular stiffened plate element for laminate analysis. *Composites Science and Technology,* 60**,** 935-943.

KUMAR, Y. V. S. & MUKHOPADHYAY, M. 2002. A New Modelling Tool for 3-D Finite Element Analysis of FRP Ships. *International Shipbuilding Progress,* 49**,** 5-35.

KUMAR, Y. V. S., MUKHOPADHYAY, M. & SARKAR, T. 2002. Development of a New Efficient Stiffened Plate Element for Dynamic Analysis of a Three-Dimensional Ship Structure. *Journal of Engineering for the Maritime Enviroment,* 216**,** 45-56.

KUMAR, Y. V. S. & SRIVASTAVA, A. 2003. First Ply Failure Analysis of Laminated Stiffened Plates. *Composite Structures,* 60**,** 307-315.

LAMBERTI, L., VENKATARAMAN, S., HAFTKA, R. T. & JOHNSON, T. F. 2003. Preliminary Design Optimization of Stiffened Panels using Approximate Analysis Models. *International Journal for Numerical Methods in Engineering,* 57**,** 1351-1380.

LEVY, S. 1942. Square Plate with Clamped Edges under Normal Pressure Producing Large Deflections. *In:* NACA (ed.) *NACA Technical Report.* NACA.

LIAO, C.-L. & REDDY, J. N. 1989. Continuum-Based Stiffened Composite Shell Elements for Geometrically Nonlinear Analysis. *AIAA Journal,* 27**,** 95-101.

LIAO, C.-L. & REDDY, J. N. 1990. Analysis of Anisotropic, Stiffened Composite Laminates using a Continuum-Based Shell Element. *Computers & Structures,* 34**,** 805-815.

LOUGHLAN, J. 1994. The Buckling Performance of Composite Stiffened Panel Structures Subjected to Combined in-plane Compression and Shear Loading. *Composite Structures,* 29**,** 197-212.

LOUGHLAN, J. 1996. The Buckling of Composite Stiffened Box Sections Subjected to Compression and Bending. *Composite Structures,* 35**,** 101-116.

LOUGHLAN, J. & DELAUNOY, J.-M. 1993. The buckling of composite stiffened plates with some emphasis on the effects of fibre orientation and on loading configuration. *Composite Structures,* 25**,** 485-494.

MARGUERRE, K. 1938. Zur Theorie der gekrümmten Platte grosser Formänderung. Proceedings of the 5th International Congress for Applied Mechanics, 93-101.

MCGUIRE, W., GALLAGHER, R. H. & ZIEMIAN, R. D. 2000. *Matrix Structural Analysis*, Wiley.

MINDLIN, R. D. 1951. Influence of Rotary Inertia and Shear on Flexuaral Motions of Isotropic, Elastic Plates. *Transactions of the ASME***,** 31-38.

MOLLAND, A. F. 2008. *The Maritime Engineering Reference Book,* Oxford, Elsevier.

MOURITZ, A. P., GELLERT, E., BURCHILL, K. & CHALLIS, K. 2001. Review of Advanced Composite Structures for Naval Ships and Submarines. *Composite Structures,* 53**,** 21-41.

MOY, S. S. J., SHENOI, R. A. & ALLEN, H. G. 1996. Strength and Stiffness of Fibre-Reinforced Plastic Plates. *Proceedings of the Institution of Civil Engineers - Structures and Buildings,* 116**,** 202-220.

MUKHERJEE, N. & CHATTOPADHYAY, T. 1994. Improved free vibration analysis of stiffened plates by dynamic element method. *Computers & Structures,* 52**,** 259-264.

MUKHOPADHYAY, M. 1981. Stiffened Plate Plane Stress Elements for the Analysis of Ships' Structures. *Computers & Structures,* 13**,** 563-573.

MUKHOPADHYAY, M. & MUKHERJEE, A. 1989. Recent Advances on the Dynamic Behavior of Stiffened Plates. *The Shock and Vibration Digest,* 21**,** 6-9.

MUKHOPADHYAY, M. & MUKHERJEE, A. 1990. Finite Element Buckling Analysis of Stiffened Plates. *Computers & Structures,* 34**,** 795-803.

MUKHOPADHYAY, M. & SATSANGI, S. K. 1984. Isoparametric Stiffened Plate Bending Element for the Analysis of Ships' Structures. *Transactions of the Royal Institution of Naval Architects,* 126**,** 144-151.

MUKHOPADHYAY, M., SATSANGI, S. K. & MUKHERJEE, A. 1990. A New Isoparametric Plate Element for the Analysis of Ship Structures. *International Shipbuilding Progress,* 37**,** 79-117.

MUKHOPADHYAY, M. & SINHA, G. 1992. A review of Dynamic behavior of stiffened shells. *The Shock and Vibration Digest,* 24**,** 3-13.

NAYAK, A. N. & BANDYOPADHYAY, J. N. 2002. On the Free Vibration of Stiffened Shallow Shells. *Journal of Sound and Vibration,* 255**,** 357-382.

NORWOOD, C. 1995. The Free Vibration of Ring Stiffened Cylinders - A Critical Review of the Unclassified Literature. *DSTO Technical Report.* Defence Science and Technology Organization.

OJEDA, R., PRUSTY, B. G. & LAWRENCE, N. 2008. Geometrically non-linear analysis of stiffened structures: a review. *Pacific 2008 International Maritime Conference.* Sydney, Australia.

OJEDA, R., PRUSTY, B. G., LAWRENCE, N. & THOMAS, G. 2007. A new approach for the large deflection finite element analysis of isotropic and composite plates with arbitrary orientated stiffeners. *Finite Elements in Analysis and Design,* 43**,** 989-1002.

PALANI, G. S., IYER, N. G. & APPA RAO, T. V. S. R. 1993. An efficient finite element model for static and vibration analysis of plates with arbitrarily located eccentric stiffeners. *Journal of Sound and Vibration,* 166**,** 409-427.

PALANI, G. S., IYER, N. R. & APPA RAO, T. V. S. R. 1992. An efficient finite element model for static and vibration analysis of eccentrically stiffened plates/shells. *Computers & Structures,* 43**,** 651-661.

PAULLING, J. R. 1964. The Analysis of Complex Ship Structures by the Finite Element Technique. *Journal of Ship Research,* 8**,** 1-14.

PICA, A. & WOOD, R. D. 1980. Postbuckling behaviour of plates and shells using a mindlin shallow shell formulation. *Computers & Structures,* 12**,** 759-768.

PICA, A., WOOD, R. D. & HINTON, E. 1980. Finite Element Analysis of Geometrically Nonlinear Plate Behaviour using a Mindlin Formulation. *Computers & Structures,* 11**,** 203-215.

PRUSTY, B. G. 2001a. Analysis of Stiffened Shell for Ships and Ocean Structures by Finite Element Method. *Ocean Engineering,* 28**,** 621-638.

PRUSTY, B. G. 2001b. *Static, Dynamic, Buckling and Failure Analyses of Composite Stiffened Shell Structures: A Finite Element Approach.* Doctor of Philosophy, Indian Institute of Technology.

PRUSTY, B. G. 2003. Linear Static Analysis of Composite Hat-Stiffened Laminated Shells using Finite Elements. *Finite Elements in Analysis and Design,* 39**,** 1125-1138.

PRUSTY, B. G., RAY, C. & SATSANGI, S. K. 2001a. First Ply Failure Analysis of Stiffened Panels - A Finite Element Approach. *Composite Structures,* 51**,** 73-81.

PRUSTY, B. G. & SATSANGI, S. K. 2001a. Finite Element Buckling Analysis of Laminated Composite Stiffened Shells. *International Journal of Crashworthiness,* 6**,** 471-484.

PRUSTY, B. G. & SATSANGI, S. K. 2001b. Finite Element Transient Dynamic Analysis of Laminated Stiffened Shells. *Journal of Sound and Vibration,* 248**,** 215-233.

PRUSTY, B. G., SATSANGI, S. K. & RAY, C. 2001b. First Ply Failure Analysis of Laminated Panels under Transverse Loading. *Journal of Reinforced Plastics and Composites,* 20**,** 671-684.

PUTCHA, N. S. & REDDY, J. N. 1986. A Refined Mixed Shear Flexible Finite Element for the Nonlinear Analysis of Laminated Plates. *Computers & Structures,* 22**,** 529-538.

QUN, Z., MU., L. & WENQUI, K. 1999. Application if the Generalized Conforming Flat Shell Element to Geometrical Non-Linear Analysis for Composite Stiffened Shell Structures. *Communications in Numerical Methods in Engineering,* 15**,** 399-412.

RAO, D. V., SHEIKH, A. H. & MUKHOPADHYAY, M. 1993. A Finite Element Large Displacement Analysis of Stiffened Plates. *Computers & Structures,* 47**,** 987-993.

RAY, C. 1997. Buckling analysis of laminated box stiffened structures under axial and shear loads *Conference On Ship And Offshore Technology.* Kharagpur India ITT Kharagpur India

RAY, C. & SATSANGI, S. K. 1996. Finite Element Analysis of Laminated Hat-Stiffened Plates. *Journal of Reinforced Plastics and Composites,* 15**,** 1174-1193.

RAY, C. & SATSANGI, S. K. 1998. Geometric nonlinear static analysis of laminated hat stiffened plates. *Journal of Reinforced Plastics and Composites,* 17**,** 1264-1280.

RAY, C. & SATSANGI, S. K. 1999. Laminated Stiffened Plate- A First Ply Failure Analysis. *Journal of Reinforced Plastics and Composites,* 18**,** 1061-1076.

REDDY, J. N. 1987. A Generalization of Two-Dimensional Theories of Laminated Composite Laminates. *Communications in Applied Numerical Methods,* 3**,** 173-180.

REDDY, J. N. 1997. *Mechanics of laminated composite plates and shells theory and analysis,* Washington, DC, CRC Press.

REDDY, J. N. 2006. *An Introduction to Nonlinear Finite Element Analysis,* New York, Oxford University Press Inc.

REDDY, J. N. & ROBBINS, D. H. J. 1994. Theories and Computational Models for composite laminates. *Applied Mechanics Reviews,* 47**,** 147-169.

REISSNER, E. 1945. The Effect of Transverse Shear Deformation on the Bending of Eleastic Plates.

RIGO, P., SARGHIUTA, R., ESTEFEN, S., LEHMANN, E., OTELEA, S. C., PASQUALINO, I., SIMONSEN, B. C., WAN, Z. & YAO, T. 2003. Sensitivity Analysis on Ultimate Strength of Aluminium Stiffened Panels. *Marine Structures,* 16**,** 437-468.

RIKS, E. 1979. An Incremental Approach to the Solution of Snapping and Buckling Problems. *International Journal of Solids and Structures,* 15**,** 529-551.

ROHWER, K., FRIEDRICHS, S. & WEHMEYER, C. 2004. Analyzing laminated structures from fibre-reinforced composite materials - An assesment. *Technische Mechanick,* 25**,** 59-79.

RUSHTON, K. R. 1970. Large Deflexion of Plates with Initial Curvature. *International Journal of Mechanical Sciences,* 12**,** 1087-1051.

SAMANTA, A. & MUKHOPADHYAY, M. 1998. Finite Element Static Analysis of Stiffened Shells. *International Journal of Applied Mechanics and Engineering,* 3**,** 55-87.

SAMANTA, A. & MUKHOPADHYAY, M. 1999. Finite Element Large Deflection Analysis of Shallow and Deep Stiffened Shells. *Finite Elements in Analysis and Design,* 33**,** 187-208.

SAMANTA, A. & MUKHOPADHYAY, M. 2004. Free Vibration Analysis of Stiffened Shells by the Finite Element Technique. *European Journal of Mechanics A/Solids,* 23**,** 159-179.

SATSANGI, S. K. & MUKHOPADHYAY, M. 1989. A review of static analysis of stiffened plates. *Journal of Structural Engineering,* 15**,** 117-126.

SATSANGI, S. K. & RAY, C. 1998. Structural Analysis of Ships' Stiffened Plate Panels in Bending. *International Shipbuilding Progress,* 45**,** 181-195.

SHEIKH, A. H. & MUKHOPADHYAY, M. 1992. Analysis of stiffened plate with with arbitrary planform by the general spline finite strip method. *Computers & Structures,* 42**,** 53-67.

SHEIKH, A. H. & MUKHOPADHYAY, M. 1993. Free vibration analysis of stiffened plates with arbitrary planform by the general finite strip method. *Journal of Sound and Vibration,* 162**,** 147-164.

SHEIKH, A. H. & MUKHOPADHYAY, M. 2000. Geometric Non-linear Analysis of Stiffened Plates by the Finite Strip Method. *Computers & Structures,* 76**,** 765-785.

SHEIKH, A. H. & MUKHOPADHYAY, M. 2002. Linear and Nonlinear Transient Vibration Analysis of Stiffened Plate Structures. *Finite Elements in Analysis and Design,* 38**,** 477-502.

SHEN, H.-S. 1998. Postbuckling Analysis of Imperfect Stiffened Laminated Cylindrical Shells under Combined External Pressure and Thermal Loading. *International Journal of Mechanical Sciences,* 40**,** 339-355.

SINHA, G. & MUKHOPADHYAY, M. 1995. Static and Dynamic Analysis of Stiffenend Shells - A Review. *Proceedings of Indian National Science Academy,* 61**,** 195-219.

SRIVASTAVA, A. K. L., DATTA, P. K. & SHEIKH, A. H. 2003. Buckling and vibration of stiffened plates subjected to partial edge loading. *International Journal of Mechanical Sciences,* 45**,** 73-93.

STARNES, J. H. J. & ROUSE, M. 1981. Postbuckling and failure characteristics of selected flat rectangular graphite-epoxy plates loaded in compression. *AIAA Paper.*

STEEN, E. & BYKLUM, E. 2005. Ultimate strength and postbuckling stiffness of plate panels subjected to combined loads using semi-analytical models. *International Conference on Marine Research and Transportation.* Ischia Island, Naples, Italy.

STEEN, E., BYKLUM, E. & VILMING, K. G. 2004a. Computer efficient non-linear buckling models for capacity assessments of stiffened panels subjected to combined loads. *International Conference on Thin-Walled Structures.* Loughborough, UK.

STEEN, E., BYKLUM, E., VILMING, K. G. & OSTVOLD, T. K. 2004b. Computerized buckling models for ultimate strength assessments of stiffened ship hull panels. *PRADS.* Lubeck/Travemunde.

STEEN, E., OSTVOLD, T. K. & VALSGARD, S. 2001. A new design model for ultimate and buckling strength assessment of stiffened plates. *PRADS.*

TAY, T. E., LIU, G., TAN, V. B. C., SUN, X. S. & PHAM, D. C. 2008. Progressive failure analysis of composites. *Journal of Composite Materials,* 42**,** 1921-1966.

THOMAS, G. 2003. *Wave Slam response of Large High-Speed Catamarans.* Doctor of Philosophy, University of Tasmania.

THOMPSON, P. A., BETTESS, P. & CALDWELL, J. B. 1988. An isoparametric eccentrically stiffened plate bending element. *Engineering Computations,* 5**,** 110-116.

WANG, S. & DAWE, D. J. 1997. Spline Finite Strip Analysis of the Buckling and Vibration of Composite Prismatic Plate Structures. *International Journal of Mechanical Sciences,* 39**,** 1161-1180.

WHITNEY, J. M. 1972. Stress Analysis of Thick Laminated Composite and Sandwich Plates. *Journal of Composite Materials,* 6**,** 426-440.

YAMAKI, N. 1959. Postbuckling behavior of rectangular plates with small initial curvature loaded in edge compression. *Journal of Applied Mechanics,* 26**,** 407-414.

YUAN, W. X. & DAWE, D. J. 2004. Free Vibration and Stability Analysis of Stiffened Sandwich Plates. *Composite Structures,* 63**,** 123-137.

ZAGHLOUL, S. A. & KENNEDY, J. B. 1975. Nonlinear behavior of symmetrically laminated plates. *Journal of Applied Mechanics,* 42**,** 234-236.

ZHANG, Y. X. & KIM, K. S. 2006. Geometrically Nonlinear Analysis of Laminated Composite Plates by two New Displacement-Based Quadrilateral Plate Elements. *Composite Structures,* 72**,** 301-310.

ZIENKIEWICZ, O. C. & TAYLOR, R. L. 1994. *The finite element method,* Oxford, Butterworth-Heinemann.